

Review

# Porous Inorganic Nanomaterials: Their Evolution towards Hierarchical Porous Nanostructures

Anitta Jose <sup>1</sup>, Tom Mathew <sup>1,2</sup>, Nora Fernández-Navas <sup>1,3</sup>  and Christine Joy Querebillo <sup>1,\*</sup> 

- <sup>1</sup> Leibniz-Institute for Solid State and Materials Research Dresden (Leibniz IFW Dresden), Helmholtzstr. 20, 01069 Dresden, Germany; a.jose@ifw-dresden.de (A.J.); n.fernandez.navas@ifw-dresden.de (N.F.-N.)
- <sup>2</sup> Faculty of Natural Sciences, Technische Universität Chemnitz, Straße der Nationen 62, D-09111 Chemnitz, Germany
- <sup>3</sup> Faculty of Mechanical Science and Engineering, Technische Universität Dresden, Helmholtzstr. 10, 01069 Dresden, Germany
- \* Correspondence: c.j.querebillo@ifw-dresden.de

**Abstract:** The advancement of both porous materials and nanomaterials has brought about porous nanomaterials. These new materials present advantages both due to their porosity and nano-size: small size apt for micro/nano device integration or in vivo transport, large surface area for guest/target molecule adsorption and interaction, porous channels providing accessibility to active/surface sites, and exposed reactive surface/active sites induced by uncoordinated bonds. These properties prove useful for the development of different porous composition types (metal oxides, silica, zeolites, amorphous oxides, nanoarrays, precious metals, non-precious metals, MOFs, carbon nanostructures, MXenes, and others) through different synthetic procedures—templating, colloidal synthesis, hydrothermal approach, sol-gel route, self-assembly, dealloying, galvanostatic replacement, and so—for different applications, such as catalysis (water-splitting, etc.), biosensing, energy storage (batteries, supercapacitors), actuators, SERS, and bio applications. Here, these are presented according to different material types showing the evolution of the structure design and development towards the formation of hierarchical porous structures, emphasizing that the formation of porous nanostructures came about out of the desire and need to form hierarchical porous nanostructures. Common trends observed across these different composition types include similar (aforementioned) applications and the use of porous nanomaterials as templates/precursors to create novel ones. Towards the end, a discussion on the link between technological advancements and the development of porous nanomaterials paves the way to present future perspectives on these nanomaterials and their hierarchical porous architectures. Together with a summary, these are given in the conclusion.

**Keywords:** evolution of emergent nanostructures; catalysis and sensing application; synthetic procedures of nanoporous gold; hierarchical nanoarrays; zeolite and silica nanomaterials; dealloying processes; multimodal porosity; surface-enhanced Raman spectroscopy (SERS); 3D-microprinting and artificial intelligence; digital designs and DLP



**Citation:** Jose, A.; Mathew, T.; Fernández-Navas, N.; Querebillo, C.J. Porous Inorganic Nanomaterials: Their Evolution towards Hierarchical Porous Nanostructures. *Micro* **2024**, *4*, 229–280. <https://doi.org/10.3390/micro4020016>

Academic Editor: Ajit Roy

Received: 1 January 2024

Revised: 4 April 2024

Accepted: 11 April 2024

Published: 18 April 2024



**Copyright:** © 2024 by the authors. Licensee MDPI, Basel, Switzerland. This article is an open access article distributed under the terms and conditions of the Creative Commons Attribution (CC BY) license (<https://creativecommons.org/licenses/by/4.0/>).

## 1. Introduction

The increasing modern technological requirements of enhanced catalytic efficiency, sensor sensitivity, device miniaturization, being lightweight, energy efficiency, multifunctionality, and sustainability, among others, have sculpted materials/device developments toward addressing these necessities. In this respect, porous materials and nanomaterials as separate fields have attracted great attention. They have become two intensively researched materials due to their potential to tackle these current technological demands for various applications [1–7], such as sensing and catalysis. Within their structures, porous materials have pores, channels, or voids, which can be of various shapes and sizes and can contribute to material properties such as increased specific surface area, improved adsorption and absorption, and better fluid permeation/transport. The porosity results in

unique properties, including afforded catalytic activity and nano-confinement in certain cases [8]. Porous materials can be found in naturally occurring and engineered forms [9], with the former having been widely used initially.

Similarly, nanomaterials draw interest due to their enhanced properties and exciting physics [5,9–11]. These materials have structures, features, and properties exhibited at the nanoscale, i.e., at dimensions typically in the range of 100 nm or less [9,10]. Compared to bulk properties, their unique properties in the nanoscale resulted in an explosion of nano-material development for different purposes. Specifically, in addition to naturally occurring ones, engineered nanomaterials have since played crucial roles in scientific, technological, and industrial settings.

Almost seemingly stemming from both advancements, in more recent years porous nanomaterials have emerged (Figure 1). Although materials with nanoscale pores are considered a subset of nanostructured materials [3,12], a new type of nanomaterials exhibits small pores within the nanoscale structures, which result in new properties and functionalities. Incorporating porosity into nanomaterials then presents exciting possibilities entailing further exploration of their physics and potential applications. Specifically focusing on porous inorganic nanomaterials and their hybrids, new materials have been developed, including porous metal nanostructures, porous oxide nanomaterials, porous carbon nanomaterials, nano-sized metal-organic frameworks (MOFs), and nano-zeolites [10,13–17]. These offer increased surface areas, enhancing mass transport and binding capacities, facilitating, for example, an efficient interaction between immobilized molecules and target species. Such enhancements in turn can improve performance in catalysis and sensing, extending their application to environmental monitoring, food safety, and medical diagnostics [15,18]. Moreover, the fascinating physicochemical properties exhibited by porous nanomaterials contribute to their versatility and potential for technological advancements.

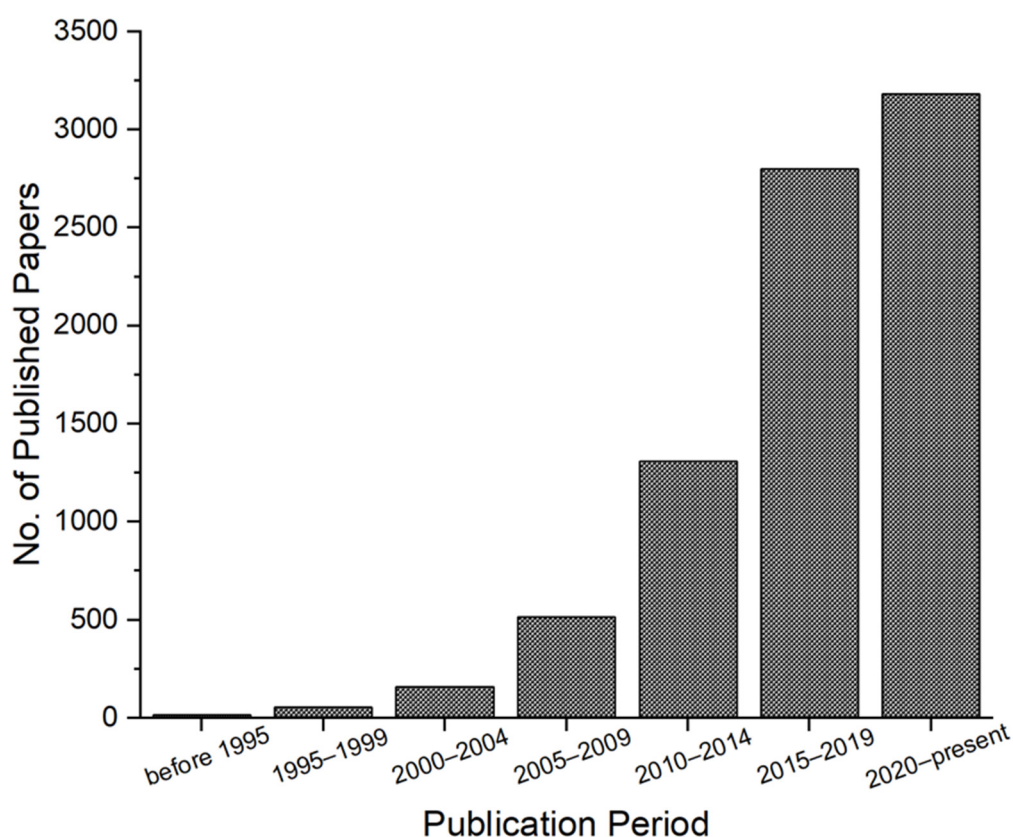


**Figure 1.** The emergence of porous nanomaterials or nanostructures. The rise of these nanomaterials is evident from the increasing number of published papers (search terms: “porous nanomaterial” OR “porous nanostructures”) over the years. Data obtained from Web of Science (8 December 2023).

It is therefore timely to look at the emergence of porous nanomaterials, specifically given catalytic, bio-, and energy applications, to further advance the development of this new type of nanomaterials. To compile this review, various references were consulted, including research articles and reviews from the Web of Science and the Internet in general. The focus is on recent publications that feature structures that exhibit both porosity and nano-size and/or multi-modes of pore sizes. The result is a review of the emergence of porous inorganic nanomaterials, focusing on said applications, towards the formation of a deemed desired architecture for modern applications—hierarchical structures. The need for hierarchical architecture has likely been one of the strongest drives toward the engineering of porous nanomaterials. This is unsurprising as interesting properties are further tapped with such architectures. For instance, nanostructured porous carbons can be used as photonic crystals when their pore arrangement follows such hierarchical architecture [15,19].

The primary focus of this review is to show how porous nanomaterials have developed towards the formation of hierarchical porous nanostructures. First, we give a brief overview of the description of porosity. Next, we introduce porous nanomaterials and their preparation techniques (templated vs. template-free approaches). Then, we present the bulk of the main body (“The Rise of Hierarchical Nanostructures”), which shows the evolution of porous nanomaterials towards hierarchical porous nanostructures for different composition types (mainly oxides and derivatives, metals, and carbon and derivatives) through different examples/studies. From these examples, specific synthetic methods applied to prepare each case of porous nanomaterial or their target applications will also be presented. For example, photonic properties and application to surface-enhanced Raman scattering (SERS) will be touched on in sections presenting porous silica, inverse opal, nanoporous plasmonic metals, and so on. Note that most applications and examples considered here are for open pore types. Hierarchical porous nanostructures can be attained by exhibiting multimodal porosity and/or as nanomaterials containing nanopores within their nanostructure [8,20–25]. This will be seen through different examples given in each subsection. As the review cannot cover everything, since other literature reviews focusing on different materials, aspects of porosity and porosity in nanomaterials, and technologies in the preparation of porous nanomaterials also exist, the readers will be referred to and encouraged to look at said reviews or research works along the course of the discussion [2,10,11,13,26–47]. The papers included here are focused on seminal works and more recent examples—especially those exhibiting both the porosity and nanomaterial aspect and/or multi-modal pore size, ultimately presenting the development of hierarchical porous nanomaterials. A section towards the end is dedicated to the interplay between technological advancements (digitalization, 3D microprinting, and artificial intelligence) and porous nanomaterial development. Finally, a summary with perspectives is given as a conclusion.

## 2. Description of Porosity

The field of porous materials, characterized by exceptional functional and structural properties, plays a crucial role in catalysis, sensing, drug delivery, and environmental applications. These materials, classified based on their pore size and network, exhibit unique properties owing to their enhanced surface area and reactivity with molecules or ions. The official terms set by the International Union of Pure and Applied Chemistry (IUPAC) to describe porous materials according to pore sizes are as follows: microporous (<2 nm), mesoporous (2–50 nm), and macroporous (>50 nm) materials [7,8,41,48,49]. Though unofficial, the term “nanoporous” has been widely used to refer to materials with pores of the size of a nanometer (or even lower) [7,41] to tens of nanometers [7] up to a maximum of 100 nm [13,41,48]. The term micropore can also be further subclassified as “super-micropore” (0.7–2 nm) and “ultra-micropore” (<0.7 nm) [41]. Figure 2a gives a schematic of the pore size scale and the corresponding terms used to describe them.

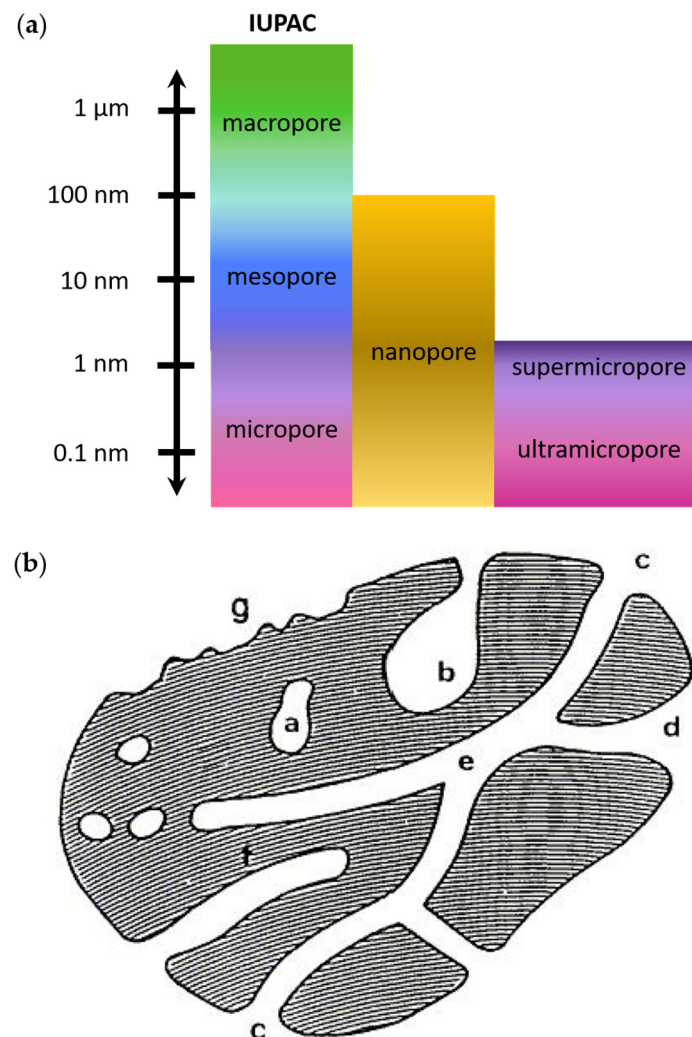


**Figure 2.** Description of pores according to size (a) and interaction with external environment (b). In (b), the pores are classified as follows: a—closed pores; b and f—dead-end pores; c, d, and g—through pores; e—open at two ends (through) pores. Figure in (a) is redrawn from refs. [7,41], whereas for (b) reprinted (adapted) with permission from [50]. Copyright 2007, Versita Warsaw. Published by De Gruyter Open Access. CC BY-NC-ND 3.0 license.

Pores are further categorized as open or closed, depending on their interaction with the environment (Figure 2b). Open porous structures, like those in sponges or foams, feature interconnected permeable pore networks, making them suitable for adsorption, catalysis, and sensing applications. They can be further subclassified as dead-end (open only at one end) or through pores (open at both ends). In contrast, closed porous structures have isolated pores, often impermeable or less permeable than open types, and their influence is often on the mechanical properties of solids such as for lightweight structural applications [50]. Moreover, based on the way the pores are organized within the structure, the porosity can also be classified as ordered or nonordered [51]. When the material has two or more kinds of pores, they are considered as “hierarchical porous structure material(s)” or “multimodal (hierarchical) porous” [8,20–22]. In hierarchical porosity, the level of pore formation can also be described as primary, secondary, or so [52].

### 3. Towards Engineering Porous Nanomaterials

One can think of porous nanomaterials as porous materials in the framework of nanomaterials, instead of the traditional (bulk) film. When the pores are found within

nanomaterials, the porous materials do not only exhibit unique properties attributed to their porosity but also from the nanoscale properties of the containing nanomaterial.

Nanomaterials are a class of materials having sizes in the range of 1 to 100 nm. The term “nano” comes from the Greek prefix referring to “dwarf”, or something very small ( $10^{-9}$  as the multiplying factor) [53–55]. Nanomaterials have been studied since ancient times, but the concept of nanotechnology has only been introduced in 1959 by Richard Feynman who proposed the idea of constructing molecular-level small machines [54,56]. More than a decade after Feynman’s concept lecture, Norio Taniguchi coined the term “nanotechnology” to refer to “the processing of separation, consolidation, and deformation of materials by one atom or one molecule” [54,57].

There is a surplus of methods for the synthesis of nanomaterials, which can be largely classified as bottom-up and top-down approaches. Top-down generally refers to the process of breaking down bulk materials into nanoscale particles, whereas the bottom-up approach involves constructing nanostructures or nanomaterials from the ground up, which for example can be done molecule-by-molecule (or atom-by-atom), i.e., via self-assembly [54]. Top-down techniques include lithography, mechanical milling or ball milling, laser ablation, sputtering, electron explosion arc discharge, and thermal decomposition whereas, techniques such as chemical synthesis, chemical vapor deposition (CVD), sol-gel, spinning, pyrolysis, and biological synthesis can be categorized under bottom-up approaches [54,55].

Due to their mitigated size, nanomaterials exhibit unique chemical, physical, electrical, magnetic and optical properties, which may differ from the bulk. Nanomaterials, therefore, also find a plethora of applications in various fields such as biomedicine, material science, engineering, industrial, and agriculture due to their compelling and innovative features [58].

Nanomaterials can be classified based on their structural configuration, origin, dimensionality, and, for the purposes of this review, the presence of pores and their sizes (as described in the previous section). In terms of structural configuration, they can be classified as carbon-based, organic, inorganic and composite nanomaterials. They can be divided into artificial and natural nanomaterials based on their origin [55]. Based on their dimensionality, nanomaterials can be categorized as zero-, one-, two-, or three-dimensional (0D, 1D, 2D, or 3D, respectively). Zero-dimensional nanomaterials include quantum dots and nanocrystals, whereas 1D includes nanotubes (NTs), nanowires (NWs), and nanorods; 2D includes nanosheets while arrays of NTs or nanospheres are considered 3D. A mix of these morphologies can also exist, adding to the intricacies of possible resulting properties and functionalities [11]. Finally, in terms of pore dimensions, nanomaterials can be classified as micro-, meso- and macroporous nanomaterials [55], which are described above. As nanomaterial dimensionality can tune different material properties, the presence of pores can then be considered by synthetic chemists and materials engineers as another means to control material properties.

### *3.1. Porous Nanomaterial Preparation Techniques*

Several methods have been reported in the literature for the preparation of porous nanomaterials [13,34,35,59–67]. To induce porosity, typical techniques for pore formation such as the templating method and dealloying can also be used. In templating method, organic or inorganic compounds are used as placeholders for the eventual void space desired in porous materials [13,35,59,61–67]. Here, the pore size and shape can be controlled [60]. On the other hand, dealloying is one of the most common methods used for the synthesis of open bicontinuous porous structures. In this case, one or several metal constituents are selectively etched from an alloy to generate porosity, in the process increasing surface roughness. The pore size distribution, pore volume, and pore interconnectivity across the dealloyed structures may be tuned by varying the bulk alloy properties and the etching conditions to enable materials with porosity levels at the nanoscale (micro-/meso-/nanoporous) and micron scale (macroporous), as presented in the review of McCue

et al. [34]. Interested readers are referred to the said review, especially for curiosities on the fundamental principles regarding the dealloying mechanism.

To generalize, one can consider subdividing these techniques as templated vs. template-free pathways (exemplary techniques shown in Figure 3), though in terms of microfabrication techniques, physical processes vs. wet synthetic processes can also be considered. Using a templated or template-free approach influences the characteristics of the pores formed within the nanomaterials. As mentioned above, in a templated approach, a pre-existing template guides the pore formation in the material, leading to a more controlled and uniform pore structure and distribution. Therefore, the technique is apt for the formation of ordered structures, and the precise control of pore parameters results in higher reproducibility of pore characteristics. However, there are possible limitations considering material-template compatibility in this technique, and it entails post-synthesis template removal [13].

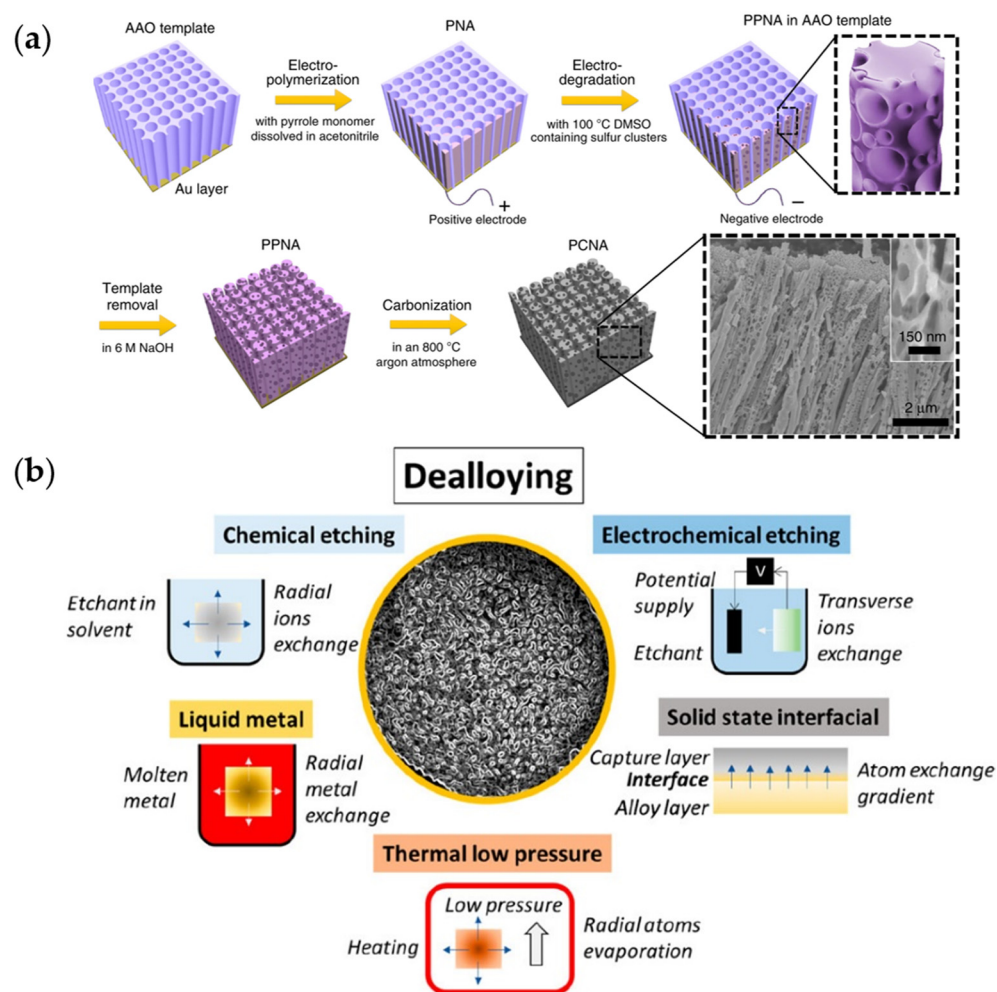


**Figure 3.** Exemplary techniques showing templated and template-free pore formation: (a) multi-step template-assisted electropolymerization to fabricate porous carbon nanowire array (PCNA) using anodized aluminum oxide (AAO) templates. After electropolymerization, the polypyrrole nanowire array (PNA) is electrically degraded into a porous pyrrole nanowire array (PPNA). Carbonization then transforms it into PCNA. Reprinted (adapted) with permission from [68]. Copyright 2020, The Author(s). Published by Springer Nature. CC BY 4.0 license; (b) different possible dealloying pathways. Reprinted (adapted) with permission from Scandura, G.; Kumari, P.; Palmisano, G.; Karanikolos, G.N.; Orwa, J.; Dumée, L.F. Nanoporous Dealloyed Metal Materials Processing and Applications—A Review. *Ind. Eng. Chem. Res.* 2023, 62, 1736–1763, doi:10.1021/acs.iecr.2c03952. Copyright 2023 American Chemical Society [14].

On the other hand, in a template-free approach, the material itself, without the aid of a pre-existing template, undergoes a process that results in the creation of pores. Therefore, this approach is often more straightforward as it does not require additional steps (such as template removal) and can lead to faster fabrication time. However, in the absence of a template, less control over pore characteristics and distribution can be achieved, often resulting in a more random or irregular pore distribution [69]. This may be unsuitable in certain applications. Therefore, the choice of whether to use a templated or template-free approach is mostly dependent on the targeted properties and applications of the end product [13]. Du et al. reviewed different synthesis strategies for producing porous nanostructures and their applications to electrocatalysis [8].

The specific surface area values that can be obtained, whether obtained by a templated or template-free approach, generally depend on the material type, specific material characteristics, and the specific methods/processes employed. For example, in the templated approach, surfactants or polymers can give mesoporous materials with relatively high surface areas (i.e., a few to several hundreds of square meters per gram,  $\text{m}^2\text{g}^{-1}$ ), whereas ordered mesoporous silica can achieve even higher specific surface areas (500–1000  $\text{m}^2\text{g}^{-1}$  or higher). On the other hand, template-free approaches have also been reported to give specific surface areas that are similar to those obtainable with ordered mesoporous silica. This includes the activation of carbonaceous materials (500–3000  $\text{m}^2\text{g}^{-1}$  or more) and the production of aerogels ( $>1000 \text{m}^2\text{g}^{-1}$ ) [70,71].

### 3.1.1. Template-Assisted Pore Formation

Different templating methods exist, and their names are based on the type of template used. Therefore, the literature includes templating methods such as soft templating, colloidal crystal templating, hard templating, and multi-templating.

The soft templating method, for example, has been widely used in the formation of porous oxides. As a relatively straightforward strategy, this method includes the use of soft organics such as amphiphilic ionic or non-ionic surfactants and/or polymers, which have been used to produce porous amorphous or semi-crystalline silica, zeolites and metal oxides [52,61,72,73]. Soft templating therefore includes those that are based on sol-gel preparation, direct self-assembly, evaporation-induced self-assembly (EISA), and spray drying [13,59,61–65]. For example, mesoporous silica nanoparticles (NPs) with diameters between 50 and 300 nm have been produced using the sol-gel method, in which surfactants or polymers serve as templates [61]. This includes using quaternary alkylammonium surfactants (e.g., cetyltrimethylammonium bromide, CTAB) under highly basic conditions or triblock copolymers, like Pluronic F127, in strongly acidic conditions [74]. Micellar objects have been used to prepare porous materials with a maximum pore size of up to 10 nm, whereas beyond this up to ~300 nm, nano-emulsion has been developed to form new templates [23]. Emulsion techniques can be used to produce different ranges of pore sizes, including micro- and macro-types [75].

Ordered porous metal oxide synthesis typically involves aqueous solution synthesis and EISA routes, i.e., self-assembly of surfactant and metal precursors to form the hybrid of metal oxides and polymers, followed by template removal by solvent extraction and/or thermal degradation. In modern EISA methods, chelating agents/acids (e.g., citric acid, acetic acid) serve as stabilizing agents [76,77]. Soft templating techniques to form porous metal oxides in non-aqueous media have also been reported [76]. Early soft templating attempts have often failed to produce ordered crystalline porous structures; however, modern research has paved the way for the preparation of robust nanoporous crystalline structures including MOFs [78].

Due to the often very small pore sizes (i.e., micropores) produced with the synthesis of earlier MOFs, strategies to increase the pore size have been developed and many of these resort to the soft-templating approach, producing so-called hierarchically porous MOFs (HPMOFs). HPMOFs enable rapid mass transport and isolation of different sizes of guest molecules. Such strategies have evolved towards rational design to overcome

incompatibilities of the surfactant templates with the MOF precursor by enhancing their interaction. This has been achieved by the group of Gu by introducing long-chain monocarboxylic acid synthesis and amphoteric surfactants in the aqueous phase to produce irregular and ordered mesoporous (OM) HPMOFs, respectively [79]. They then achieved mesopores to macropores using salting-in species-induced self-assembly strategies coupled with copolymer templating.

In addition to coupling different templating strategies, other processes can also be combined with templates to synthesize porous material. This includes modern mechanochemical procedures [80] and electrochemical approaches [81]. The latter comprises of methods such as electrochemically controlled assembly of soft templates and electrosynthesis around soft templates. The first one includes potential-controlled surfactant self-assembly [82], whereas an example under the second one is the electrochemical deposition of copper using polymeric micelle assembled templates [83]. A combination of both can also be incorporated in a method that fully utilizes electrochemical effect not only to influence the template assembly but also to induce the electrodeposition. For example, this concept can be seen in electrochemical surfactant templating [81,84].

Closely related to electrochemically controlled assembly of self-templates, only performed indirectly, is the electro-assisted self-assembly (EASA). In EASA, surfactants can be used as pore templates, whereas the applied potential can be used to control the local pH, which can then result in the formation of surfactant hemimicelles that could then orient/guide structural growth by self-assembly [81,85].

In colloidal-crystal templating, the space or void between closely packed uniform spheres is filled with liquid (metal) precursors and treated subsequently for solidification into the target material. In the case of porous metal oxide formation, a 3D-arranged porous structure is then obtained by calcination, which also removes the template [35,76]. The colloidal-crystal templating method is versatile and could be used to produce metal oxides of different metals, such as titanium [86].

Hard templating, on the other hand, uses harder materials—often inorganic—as templates, such as silica, anodic aluminum oxide (AAO), inorganic salts, organometallic salts, and carbon molds [13,35,59,66,67] (Figure 3a), which serve as negative replica for the resulting structure [81]. For example, hard templating can also be used for porous metal oxide preparation [35], which, unlike soft templates, mainly forms crystalline ones. As such, sometimes hard templating is termed nanocasting. Meanwhile, a comprehensive and updated review on templated porous carbons and precursors is given by Pavlenko et al. [13].

Multi-templating involves using more than one template (termed dual-templating for two templates), which for instance can involve soft and hard templates, as well as templates that introduce different pore sizes [13]. This can be done as a one-step—i.e., templates are introduced simultaneously—or as a multi-step [74,87–91] approach. In some examples, a template is pre-formed using a second template into a desired pattern [21], which is then used as a scaffold for the templated synthesis of the desired material. In such cases, the term two-(or multi-)step templating is used, such as in the work of Liu et al. [92]. This approach can be done to overcome the limitations of using single-templating methods [59].

In some cases, the precursor templates already contain porosity (such as MOFs, zeolites, silica, and perovskites), and the applied technique induces the chemical transformation [13,93,94]. These precursor templates can also be considered self-templating, and their use blurs the line between a templated and template-free approach (see the next subsection for further discussion on self-templating). However, here, precursors containing porosity such as MOFs and zeolites (or their evolved form), which are carried over into the final product, will be considered precursor templates and are therefore classified under the templated approach. This type of technique has been explored, additionally to induce doping of the material, aside from the (hierarchical) pore formation [13].

Furthermore, techniques that can be used to form porous (nano)materials requiring masks or templates such as lithography [21] can be categorized as soft or hard templating, depending on the templates used.

### 3.1.2. Template-Free Pathways to Form Porous Materials

Other techniques that do not use templates to form porous (nano)materials include hydrothermal/solvothermal/thermal techniques, and other physical, chemical, and electrochemical techniques [16,65,93,95–101]. The last ones include mechanochemical techniques, electrospinning, vapor deposition, acidification, plasma treatment, dynamic bubble method, self-templating, hydrothermal hot-press, metal encapsulation, dealloying, anodization, electrodeposition, other electrochemical techniques, and 3D-microprinting [34,97–105]. Some of them will be described here.

Mechanochemical preparations, in particular, are promising for the large-scale production of porous metal oxides for different applications, such as battery technology, adsorption, catalysis, and medicine [106–109]. For instance, the nanoporous tin oxide was obtained via a simple manual grinding of ammonium carbonate, stannous chloride, and glucose, followed by calcination at 600 °C, and used as an advanced sorbent material [109].

The dynamic bubble template method is considered template-free as the use of a pre-formed template or scaffold is avoided. Instead, gas bubbles—such as hydrogen—which serve as pore/void templates are generated during the synthesis process. The technique is initially used for more active metals according to the volcano curve, in terms of activity towards the water-splitting reaction (specifically, the cathodic portion for dynamic hydrogen bubble templating, DHBT) [110].

Several metals such as Zn, Cu, Sn, Ag and Au can be employed to produce multimodal (nano)porous foams via the DHBT technique. Metals can be classified into three distinct groups based on their exchange current density and melting point. Metals having high exchange current densities and low melting points are termed “normal” metals (e.g., Cd, Zn, Sn, Ag), whereas “intermediate” metals are those that have intermediate exchange current density and melting points (e.g., Au, Cu, and Ag). The “inert” metals are those that have low exchange current density and high melting points (e.g., Fe, Ni, Co, Pt, Cr, Mn). Chung et al. postulated that only metals categorized as “normal” or “intermediate” can be used in the electrodeposition of multimodal nanoporous foams [111].

A general flow of how the DHBT process works is as follows: for generation, as an example of nanoporous gold (Np-Au) via the DHBT method, a low concentration of chloroauric acid (~0.1 M) with a quantity of ammonium can be used. This comprises the electrolyte in a three-electrode cell, with a Pt or Ti working electrode and typically a Pt counter electrode. A potential within the H<sub>2</sub> evolution regime, normally between −4 V and −8 V, is then applied to the working electrode. The evolution of H<sub>2</sub> and the reduction of Au ions occur simultaneously at the electrode surface. Continuous gas nucleation, coalescence, and desorption at the electrode surface result in a self-supporting Au thin film composed of micrometer pores with nanoporous features [42].

Self-templating or self-generated templating approach somehow blurs the line between the distinction of being a templated technique or a template-free one. The latter entails that the precursor material itself (not necessarily porous at the start) serves both as the source of the material and the pore-forming agent [13,59]. The precursor material can be naturally occurring or synthetic. An example is a substance that undergoes direct pyrolysis to form a carbon composite from which the second phase is removed to form porous carbon [13]. Since no additional agent was added as an external template or scaffold, here, this is considered template-free.

Dealloying is a convenient synthetic procedure to produce bicontinuous open nanoporous metallic structures based on selective corrosion processes, resulting in a large specific surface area that can also then serve as active reaction/process sites [34,102–105]. Facile dealloying techniques include chemical and electrochemical ones. In these cases, the porous material is produced from an alloy that can be fabricated, for example, by casting, co-sputtering or

deposition onto a substrate [112]. The alloy is then immersed in an electrolyte to induce the selective dissolution of the least noble element(s) (e.g., Zn, Cu, and Ag for porous gold) from the alloy. This leaves behind the most noble element with a porous structure and generates, in the process, surface roughness [113]. Figure 3b shows the general dealloying pathways available. For example, chemical dealloying takes place by immersion of the alloy material in acids (such as sulfuric, hydrochloric, or hydrofluoric acid), bases (such as sodium hydroxide), or solution/electrolyte that is corrosive to the material. On the other hand, in electrochemical dealloying, an electric field is applied to induce selective etching. The less noble atoms having lower corrosion potential will be removed first, resulting in the formation of porous structures [14].

Electrochemical dealloying results in better control of the pore dimensions and uniformity over the corrosion process [42]. Therefore, the material's composition and porous structure can be fine-tuned, although challenges related to thermodynamics and kinetics must be addressed through innovative strategies [114]. Electrolyte composition is also a crucial factor in electrochemical dealloying, influencing the reconstruction and diffusion processes [115]. The electrolyte can also be used to control the shape of ligaments and pores. For example, in preparation of Np-Au, smaller pores are expected upon thiol addition [116,117], whereas bimodal pore sizes can be achieved with halide salt addition [115]. Dealloying times [118], temperatures [119–121], or the addition of other elements and electrolyte additives [116,117] can be explored to tailor the characteristics of the porous material to suit various applications.

Other electrochemical approaches include combining alloying by electrodeposition, and then dealloying electrochemically. For example, recent electrochemical techniques have allowed for the creation of nearly pure Np-Au from AuCu (only 3% Cu remaining) through carefully designed deposition and dealloying processes [122]. The preformation of alloys can also be effectively removed by doing instead an in situ electrochemical alloying/dealloying process using pulsed electrochemical techniques [123], or cyclic voltammetry. In cyclic voltammetry, the oxidation-reduction potential of the systems can be studied. The cathodic sweep reduces metal ions in solution at the working electrode to form an alloy. Then, the anodic sweep oxidizes the alloyed metal and removes it from the working electrode, which leaves a pitted surface behind. By continuing this alloying-dealloying process, the pitting deepens and widens, creating a porous structure [42]. Square wave potential pulse voltammetry can also be implemented to produce porous materials [124].

Another electrochemical technique for the formation of porous materials is anodization. This technique is an electrochemical oxidation process, which can be done in potentiostatic or galvanostatic modes. Sulka gives an updated introduction to metal anodization as a book chapter [125]. Readers are encouraged to take a look at it when interested.

Diffusion of vacancies can also be taken advantage of to form voids resulting in porous materials. The so-called Kirkendall effect, typically used in metals and their oxides to form hollow nanoparticles, can result in void formation at the interface of two different metals. In such a case, the difference in the diffusion rate of different phases results in a simultaneous vacancy diffusion associated with the diffusion of the phases. This results in void (or gap) formation in the interface of the phase near the component with a faster diffusion rate. For details and examples on the said strategy, readers are encouraged to look at the review of Du et al. [8].

A recent paper features high-precision 3D microprinting applicable to a vast variety of porous inorganic materials by solidification of inorganic nanocrystals [44]. This was possible by immediately controlling the dispersibility and subsequently chemically linking the nanocrystal surfaces in a nonsolvent linker bath to create multibranching gel networks. This work specifically presents a hierarchical 3D-microprinted porous microstructure of Au nanocrystals made of extremely thin wires (5–10 nm) with multi-branching features, interconnectivity, and a wide range of resulting pore sizes (few nanometers to hundreds of nanometers) formed in the process. Readers are encouraged to read this cutting-edge work.

#### 4. The Rise of Hierarchical Nanostructures

The term “hierarchy” has Greek roots and means “rule of a high priest”, fitting well its current definition which describes ranking [23]. Hierarchical nanostructures refer to materials or systems that exhibit a multi-level organization of nano-sized building blocks, creating a complex and ordered architecture. These structures often feature variations in size, shape, and composition at different length scales. The hierarchical arrangement imparts unique properties and functionalities to the materials, making them valuable in various fields [126–128].

Delving into the literature on nanomaterials, one will see the significance of hierarchy in different applications and performance, affected by structure and morphology, including porosity [23]. Although porous materials have higher surface area than unmodified ones, they may at times exhibit an adsorbed molecule packing density that is smaller or just comparable to unmodified metallic surfaces [129,130]. This occurs when not all of the surface area is accessible to adsorbing species due to restricted mass transport. The introduction of hierarchy into the porous structure morphology could therefore benefit the “porous function” of the material in different ways, including the following [51]:

- An increased surface area and pore volume, enabling species to interact and functionalize pore walls;
- Providing more accessible mass transport pathways within the structure framework and allowing more molecules to flow within or out of the porous matrices;
- A more effective diffusion and possibly simultaneous loading of target/adsorbing molecules.

Porous hierarchy refers to having two or more modes (i.e., bimodal or multimodal) of distribution of pore sizes at different scales (micro-, meso-, macropores, etc., as described above) in a single body. Such structure could achieve large specific surface area and fast mass transport for high efficiency of reactions and exchanges. However, such modalities are only hierarchical when the overall pore system shows a well-ranked, interconnected pore system and when regularity in pore structure is displayed at each level. Thus, hierarchical porous materials should exhibit (i) multiple levels, (ii) interconnectivity, and (iii) regularity [24].

In addition to porous hierarchies, other types of hierarchies also exist in natural materials. These include structural hierarchy, morphological hierarchy, and compositional hierarchy. In the structural hierarchy, a strict and precise repetitive combination of structural elements could result in a very stable construction, whereas morphological hierarchy refers to having multiple levels of microstructural units of specific morphologies useful for a concerted coupling of their functions. In the compositional hierarchy, smart assembly of units—such as objects and chemical compositions—could result in system formation exhibiting both systematic and local variables [24].

Hierarchical nanostructures are also often integrated with well-ordered nano subunits with 0D, 1D, 2D, or 3D architectures. By fabricating materials that exhibit porous hierarchy in different orders, natural systems with different functionalities can be mimicked. Therefore, the relation between the architectures and their functionalities is also investigated to further design and develop advanced hierarchical porous morphologies [126–128].

Though the strict definition of porous hierarchy involves the presence of bimodal to multimodal porosity in materials [25], another way to achieve hierarchical structures containing porosity would be to combine porosity with nanostructural design. Both strategies involve increasing the readily available surface area for adsorbing species in catalytic, sensing, energy storage, and bio-related applications [126–128], ultimately improving the overall performance of porous materials. Both approaches are also being utilized and developed to enhance the diffusivity of the electrolyte and dissolved species. In this section, examples of different porous nanomaterials will be given, with emphasis on their development into hierarchical types.

#### 4.1. Porous Oxide Nanostructures and Derivatives

Among many porous materials, porous oxides, especially transition metal-based ones, evoke great interest due to their unique properties and potential (e.g., for energy storage and conversion [109]). Initially, close-packed mesoporous ones were mainly silicates and aluminosilicate-based, which to form uniform pore sizes can be achieved through different methods including wet chemistry (e.g., sol-gel and micelle-assisted synthesis). This is likely due to their stability and resistance to reactions and transitions that can compromise their structural integrity [35]. Nevertheless, from thereon, non-silicate-based oxides were pursued with the first stable mesoporous non-silicate oxide preparation using wet chemistry reported by Ying et al. in 1995. They prepared mesoporous TiO<sub>2</sub> by sol-gel technique using a combination of the alkoxide and surfactant, resulting in an average pore size of 30–40 nm [131]. With the desire to produce non-silicates, newer techniques were developed to also circumvent limitations such as the use of aqueous solutions, which are not suitable for the fabrication of some materials (such as non-silicate oxides). Gu and Shüth gave a comprehensive review of mesoporous non-silicate (metal) oxides, their preparation, and control of their properties [35]. There, they tried to give prototypes for each method, though they noted that a general facile synthesis of mesoporous metal oxides still needs to be developed and the difficulty of finding one is likely due to, for example, the sensitivity of composition and phases to preparation conditions.

While different techniques to prepare porous metal oxides were being developed, the formation of hierarchical structures was also becoming a focus of interest. Such development has been observed for porous metal oxide, for which it was observed that the hierarchical structure of these porous oxide materials can be formed. Some of the common metal oxide nanomorphology by design have pores in them. This includes NTs and nanosheets, which contain nanopores with their cylindrical or sheet structures, respectively. It seems therefore that the self-organization of porous hierarchical structures naturally occurs, especially in certain situations such as in the presence of high electromagnetic fields, as these are observed with electrochemical (anodic) preparation, say of TiO<sub>2</sub> [132–137] or Al<sub>2</sub>O<sub>3</sub> [138–140], and even of mixed metal (alloy) oxides [141,142].

##### 4.1.1. Porous Metal Oxides, Phosphides, Nitrides and Other Derivatives

Many of the metal oxide nanomaterials are easily synthesized as porous nanomaterials. As mentioned, many of the common metal oxide nanomorphologies have pores in them (e.g., nanosheets and NTs). Therefore, much of the advancements in this field are on the formation of these porous morphologies, hierarchical structuring, and their composites. Recently, Querebillo made a review on the different TiO<sub>2</sub> and Ti-based oxide nanomorphologies, which include many porous ones, and their (photo)catalytic and bio applications [11]. The review showcases not only the influence of morphology/structure, such as porosity, on the photocatalytic activity of TiO<sub>2</sub> [11,96] but also gives a discussion on the (photo)catalytic bio-applications, such as photocatalytic disinfection against critical pathogens (e.g., *E. coli*, *S. aureus*, human coronaviruses, and others) [11,143]. The readers are encouraged to refer to the said review for further interest.

Since mesoporous TiO<sub>2</sub> is a well-known catalyst, catalyst support, and material for dye-sensitized solar cells (DSSCs), many studies have been done on porous titania and porous TiO<sub>2</sub> nanomaterials [11,65,95,96,144]. Several studies on metal oxide (porous) nanomaterials, for the same reason, were explored for catalysis and DSSCs (i.e., to substitute TiO<sub>2</sub>, to explore for enhancement, and/or to form composites with titania) [11,145]. For example, the use of ZnO in DSSCs is aimed at improving electron transport. Li et al., produced a nanoporous ZnO nanosheet for high-performance DSSC [145]. The benefit of such hierarchical porous nanomorphological structure does not only include attributes due to its porosity and nano-thin “thickness”, i.e., large surface area, enhanced dye adsorption, and efficient electrolyte diffusion, but also due to the hierarchical configuration formed: generation of aggregation-induced light scattering center (enhancing light absorption and propagation in the process), improved transport channel of injected electrons due to adjacent spherical

structures, and faster electrolyte diffusion due to large pores formed by the assembly. This resulted in a higher light conversion efficiency compared to non-hierarchically assembled counterparts. On the other hand, an earlier work on DSSC made with hierarchically assembled TiO<sub>2</sub> nanosheets still reported a higher energy conversion efficiency [95]. Nevertheless, in both cases, the porosity in the nanosheets (instead of mesoporosity via spherical aggregates) should minimize any effect due to the grain interfaces.

Hierarchical composites of porous TiO<sub>2</sub> have also been developed for DSSCs using double-shell nanostructures made of inner tin (IV) oxide hollow spheres and outer porous titania nanosheets [65]. The multiple-shelled hollow spheres resulted in an overall high reflectivity due to multiple reflections and scattering between the shells. These were then uniformly distributed in a mesoporous titania nanosheet matrix, giving an overall excellent solid-state DSSC performance that was reported.

Other porous metal oxides, such as NiO, are also attractive catalysts. The development of porous mixed oxide nanocomposites is also gaining traction, especially for catalysis [146]. Using multi-metal lends several advantages that cannot be obtained with the use of single metal. In fact, in the work of Pang et al., though the oxide is primarily NiO, the presence of Mo (likely within the oxides) stabilizes the porous oxide [102]. In catalysis, multi-metal hybridization results in better catalytic performance as adding foreign metals can be used to adjust the catalyst's electronic structure and optimize the active sites' energy for adsorption [146]. The resulting use of composites, for example, can then improve the charge transfer between the catalyst and the reactant by creating new electronic states. Such is the case with TiO<sub>2</sub> and ZrO<sub>2</sub>, which are both mediocre hydrogen evolution reaction (HER) catalysts but display improved performance as a composite. This micro-/mesoporous composite was then reduced to improve its conductivity by inducing semi-metallic properties and producing oxygen vacancies. This results in a highly stable catalyst, with increased HER current density at  $-0.6$  V, and a small overpotential of  $\sim 160$  mV [147]. Another example is Ni-Fe oxides and hydroxides, which are being considered for alkaline water-splitting. Figure 4a illustrates the water-splitting process and related reactions (HER and OER). Additionally, ORR, which takes place in fuel cells, is also shown. To obtain an ordered porous structure, Kumar et al. produced porous nanocubic Ni-Fe oxide from a mesoporous MOF precursor, achieving  $10 \text{ mA} \cdot \text{cm}^{-2}$  for water splitting at a cell voltage of  $1.67$  V and in an alkaline environment with reasonable stability and outperforming the electrocatalytic activity of spherical counterparts [93] (Figure 4b). There, the presence of  $\alpha$ -/ $\gamma$ -Fe<sub>2</sub>O<sub>3</sub> phases not only serves as efficient current collectors but also provides efficient electron-transfer paths, which effectively lowers the OER/HER overpotentials, and suppresses further oxidation of Ni<sup>2+</sup>. The Ni<sup>2+</sup> and Fe<sup>3+</sup> serve as the active site and electrode kinetics enhancer, respectively.

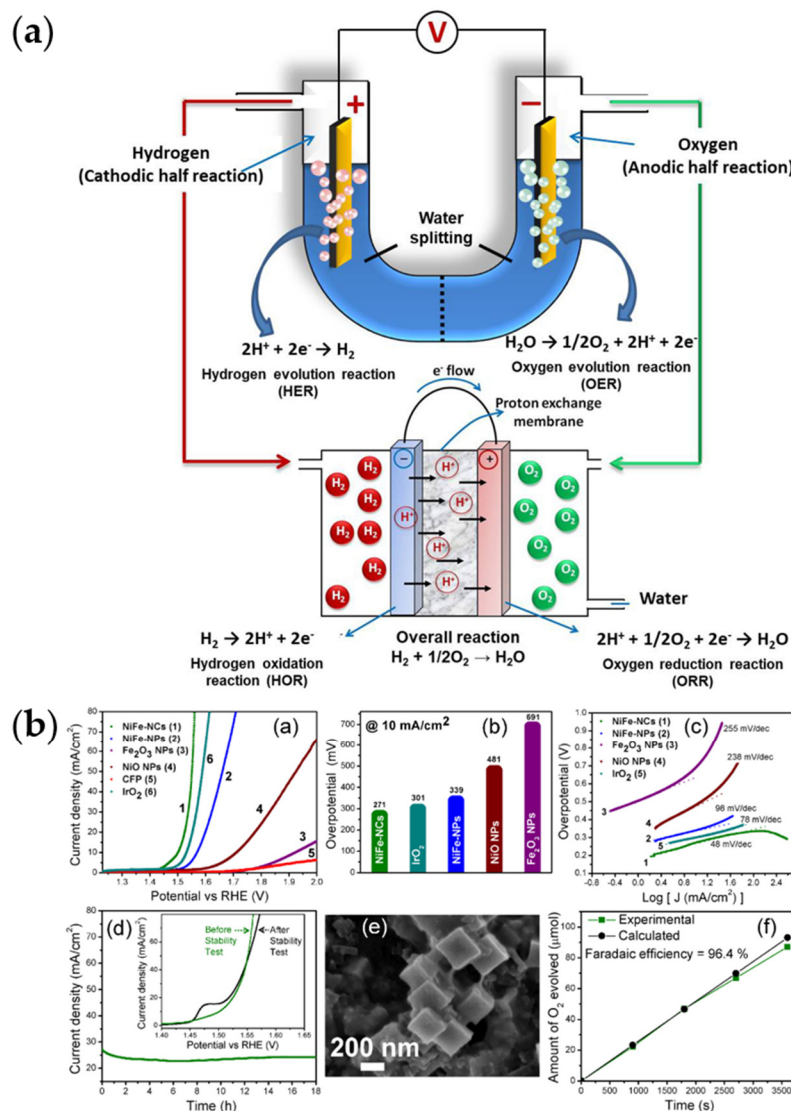


**Figure 4.** Porous metal oxide nanomaterials and common electrocatalytic reactions: (a) an illustration of the relevant reactions (hydrogen evolution reaction or HER, oxygen evolution reaction or OER, and oxygen reduction reaction or ORR) in energy conversion and storage, which are currently some of the most significant applications of porous nanomaterials. The first two reactions (HER and OER) occur in water hydrolysis, whereas ORR takes place in fuel cells (energy storage). Reprinted (adapted) with permission from Vij, V.; Sultan, S.; Harzandi, A.M.; Meena, A.; Tiwari, J.N.; Lee, W.G.; Yoon, T.; Kim, K.S. Nickel-based electrocatalysts for energy-related applications: oxygen reduction, oxygen evolution, and hydrogen evolution reactions. *ACS Catal.* 2017, 7, 7196–7225, doi:10.1021/acscatal.7b01800. Copyright 2017 American Chemical Society [148]; (b) porous NiFe oxide-based nanomaterials as bifunctional catalyst for electrochemical HER/OER. (a) LSV polarization curves for OER and (b) the required overpotentials to achieve  $10 \text{ mA cm}^{-2}$ . (c) Tafel plots with the corresponding Tafel slopes for the OER process. (d) Chronoamperometric durability test at a constant overpotential of 305 mV. The inset shows the LSV curves before and after the durability test. (e) FESEM image of NiFe-NCs after the OER durability test. (f) Faradaic efficiency measurement of NiFe-NCs showing the theoretically calculated and experimentally measured  $\text{O}_2$  gas with time at 0.62 V vs. Ag/AgCl. Reprinted (adapted) with permission from Kumar, A.; Bhattacharyya, S. Porous NiFe-Oxide Nanocubes as Bifunctional Electrocatalysts for Efficient Water-Splitting. *ACS Appl. Mater. Interfaces* 2017, 9, 41906–41915, doi:10.1021/acsaami.7b14096. Copyright 2017 American Chemical Society [93].

Not surprisingly, porous iron oxide nanostructures themselves are also popular metal oxides. OM iron oxides of different oxidation states and structures can be prepared by several methods such as soft [149] and hard templating [150]. Smarsly and his team [149] reported the synthesis of crack-free mesoporous  $\alpha$ -Fe<sub>2</sub>O<sub>3</sub> and  $\alpha$ -FeOOH thin films, using the EISA method with diblock copolymer poly(isobutylene)-blockpoly(ethylene oxide) (PIB-b-PEO) as a template. Jiao et al. [150] synthesized OM Fe<sub>3</sub>O<sub>4</sub> with crystalline walls for the first time by reducing OM  $\alpha$ -Fe<sub>2</sub>O<sub>3</sub> (corundum structure) to Fe<sub>3</sub>O<sub>4</sub> spinel and then to  $\gamma$ -Fe<sub>2</sub>O<sub>3</sub> by oxidation. Porous iron oxides have various applications, including anticancer drug carrier [151], potential electrode for lithium-ion batteries [152], and photocatalysts (especially, haematite ( $\alpha$ -Fe<sub>2</sub>O<sub>3</sub>)) [153].

Perovskites have also been used as a source of hierarchical porous structures. Xu et al. formed hierarchical porous  $\varepsilon$ -MnO<sub>2</sub> from a manganite perovskite (LaMnO<sub>3.15</sub>) using a template-free mineral acid etching process [94] to produce catalysts for low-temperature formaldehyde oxidation. The perovskites themselves are also porous metal oxides that also find application as catalysts [154]. Due to the prevalence of perovskites in solar cells, it is not surprising that hierarchically (nano-,meso-)porous perovskites have also been developed for this purpose [25].

Porous perovskite oxides (ABO<sub>3</sub>) have also been used in fuel cells, batteries, and supercapacitors [37,101,155–157]. A hierarchical meso-/microporous La<sub>0.5</sub>Sr<sub>0.5</sub>CoO<sub>3-x</sub> perovskite NT was developed for Li-O<sub>2</sub> batteries using an electrospinning-post-annealing approach [101]. The hierarchical porous structure complements the high catalytic activity resulting in batteries with good rate capacity and excellent stability (up to 50 cycles at a current density of 0.1 mA cm<sup>-2</sup>; upper limit capacity ~500 mAh g<sup>-1</sup>). Li et al. used a sol-gel method to form 2D LaNiO<sub>3</sub> perovskite oxide nanosheets (50 nm thick) with 10–50 nm pores [157]. In the micron-scale, these nanosheets form an open-porous honeycomb-like structure further adding to the hierarchical architecture, increasing the surface area and pore volume and achieving a specific capacitance of 139.2 mAh g<sup>-1</sup> at a current density of 1.0 A g<sup>-1</sup>, with excellent stability and good rate capability. When combined with graphene in an asymmetric capacitor device, a high energy density of 65.8 Wh kg<sup>-1</sup> at a power density of 1.8 kW kg<sup>-1</sup> and 92.4% retention after 10,000 cycles can be achieved. Such nanosheets can also form into more intricate structures. Hussain et al. also used the sol-gel route and fabricated hierarchical mesoporous structures of LaCrO<sub>3</sub> perovskite oxides comprising micrometer-sized flowers made of nanosheets (10–15 nm thick) with pores of <20 nm size [156]. With a carbon cloth as a current collector, a maximum capacitance of 1268 F/g at 2 A/g was achieved, also retaining an excellent cyclic ability of 91.5% after a charge–discharge of 5000 cycles. An up-to-date review by Yu et al. also presents advances in this field, including porous NPs, porous hollow nanospheres, porous NTs, and porous nanofibers, and the influence of the porous structure and morphology on the catalytic performance [37].

The push for sustainable and more cost-effective sourcing also resulted in these emergent materials being developed with certain metals reduced in amounts or replaced. Due to the vast usage of cobalt in batteries, cobalt-free battery materials are also being developed. Jiang and co-workers developed cobalt-free 3-D hierarchically porous ceramic (SrNb<sub>0.1</sub>Fe<sub>0.9</sub>O<sub>3- $\delta$</sub> ) electrodes, reaching a target area specific resistance of 0.15  $\Omega$  cm<sup>2</sup> at 600 °C and able to generate power as a solid-oxide fuel cell (SOFC) cathode below that temperature [158]. This was possible due to their enhanced oxygen reduction reaction (ORR) activity brought about by their large active area and optimized gas transport pathways. Another cobalt-free perovskite for the rechargeable Li-O<sub>2</sub> battery was developed by Zhang et al. by focusing on catalysts for the oxygen evolution reaction (OER) [155]. This comprises porous LaNiO<sub>3</sub> nanocubes, which were then used to fabricate batteries with reduced overpotential (3.40 V) and excellent charging capabilities.

A nanocomposite of MOFs and perovskites (CsPbX<sub>3</sub>@MOF) has also been reported wherein the MOF serves as a template and encapsulation host, confining and growing monodispersed metal-halide perovskites in situ [159]. This prevents the perovskites from

aggregating and interacting with the external environment. The hierarchical porosity of the MOFs enabled perovskite precursor impregnation in one step and allowed reactants to easily diffuse, resulting in high-loading uniform perovskite distribution within. This enabled the fabrication of light-emitting nanocomposites, which can be tuned to green or red depending on the halide used.

Along with the advancement of porous metal oxides, alternatives such as chalcogenides, phosphides, carbides, nitrides, and so on have also been explored for catalysis [100]. Porous mixed metal oxide hierarchical nanostructures, though effective water-splitting catalysts, can be made more effective by converting them to phosphides since P can act as a base and trap protons for the HER part, whereas the peroxide intermediate-formation induced facilitates OER. Such emerging catalysts can be prepared through porous metallic or metallic oxide precursors. Hu et al. presented a template-assisted strategy forming Ni-Co precursor 2D nanosheets and  $\text{Ag}_2\text{WO}_4$  anisotropic cuboids [160]. Then, the cuboids were selectively removed, and the Ni-Co were oxidized and subsequently phosphorated by heating, etching, and phosphorylation. The end result is open porous hierarchical Ni-Co-P hollow nano bricks made from nanosheets, which exhibit exposed active sites and electrolyte permeation, facilitating electrochemical reactions.

Porous transition-metal nitrides also present attractive traits such as excellent corrosion behavior, high electrical conduction, high melting point, stability, and superior mechanical strength. The addition of N to transition metal modifies the d-band of the metals, reducing their electron deficiency and making the nitride surface behave as an electron donor similar to noble metals. As such, the metal nitrides are expected to have higher catalytic activity than their parent metals. For this reason, hierarchical porous metal nitrides have also been developed, including the work of Zhang et al. [100]. There, they presented a hierarchical porous dendritic Ni-Mo nitride for HER catalysis achieved using  $\text{N}_2$  plasma treatment of Ni-Mo alloy, exhibiting only a small overpotential of  $\sim 109$  mV and durability at various current densities.

#### 4.1.2. Zeolites

Zeolites are ordered porous inorganic materials composed of (alumino-)silicate as  $\text{M}_{x/n}(\text{AlO}_2)_x(\text{SiO}_2)_y \cdot w\text{H}_2\text{O}$ , where M is a cation of valence  $n$ ,  $w$  is the number of water molecules, and  $x$  and  $y$  are the molar concentrations of the tetrahedra in the structure (typically,  $y/x$  between 1 and 5, but can increase to 100 in siliceous zeolites). The framework may contain cages and channels of discrete size, which are normally occupied by water [38,161] (Figure 5). Figure 5a shows the influence of the negatively charged aluminum on the zeolite. To neutralize this apparent negative charge, the protons on the neighboring oxygen become highly acidic, or metal cations are attracted. As such the zeolite's Al content determines largely the material's acidity or cationic content.

Usually, zeolites are crystalline and mostly microporous, but they can also be meso- or even microporous, for instance, due to modifications [17,36]. Some of the characteristic features of zeolites and their analogues are their high surface area ( $\sim 1000$   $\text{m}^2/\text{g}$ ), highly ordered micropore channel system with uniform pore sizes and shapes [60,162], and the presence of charges and ions at well-defined sites in the framework. The well-defined pore system results in their molecular sieving property, excluding molecules with larger diameters than the pore system. The presence and particular distribution of the charges and ions create a specific electric field within the framework, enabling the control of their hydrophilicity and introducing their ion-exchange properties [60]. As such, zeolites have found widespread applications as dehydrating agents, selective adsorbents, atmospheric purification, ion exchangers, and, most importantly, catalysts of both high activity and selectivity for a huge number of reactions, including hydrocarbon reactions (Figure 5b) [36,38].

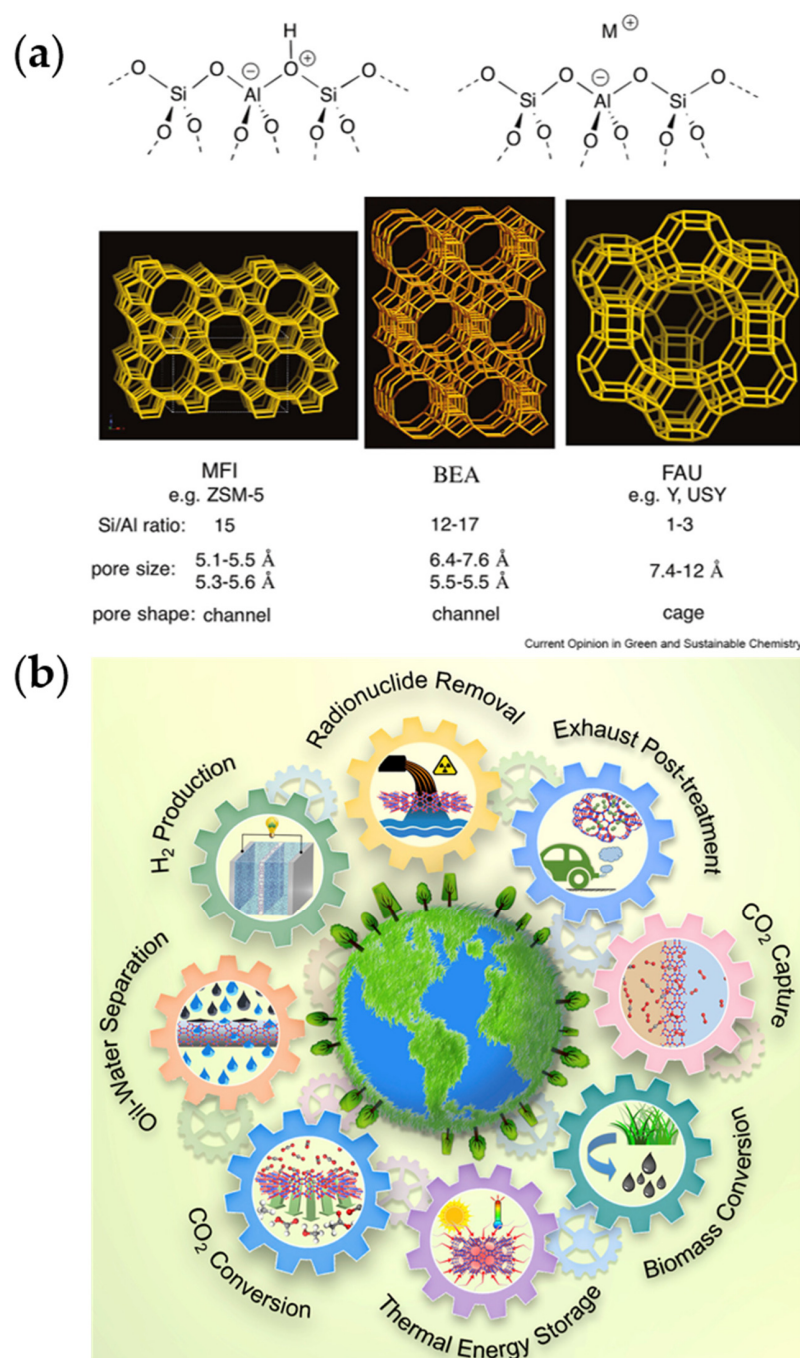


**Figure 5.** Schemes of zeolites showing model structures (a) and their common applications (b). (a): Reprinted from *Current Opinion in Green and Sustainable Chemistry*, 10, Chassaing, S., Bénétteau, V., and Pale, P., Green catalysts based on zeolites for heterocycle synthesis, 35–39, Copyright 2018, with permission from Elsevier B.V. [161]; (b): Reprinted from *Chem*, 3, Li, Y., Li, L., and Yu, J., Applications of Zeolites in Sustainable Chemistry, 928–949, Copyright 2017, with permission from Elsevier Inc. [163].

Synthetic zeolites can be prepared by crystallizing gels containing alumina and silica in an aqueous medium at 100–190 °C for several days or weeks [36]. Zeolites have long been used, with their first usage and laboratory synthesis already being a century or two. A large number of zeolites has been produced thereafter, mainly for use as catalysts [164]. Cundy and Cox give an extensive review of the history of hydrothermal synthesis of zeolites until the early 2000s [36], whereas Derakshankhah and co-authors give a comprehensive review of the use of zeolite NPs for biomedical applications [38]. A book on the use of

artificial intelligence (AI) to guide the design and predict the properties of nanoporous materials, including zeolites has also been published recently [39].

In particular, the zeolite NPs, or nano zeolites, are interesting for different applications [16,38] and can be synthesized using different techniques (see possible techniques in Section 3.1) such as templating approaches [165]. But as with any nanomaterial, their nanoscale properties and, in the case of drug-delivery and in vivo applications, scrutinizing their toxicity becomes crucial. Despite this, zeolite NPs are desirable among porous nanomaterials due to their relatively low toxicity, adjustable payload capacity (i.e., increased loading in the pores), and improved intracellular targeting specificity and efficacy. In addition to their possible use in drug delivery, and in developing treatments for Alzheimer's disease, their usage also includes bone regeneration for implants [38]. In cases of in vivo applications, due to their affinity for protein adsorption, their envelope or corona comprises of protein, which can be tuned mainly by their zeolite type (e.g., FAU- and EMT-types, which have one and two cages, respectively) and the (plasma) protein concentration [38,162]. For example, at high (human) plasma concentrations, higher selective adsorption for apolipoprotein C-III (APOC-III) and fibrinogen is seen, whereas at low concentrations, the preference is towards immunoglobulin gamma proteins. With more hydrophilic EMT-types, more proteins are also adsorbed. Therefore, one potential use of zeolite NPs is for the selective capture of proteins for therapy, drug delivery, and other bio-applications [162].

As catalysts, the nano size of NPs allows for easier access to reactants, resulting in higher diffusion, exchange, product yield, and selectivity [16,52]. Often, these NPs contain hierarchical porosity, having also meso- (and macro-)pores, in addition to their micropores [52,97,162]. The idea behind hierarchical modification is to reduce steric hindrance, allowing easier access to active sites [52], which is difficult with only the microporous channels [40]. However, the hierarchical porosity does not always result in pronounced catalytic effect [97]. When their size is <200 nm, they also exhibit colloidal stability [162]. Wawrzyńczyk et al. [52] has shown that hierarchical zeolites also have the potential as bioactive molecule carriers, with a cumulative ibuprofen release being almost complete after 8 h. In their work, the controlled release behavior of the active substance depends on the zeolite matrix. The hierarchical pores can be produced using bottom-up or top-down approaches, and result in pure zeolitic phases (i.e., true hierarchical since the secondary porosity is located within the zeolite phase) or composites (i.e., the hierarchy results from other phases, binders or carrier).

Porous zeolites as catalysts, sorbents, and container composites can also serve as support for metal catalysts [16,99] and other materials [17]. The rigid porous framework of zeolites makes them ideal inorganic supports. An aim in doing so is to prevent catalyst/material aggregation, and the associated loss of (catalytic) function [40]. Different architectures have been reported, including simply containing the metal catalysts in the mesoporous (nano)zeolites [16,17] or as layered zeolites [99]. For interest in zeolites and their catalytic activity, readers are referred to available reviews on the topic such as Xu et al.'s [40]. Also, a tutorial review on textural characterization—mainly on physisorption methods for micro- and mesopore analysis, macropore analysis by mercury porosimetry—of nanoporous materials, specifically of hierarchically ordered materials like hierarchically ordered zeolites, is given by Schlumberger and Thommes [41].

#### 4.1.3. Porous Silica

Silica in the form of mesoporous nanoparticles presents promising features, such as tunable pore sizes and pore volumes, low mass density, facile synthesis, and large-scale production. These features make them promising as materials for therapeutic and diagnostic purposes [166,167]. Mesoporous silica materials were first reported by Kuroda et al. (Japan) and the Mobil Oil scientists (USA) back in 1990 [61,168]. The most common technique in preparing mesoporous silica NPs is based on the supramolecular self-assembly of the surfactants (or templates), such as sol-gel synthesis-based. The surfactants self-organize themselves in the solution, while hydrolyzed inorganic silica precursors arrange them-

selves in the micelles to form the composites of silica with the templates [169]. With the sol-gel method, these NPs present diameters between 50 and 300 nm [61]. The removal of templates such as by calcination or solvent extraction then reveals the arrangement of the silica network, which could be cage-type, 2-D cylindrical, or bicontinuous cubic [169]. The typical process of preparing mesoporous silica is given in Figure 6a. Gruner et al. reported a sponge phase-type porous silica using cetyl pyridinium chloride [170]. Mesoporous silica NPs have shown bioactivity [171] and therefore find applications in drug delivery [166,167]. Similarly, they have been used as carriers for the gradual release of antioxidant molecules (Figure 6b) [172]. They can also be used for energy storage [169], sensors [173], and catalysis (e.g., as catalyst supports) [150,174].

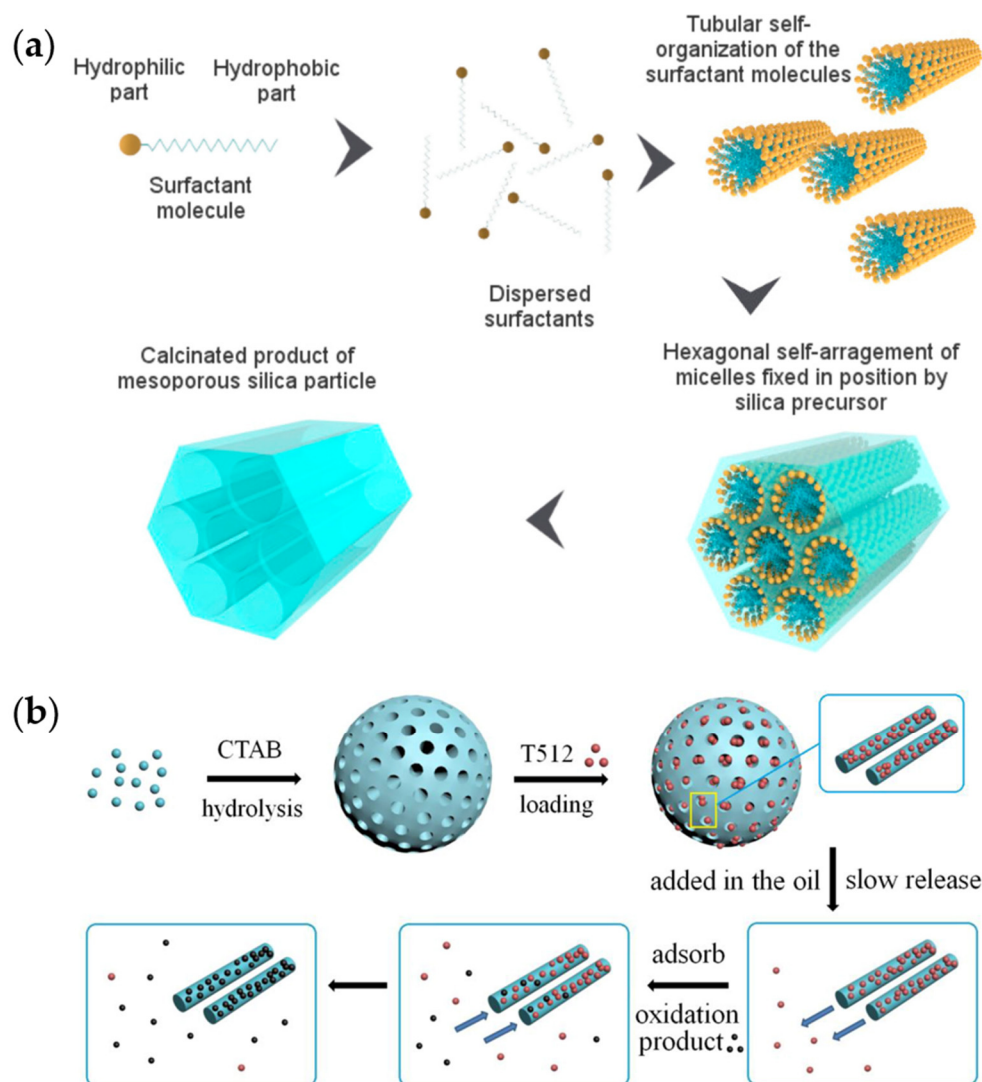


**Figure 6.** Typical formation of mesoporous silica (a) and gradual release carrier as an exemplary application (b). For the scheme in (a): Reprinted from *Microporous and Mesoporous Materials*, Vol. 289, Mikšík, F., Miyazaki, T., and Inada, M., Detailed investigation on properties of novel commercial mesoporous silica materials, 109644, Copyright 2019, with permission from Elsevier Inc. [175]; for the scheme in (b): Reprinted from *Tribology International*, 121, Huang, L. et al., Mesoporous silica nanoparticles-loaded methyl 3-(3,5-di-tert-butyl-4-hydroxyphenyl) propanoate as a smart antioxidant of synthetic ester oil, 114–120, Copyright 2018, with permission from Elsevier Ltd. [172].

Introducing hierarchy in the porous structure of silica nanomaterials has been a major advancement in the field. The natural gemstone opal consists of mesoporous silica nanospheres embedded within its structure [176]. Opal is an example of a photonic crystal

made of mesoporous silica nanomaterial. Photonic crystals (PCs) exhibit periodic changes in their dielectric function which influences the propagation of photons within, enabling them to control the flow of light. These materials are used in many modern technologies including energy storage and conversion, (bio)sensors, optoelectronics, and optical devices. Some examples include artificial opals, and inverse opals (IOs), which can also be made of mesoporous silica. Such hierarchical structures are mainly prepared by colloidal assembly but can also be prepared in other ways such as lithography and sol-gel routes. Hierarchical meso-, microporous IO silica, displaying a very thin silica framework with macropores of ~500 nm and mesopores of ~4 nm, were used for the fabrication of biosensors for the detection of glucose [177,178]. 3D IOs can also be prepared by preparing opal PC templates made of silica microspheres [179,180]. Therefore, an important application of silica PCs includes their use as templates to prepare other PCs or hierarchical architectures. For interest in photonic crystals, readers are advised to look at reviews available in the literature [176,177,181]. Specifically, the review of Fathi et al. on IO PCs for bio applications is fairly recent [177].

Hierarchical porosity in silica NPs, in particular, would allow diffusion of different sizes of molecules within the inorganic structure and also possibly harmonize the diffusion of molecules of different sizes for simultaneous loading in the case of multi-scale pores. The use of hierarchical structures was thus demonstrated by Du and He for drug release (of ibuprofen), which achieved quicker rates than conventional counterparts [51]. Additionally, they also demonstrated their use as antireflection and superhydrophilic coatings. Due to the said reflection/scattering properties, they were also used as dye-sensitized solar cells (DSSCs) scattering layers [75]. There, Ryu et al. fabricated a composite by coating the porous silica NPs with a thin layer of TiO<sub>2</sub>. Investigation of their light scattering properties shows their outstanding performance, likely due to the large surface area and multiple scattering possibilities they afford. Such hierarchical structures were obtained using microemulsion techniques.

To go even smaller, nano-emulsions have also been used to form hierarchical porous silica nanoparticles [23,182]. For example, multi-chambered networks that can be spatially isolated to accommodate different nanomaterials in the compartmentalized chambers of a hierarchical mesoporous calabash-shaped silica have been developed [182]. This has been shown to be useful as a double-chambered nanoreactor, but can also be used in biological applications such as in drug delivery.

#### 4.1.4. Porous Amorphous Oxides

Since a significant amount of porous oxides are amorphous and/or made from amorphous materials, a subsection on porous bulk metallic glasses is therefore dedicated. Firstly, the improvement in the structural properties of these materials has been a subject of research due to their tendency to undergo catastrophic failure with their poor uniaxial ductility. The presence of pores acting as the gaseous second phase in such materials was found to mitigate this weakness, enabling compressive strains without fracture [183].

Additionally, a strong motivation in the development of porous amorphous alloys and their oxides is their potential application as bone implant materials. Bioactive glasses (made of silicates, and possibly additional network modifiers) have been considered as scaffolds for bone tissue engineering and regeneration [184]. With such materials, the bone can bond by forming a layer of carbonate-substituted hydroxyapatite (HCA) on the material's surface once implanted. Interestingly, these materials do not only exhibit bone growth stimulation but also resorbability, which, in the process, results in products that further induce bone-cell formation. By resorting to sol-gel-derived bioactive glasses, nanoscale textural porosity can be achieved. This results in an increased material surface area, exposure of more HCA nucleation sites, and an enhanced cation exchange and network dissolution. However, their mechanical properties are low, which limits their implant applications. As such, a separate subsection (given above) is dedicated to porous silica because of its numerous examples.

In recent decades, there has been significant progress in the development of multi-component metallic glasses, especially titanium-based ones (Ti-BMGs). New alloys with

high GFA that are free of toxic elements such as Be, Ni, and Al are considered promising candidates for biomedical applications [185,186]. The materials are mostly suitable for small bone implants in dentistry and trauma surgery. Compared to implants in clinical use, Ti-BMGs are advantageous due to their high mechanical bio-functionality, i.e., higher strength and hardness as well as good corrosion resistance [187,188].

Currently, Ti-Cu-based alloy types are being investigated for potential implant applications. Several studies assessed the biocompatibility of amorphous alloys such as  $(\text{Ti,Zr,Cu})_{92.5}\text{Fe}_{2.5}\text{Sn}_2\text{SiAg}_2$  and  $\text{Ti}_{40}\text{Zr}_{10}\text{Cu}_{34}\text{Pd}_{16}$ , and their derivatives [189–191]. They showed good results in short-time implantation. However, these alloys present a high amount of Cu which generally leads to high pitting corrosion sensitivity as well as cytotoxicity due to the release of Cu near the surface region in contact with the physiological environment [192,193]. For these reasons, in long-term exposure, Cu could be detrimental to the implant performance.

Selective dissolution processes (i.e., dealloying [14,34,105]) emerge as an option to remove Cu from the near-surface regions of the glassy alloy while at the same time introducing surface roughness, which can create bioactive states for the optimal growth of bone tissue. Using an alkaline approach for the removal of Cu, Blanquer et al. modified the surface of  $\text{Ti}_{40}\text{Zr}_{10}\text{Cu}_{38}\text{Pd}_{12}$  by polarizing the bulk samples in a 5 M NaOH solution at 25 °C. They obtained a porous structure layer of 200 nm thickness, which improved the corrosion resistance of the alloy. The layer was rich in Ti and Cu oxides, the latter with a lower amount [194]. Similarly, J.-J. Oak et al., using the same electrolyte but varying the temperature for ribbons with the composition  $\text{Ti}_{42}\text{Hf}_{11}\text{Cu}_{11}\text{Pd}_{36}$  obtained nanostructures consisting of a 200 nm connective framework of O, Ti, and Pd. The synthesized nano-meshes induced calcification in simulated body fluid, therefore showing its improved bioactivity in comparison to Ti alloys, which are bioinert [195].

Another line of study for these types of Ti-Cu-based BMGs for biomedical applications is the improvement of their mechanical properties. Even though Young's modulus of these amorphous alloys (80–100 GPa) is reduced in comparison to cp-Ti (102–108 GPa), it is still too far from that of the bone's (10–30 GPa) [192,196]. This can lead to implant loosening due to stress-shielding effects. By incorporating porous structures, Young's modulus can be effectively lowered. Several studies investigated the effect of porous structures introduced by additive manufacturing (AM) [197,198] or spark plasma sintering (SPS) [199,200] on amorphous alloys (including Zr- and Fe-based BMGs). Their Young's Modulus was decreased to a value closer to that of the natural bone's, resulting in improved biocompatibility. However, there was a significant reduction in compressive strength. In this case, introduced pores can induce microcracks, which degrade the mechanical properties of the BMG and result in the failure of the implant. That is why better parameters/strategies or post-processing techniques are needed [201], and further studies have to be carried out regarding the effect of porosity in amorphous materials. Nevertheless, the introduction of porosity in Ti-based BMGs as future bioimplants presents potential substitutes to the current ones in clinical use (Ti-6Al-4V, cp-Ti, Co-Cr) by improving their osseointegration.

Hierarchical structures also seem to correlate with their bioactivity and biological properties [202–205]. Several studies of hierarchical inorganic structures and hybrids, especially those for bone-implant applications, show bioactivity [204,205]. Foamed sol-gel-derived bioactive glasses produced hierarchical structures that enable tailoring of bioactivity, which can be optimized for target applications such as scaffold usage [184]. The 3D porous network in bone implant materials allows for tissue ingrowth and enhanced osteogenic activity, by not only providing the desired surface properties [205], but also in some materials, the needed mechanical strength [206] for such processes. Specifically, a Ti-based implant material with a hierarchical structure displayed not only osteogenic activity but also antibacterial properties due to its topography [205].

A two-pronged approach of enhancing biocompatibility while providing antibacterial properties is currently being implemented in many surface modification studies for bioimplant applications to address infection-associated failures of implants [11,205]. This was

effectively shown in the work of Huang et al. [205], on amorphous titania consisting of hierarchical structures. There, they attribute the effective biological properties of the material to surface properties brought about by the hierarchical structure. Specifically, the decreased bacterial adhesion was ascribed to the porous nanoscale structure which seemed to have reduced the contact of the bacteria with the substrate and increased the surface free energy of the material, the latter possibly deforming the bacterial membrane. On the other hand, the same nanoscale features and surface free energy result in high adsorption of proteins and cells for osteogenic properties. However, cell differentiation seemed to be more effective when the nano-features were combined with (micron/)submicron structures, i.e., in hierarchical structures [205,207]. Smaller micron-sized pits and lower roughness seem to allow faster cell propagation, though larger ones were correlated with elevated osteogenic-specific genes. Moreover, the hierarchical structure seemingly also modulates the Wnt/ $\beta$ -catenin signaling pathway crucial in cell osteogenic differentiation [207]. Figure 7 shows a scheme of the influence of hierarchical nano-microstructure on cell behavior.

Overall, hierarchical structures favor cell differentiation and proliferation, as well as antibacterial property. Although many of the bone implant applications are on porous (micron/)submicron materials, rather than porous nanomaterials, these examples point to the need for hierarchical structures driving the development of porous (nano and) submicron materials forward.

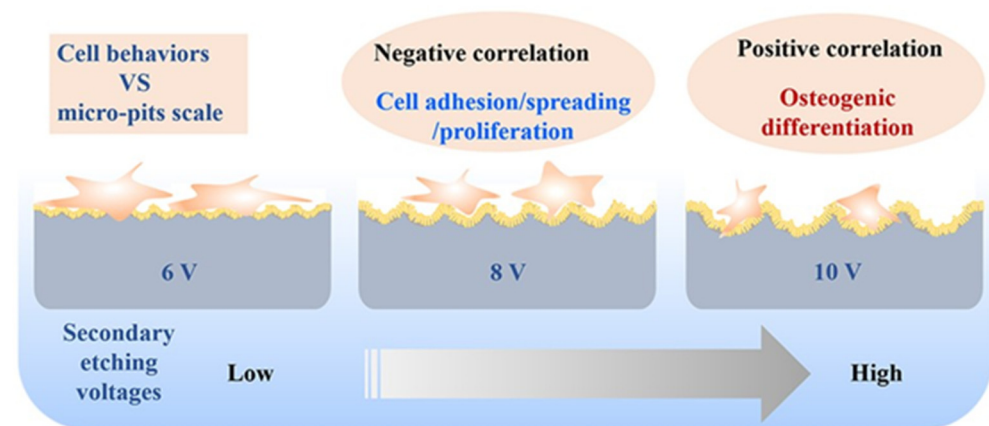


**Figure 7.** A scheme showing the influence of the secondary etching voltage on the formed micro-pits and the correlation between the cell-behavior and the formed nano-microstructure. For example, osteogenic differentiation was observed for larger micro-pit array. Reprinted with permission from [207]. © The Author(s) 2022. Published by Oxford University Press. This is an open access article distributed under the terms of the Creative Commons Attribution License, which permits unrestricted reuse, distribution, and reproduction in any medium, provided the original work is properly cited.

#### 4.1.5. Porous Nanomaterial Ordered Structures and Arrays of Oxides and Derivatives

To further introduce hierarchy and 3D order in porous nanomaterial morphology, arrayed construction can be included in the design. As mentioned in Section 4.1, many of the metal oxides when anodized, self-assemble into arrayed porous forms. These include NTs and porous nanosheets, e.g., of titania and alumina [132–140]. As many derivatives can be formed from porous oxides, NTs of nitrides have also been formed. An example is TiN, which can also be in the form of porous nanotubular arrays [208]. Therefore, a subsection is allotted here for these emergent materials.

Mixed metal oxides were also developed into porous HNAs. An example is the work of Yan et al. on nanoporous (~5 nm pore size) NiCoFe spinel oxides arranged hierarchically into nanorod arrays (up to 50–250 nm in rod diameter, hundreds of nanometers in spacing) to form excellent OER electrocatalysts with a low overpotential of 280 mV in alkaline medium [146]. With such HNAs, both the surface area and mass transfer are increased, whereas both the diffusion and transfer paths of the reactants are shortened.

Three-dimensional ordered microporous (3DOM) perovskites have also been created using polymethyl methacrylate (PMMA) colloidal crystal templated synthesis. Dai and co-workers prepared 3DOM LaFeO<sub>3</sub> perovskite with a honeycomb structure using monodispersed PMMA (330 nm in diameter) [37,209]. Their ordered interconnected pores are effective for electrocatalysis.

In the field of perovskite solar cells, ordered hierarchical porous TiO<sub>2</sub> has been used as a scaffold to support an ordered-growth perovskite [210]. The hierarchical porous TiO<sub>2</sub> was produced from MOFs (air-sintered MIL-125(Ti)), which lend to its ordered porosity. A quasi-mesoscopic scaffold was obtained by a scattered distribution of the produced porous structure on planar and compact TiO<sub>2</sub>, resulting in grown perovskite solar cells with a PCE of 16.56%, which is higher than those formed without these scaffold structures.

An interest in porous HNAs of metal oxides and their derivatives, in addition to their use as scaffolds/templates, is PC-like materials. This makes them effective light scatterers based on the Mie theory, pointing to their suitable application as light-harvesting solar cell materials or as substrates for SERS [211,212]. The SERS effect on metal oxides and other semiconductors has been well-observed [213,214], and the influence of their nanostructure has been well studied on oxides such as TiO<sub>2</sub>. IO structures exhibit this PC-like character and have been reported to achieve SERS EF~10<sup>4</sup> [136,215,216]. This value though is likely due to both electromagnetic (EM) and chemical contributions. Such IO structures can also be made from TiO<sub>2</sub> and other metal oxides, such as Al<sub>2</sub>O<sub>3</sub>, ZnO, V<sub>2</sub>O<sub>5</sub>, and NiO (though they can also be made from other materials, such as silica (as presented above), carbon, silicon, hydrogels and polymers; V<sub>2</sub>O<sub>5</sub> was the first one for metal oxide anode design) [176,177,217–219]. Hierarchical mesoporous IO V<sub>2</sub>O<sub>5</sub> (with a wall thickness of ~150 nm), for example, has been prepared for battery electrodes [180]. IO TiO<sub>2</sub> is promising as a photocatalyst since it can harvest light up to the visible range and generate slow photons, which enhance the light-matter interaction to further enhance catalysis [217–221].

The SERS effect has also been investigated on TiO<sub>2</sub> NTs and nanofibers, particularly on the distinction of the EM from the chemical contribution to understanding the morphological influence on the EM enhancement [136,222]. The contribution of the EM—in addition to chemical—enhancement has already been observed for high-aspect-ratio TiO<sub>2</sub> nanostructures [136,216,222,223]. This has been demonstrated by SERS studies using indirectly attached probes, including TiO<sub>2</sub> NT arrays (NTAs), showing a morphology-dependent EM enhancement [136,216,223]. EM field (EMF) calculations show that the aspect ratio of particles increases the regions of enhanced EMF, i.e., “hotspots”, at the metal oxide-water interface [223], thereby improving their “light harvesting” capabilities. For TiO<sub>2</sub> NTAs with diameters of ~70 nm, wall thicknesses of ~10 nm, and tube lengths of ~700–900 nm—a structure exemplifying higher morphological anisotropy—EMF calculations show hotspot variation along the tube length, which fits the observed different Raman enhancements depending on the NT length (Figure 8a) [136,216]. The high EMF enhancement of TiO<sub>2</sub> NTAs results in a better visible-light photodegradation of an azo dye pollutant chemisorbed on the NTA, based on the observed correlation of the EMF enhancement with the calculated photocatalytic degradation rate (Figure 8b) [135]. This effectively shows the influence of the nanomorphology of these porous HNA on the photocatalytic activity of the nanomaterial. The enhanced catalytic activity of such TiO<sub>2</sub> NTAs can be further achieved by forming nanohybrids and nanocomposites with other nanomaterials to improve their light harvesting and charge separation. Examples of these include S-doping and the addition of CdS or ultrafine Pt NPs [224–226].

Structures derived from TiO<sub>2</sub> NTAs, such as their nitridated form resulting in TiN NTAs, also exhibit light enhancement due to the periodic arrangement. Interestingly, such porous HNAs of TiN NTs show wavelength-dependent EMF enhancement (Figure 8c) [208]. Recent work shows a general polymerization-induced strategy to form wide-scale mesoporous arrays of transition metal nitrides (which, in addition to TiN, also includes MoN, VN, and WN) and their doped counterparts [227]. This was developed towards their use as effective and durable SERS substrates, exhibiting up to a Raman EF of ~10<sup>7</sup> and detection

limits in the range of pM for TiN mesoporous arrays (rod diameter in the sub-micron to micron range; 508 nm excitation).

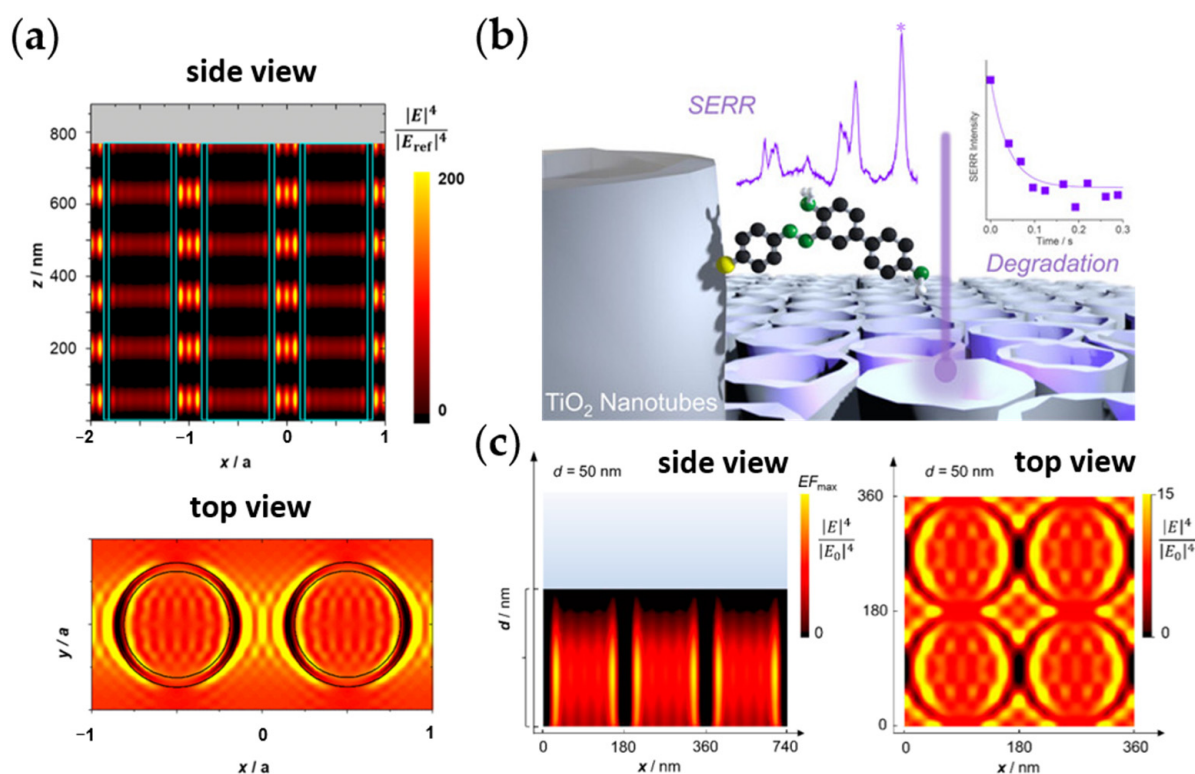


**Figure 8.** Electromagnetic field (EMF) enhancement studies on porous hierarchical nanotubular arrays of TiO<sub>2</sub> and TiN: (a) calculated EMF enhancement for the TiO<sub>2</sub> nanotube array (TiO<sub>2</sub> NTA). The side and top view of the calculation show the localized field hotspots along the tube length for three and two tubes, respectively. The enhancement factor (EF) scale bar is on the left of the side view image. Adapted with permission from [136]. Copyright 2018 Wiley-VCH Verlag GmbH and Co. KGaA, Weinheim. (b) The photocatalytic azo-dye degradation on TiO<sub>2</sub> NTA correlates with its EMF enhancement. The inset shows the surface-enhanced resonance Raman (SERR) spectra of chemisorbed dye on TiO<sub>2</sub> NTA of high EMF enhancement and the corresponding fit of the decay rate of the SERR intensity of the dye peak marked by \*. Adapted with permission from ref. [135]. Copyright 2019, the authors. Published by Wiley-VCH Verlag GmbH and Co. KGaA. Open access article. CC BY 4.0 license; (c) EM enhancement calculations for the TiN NTA from nitrated TiO<sub>2</sub> NTA. The side and top view of the calculation show the localized field hotspot distribution for three and four tubes, respectively. The EF scale bars are on the left of the images. Adapted with permission from [208]. Copyright 2022 by the authors. Licensee MDPI, Basel, Switzerland. This article is an open access article distributed under the terms and conditions of the Creative Commons Attribution (CC BY) license. Exact image construction reprinted from [11].

#### 4.2. Porous Metallic Nanostructures

Porous metals, specifically those containing small (micro-, meso-, nano-)pores are attractive for many applications due to the combined advantages provided by the metallic aspect (conductivity, catalytic activity, desirable structural property, and optoelectronic properties, among others) and the porosity (increased surface area, improved mass transport, more available active sites, lightweight, altered mechanical properties, light scattering/harvesting, etc.). A common strategy for producing such structures is by dealloying [14,34,105] (Figure 3b), which is more extensively discussed within Section 4.2.1 and has been introduced in Section 3.1.2, together with the other strategies to prepare porous materials. Here, a subsection is dedicated to porous gold and other porous noble metal

nanostructures since many earlier studies for various applications were carried out on these metals. It is interesting to see how the development of hierarchical porous nanostructures took place coming from the creation of multimodal porosity and/or nanopores within precious metal nanomaterials. Even with hierarchical structures that consider large-scale superstructures, looking at the micro- and mesoscopic scale structures (including their porosity) is crucial as these features could influence the macro-scale behavior of the material.

The next subsection is then dedicated to the non-precious metal porous nanostructures, which are important considering sustainability and economic viability. Such nanoporous metals (Np-metals) can also be prepared with similar techniques as the precious metals, which include dealloying and galvanic replacement reactions [228], also towards hierarchical porous nanostructures. There, MOFs and nanoMOFs will also be mentioned, considering that most examples of this class of materials incorporate non-precious metals. However, as these are hybrids and are too broad a classification of porous nanomaterials to be included here, an in-depth discussion on these is excluded from this review.

#### 4.2.1. Porous Gold Nanostructures and Other Precious Metals

Gold is one of the most important precious metals with a plethora of applications in various sectors due to its biocompatibility, high stability, and conductivity. However, its high cost makes bulk gold economically prohibitive for some applications [229]. Therefore, the implementation of nanostructured Au is attractive since an increased surface area-to-volume ratio can be achieved, effectively reducing cost as less material is then needed for the same surface area required for the application. The fabrication of Au NPs has thus been widely employed as a facile technique to achieve the desired surface area optimization.

Another way to achieve a large surface area is by introducing porosity to the material. Porous metals and porous metallic nanostructures for catalysis, sensing, actuation, other electrochemistry-based applications, and SERS-based applications are typically based on nanoporous silver (Np-Ag), nanoporous gold (Np-Au), nanoporous platinum (Np-Pt), and nanoporous palladium (Np-Pd) [14,42,43,113,229–234]. With Np-Au, the large surface area combined with its conductivity makes it an attractive electrode for electrochemical studies. As it can be achieved with simple fabrication techniques, Np-Au has been widely applied for different purposes in various sectors, such as catalysis, biosensors, biofuel cells, and drug delivery [42,43,112,113,231].

Specifically, for (bio)sensing and catalysis, the porous structure of Np-Au allows for increased loading of (bio)molecules and efficient mass transfer necessary for both catalysis and (bio)sensing. Its excellent conductivity is also useful for such purposes that benefit from an effective electron transfer [113,230,231,235–239]. Np-Au exhibits good oxidative activity for a variety of small organic molecules, such as methanol, ethanol, phenols, H<sub>2</sub>O<sub>2</sub>, glucose, and dopamine. It can also be effectively used in various biosensors, such as enzyme-, aptamer-, or immune-based biosensors. Direct electrochemical sensing of various molecules and ions also finds use in medical, environmental, and food safety applications [42].

Np-Au plays a crucial role in detecting biomolecules like nucleic acids and proteins. Moreover, Np-Au can combine with active biological elements such as enzymes or whole cells to construct a biological composite material, which shows a wider range of applications than Np-Au or active biological elements alone [43]. It can therefore also act as a carrier for biorecognition elements, such as enzymes, DNA, antigens, and antibodies. Further, it can be prepared and modified easily. Np-Au can be synthesized using different methods, such as dealloying, other (electro-)chemical and physical approaches, and DHBT (please see Section 3.1 for the different possible techniques; electrochemical dealloying will be given a focus later here).

The same characteristics of Np-Au having a high specific surface area, lightweight, high porosity, good biocompatibility, and high electron transfer efficiency also make it an ideal biofuel cell (BFC) electrode material [43]. As a truly renewable green battery, BFC refers to a power generation device that uses enzymes or microorganisms as a catalyst to

convert the chemical energy of fuel into electricity. Np-Au in BFC is mainly focused on applications such as enzyme and microbial biofuel cell types [240].

The successful applications of porous nanomaterials and gold nanoparticles in drug delivery imply the potential of Np-Au with unique properties as drug carriers to achieve drug delivery [241]. The advantages of using Np-Au for drug delivery are its large specific surface area and porosity and low toxicity to enzymes or cells, indicating its biocompatibility. In addition, when produced as a nanomaterial, Np-Au can easily penetrate various membrane structures, making it conducive for drugs to enter the target tissues or cells. Np-Au nanomorphologies have also been studied *in vitro* and *in vivo* to investigate the immune response towards their presence [242] (Figure 9a). The surface of Np-Au nanomaterials can be further modified for different purposes to allow drug delivery to different tissues or organs in a directional manner [43].

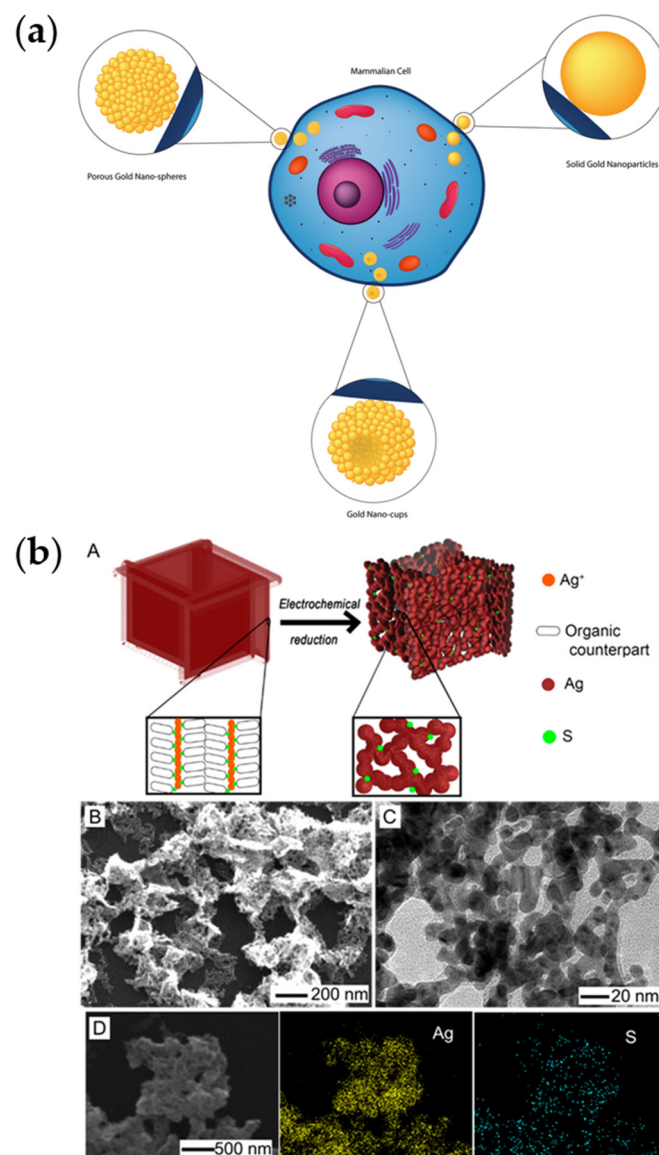


**Figure 9.** Hierarchical porous nanomaterials made of precious metals, gold and silver: (a) a scheme showing different gold nanomorphologies (porous gold nanospheres, solid/smooth gold nanoparticles, and porous gold nanocups) interacting with a mammalian cell. The different nanomaterials are expected to interact with the immune system of the cell/organism. Reprinted from NanoImpact, 28,

Usman, M.; Sarwar, Y.; Abbasi, R.; Ishaq, H.M.; Iftikhar, M.; Hussain, I.; Demirdogen, R.E.; Ihsan, A., Nanogold morphologies with the same surface chemistry provoke a different innate immune response: an in vitro and in vivo study, 100419, Copyright 2022, with permission from Elsevier. [242]; (b) a schematic diagram of the electrochemical reduction of the Ag nanobox precursor to a 3D porous Ag nanobox/nanocage (A). Scanning electron microscopy (SEM) (B) and transmission electron microscopy (C) images of the synthesized 3D porous Ag nanoboxes. Images in D show the SEM image and corresponding EDX analysis. Reprinted (adapted) with permission from Abeyweera, S.C.; Yu, J.; Perdew, J.P.; Yan, Q.; Sun, Y. Hierarchically 3D Porous Ag Nanostructures Derived from Silver Benzenethiolate Nanoboxes: Enabling CO<sub>2</sub> Reduction with a Near-Unity Selectivity and Mass-Specific Current Density over 500 A/g. *Nano Lett.* 2020, 20, 2806–2811, doi:10.1021/acs.nanolett.0c00518. Copyright 2020 American Chemical Society [243].

Reported Np-Au studies are primarily based on dealloying of AuAg alloys, but there is also a growing interest in exploring other gold alloys like AuCu, AuPd, and Au metallic glasses for Np-Au synthesis. Compared to the well-studied AuAg for Np-Au production, there have been relatively fewer investigations using the AuCu system as a starting material, despite copper's lower cost compared to silver and that initial dealloying studies mainly started with brass and AuCu alloys. This discrepancy is likely attributed to the partial miscibility between gold and copper, which complicates the process [244]. Nevertheless, AuCu has been used to produce Np-Au and Np-Au nanomaterials and its different parameters have been investigated. Similar to AuAg, AuCu exhibits critical potential and parting limits that depend on the condition.

Noble metal-based alloys display distinct electrochemical behaviors compared to their individual constituent metals. The dissolution behavior of these alloys is notably influenced by the differences in standard potentials between their components. Consequently, the anodic polarization pattern of an alloy differs from that of the constituent metals. Selective or nonselective dissolution can then occur depending on the composition. At lower potentials, surface passivation from the enrichment of the more noble element overpowers the dissolution of the less noble component. This manifests as a limited current regime which continues until the critical dealloying potential ( $E_c$ ) is reached. At this point, sudden increased dissolution of the less noble element occurs, which when combined with surface diffusion of the more noble element forms the desired 3D porous structure. In more noble compositions where  $E_c$  affects the dissolution of both the noble and less noble elements, nonselective dissolution occurs, and a nonporous structure is formed. Therefore, alloy composition is also a key factor influencing electrochemical dealloying, with the selective dissolution not only being influenced by the difference in standard potential of the elements but also by the proportion of the more noble component. Limits therefore exist for determining an appropriate alloy composition for porous structure formation: an upper limit on the quantity of the more noble element for selective dissolution to occur, and a lower limit to ensure that the remaining atoms adhere to form the desired 3D structure. In cases like AuCu alloys with partial miscibility, intermetallic compositions should also be noted [245,246].

Np-Au typically exhibits an average pore size of 10–50 nm [247–249], but finer nanopores (ca. 4–5 nm) can be achieved with specific preparation methods [119,250], such as shorter dealloying times [251], lower temperatures [119–121], use of pulsed electrochemical techniques [123], or the addition of platinum or thiol [116,117]. These approaches allow for tailored Np-Au characteristics suitable for various applications. In multiscale pores, such as with bimodal pore sizes, mesopores, nanopores or micropores provide the increased surface area and often also the functionality, whereas macropores facilitate the overall transport [18,252,253]. For example, hierarchical porous AuCu films exhibiting features in the microscale (0.5–1  $\mu\text{m}$  ligaments and 1  $\mu\text{m}$  pores) and nanoscale (70 nm ligaments and 50 nm pores) (Np-Au-like, with Cu of ~33%) [253] have been reported. Such hierarchical nanoporous Au (or AuCu) structures have been heavily investigated in catalysis-oriented research such as for methanol electro-oxidation. Recently, Zhang

et al. showed similar hierarchical Au (or AuCu) structures (so-called black Au) exhibiting ultrahigh porosity for potential use in solar-steam generation. There, they showed that the structure differs in the final film composition with a hierarchical structure similar to porous NW being exhibited for those with greater final residual Cu content, whereas those of ultrahigh Au purity display typical 3D-bicontinuous open structure [254]. Other porous Au alloy structures such as PtAuCu porous nanoparticles in core-shell configuration have also shown enhanced electrocatalytic activities compared to commercially available counterparts. In this case, the addition of residual amounts of Au and Cu improves the performance of Pt for oxygen reduction by ensuring the availability of active Pt atoms at the surface, modifying the (electronic) structure and enhancing the adsorption-desorption process of oxygenated species [255].

Several techniques have been used to form hierarchical Np-Au (alloy) structures including combined alloying-annealing-dealloying [253–255], which were used to produce the abovementioned structures. The alloying can be done by electrodeposition, chemical co-reduction, or high-frequency heating (co-melting). Other techniques based on similar steps and using dynamic templates have also been reported for the production of hierarchical porous structures. A combination of nanocasting-dealloying-annealing, in which colloidal bicontinuous emulsion gel templates can be used, has also been reported for hierarchical porous structure formation [256]. Multiple dealloying steps and direct printing have also been incorporated as steps to produce hierarchical macro-/mesoporous nanostructures [252,257].

To facilitate electrochemical transport, nanorod or NW arrays of Np-metals have also been shown to provide fluid accessibility throughout the pore network similar to the multiscale pore hierarchical structures [258]. In such systems, the inter-nanorod distance and the nanoporosity can be tailored for these purposes [259]. As porous nanomaterials, Np-Au NW arrays have been produced using AAO [260] combined with dealloying [1]. Porous gold wires with micrometer-size diameters have also been shown recently for their applicability in *in vivo* electrochemical sensors [130]. Micrometer-wide porous gold wires have been well reported in the literature due to the easier preparation at this diameter scale [261].

AuAg alloy has been developed as a free-standing, single porous NW with a diameter of ~100 nm and pores of 5–30 nm. In studies on the influence of plasmonic properties on IR absorption, the strong impact on the plasmonic properties of porous gold NWs resonant with the vibrational modes (in the fingerprint region) result in strongly redshifted, broader plasmonic bands compared to those of smooth wires, which are likely due to the lowered average electron density and enhanced electronic surface scattering on the irregular porous surface. Overall, though, no significant surface enhancement in the infrared (IR) absorption due to porosity is apparent with its lower near-field strength counterbalancing the increased surface area. However, considering that the same vibrational signal contrast is obtained between smooth wires and porous wires (both were at 20%), less gold material is therefore needed to obtain the same surface-enhanced IR absorption spectral quality with porous wires [262].

On the other hand, the performance of porous gold nanomaterials—including those of NW arrays—as SERS substrates is more straightforward and apparent. The experimental enhancement factor (EF) obtainable is in the range of  $10^5$  (similar can be achieved with porous gold nanoparticles from AuAg alloys for non-resonant SERS conditions, i.e., 705 nm with methylene blue) [263]. Bunched porous Au-Ag NW arrays have also been used as SERS substrates, giving an  $EF \sim 10^6$  for 4-mercaptobenzoic acid at 632.8 nm excitation [264]. The bunching of the porous wires is due to the action of the capillary force during solvent drying [265] and can be controlled by tuning the wire length. In fact, this bunching is advantageous in the case of SERS as this also contributes to greater electromagnetic field enhancement [266]. Recently, single porous gold NW has been used as a SERS-based nano-sensor platform. An  $EF \sim 10^6$  for optimized conditions was achieved in pre-studies using rhodamine-6G as a model dye and at 633 nm laser excitation. It was

then used for in situ monitoring of the catalytic reaction of 4-nitrophenol (4-NTP) to 4,4'-dimercaptoazobenzene [231].

For interest in porous gold, readers are encouraged to look for excellent reviews on the topic. These include van der Zalm et al. [42] and Xiao et al. [43], which are updated reviews of Np-Au and hierarchical Np-Au materials for sensing applications and for biotechnological and biomedical applications, respectively. A recent review of Wittstock et al. on Np-Au and its evolution for catalysis and electrochemistry is also recommended [113]. The last two give examples on nanoporous nanomaterials. Especially the last one exhibits sections and subsections addressing hierarchical porosity and engineered nanoporous gold (nano)materials. Also, a recent article on high-precision 3D microprinting includes and prominently features a gold structure made from a few nanometers thick Au wires (or rather, fibers) that are multi-branched and interconnected, resulting in porosity at a wide range of sizes (a few nanometers to several hundreds of nanometers). This work shows a perspective on the possible direction of the fabrication of nanoporous gold and other metals in general [44].

Hierarchical porous Ag nanostructures have also been fabricated as catalyst for CO<sub>2</sub> reduction (CO<sub>2</sub>RR). An example is the work of Abeyweera et al. which features Np-Ag nanoboxes (pore/ligament in the order of 10 nm) fabricated by electrochemical reduction of silver benzenethiolate nanoboxes [243] (Figure 9b). Such structures display impressive catalytic electrochemical CO<sub>2</sub>RR and because HER is inhibited, a near 100% Faradaic efficiency at high cathodic potentials can be achieved.

Silver is another well-known SERS substrate, having a broader and stronger plasmonic absorbance in the visible range than bulk Au or Cu. Therefore, the development of hierarchical porous Ag nanostructures for SERS is expected [267,268]. Capaccio et al. fabricated Np-Ag nanofilms (10–200 nm) using an approach based on plasma treatment of Ag films [268]. With the 30 nm Np-film treated under plasma for 90 s, an EF  $\sim 6.5 \times 10^7$  was achieved for 4-mercaptobenzoic acid at 532 nm. Tian et al. prepared highly OM Ag superstructures (nanowire diameter of 10 nm with gaps of  $\sim 2$  nm) using nanocasting with mesoporous silica templates [267]. Due to the uniform hotspot distribution, a high Raman EF of up to  $10^9$  was achieved at 514 nm with crystal violet as reporter molecules, allowing for detection down to 0.1 pM concentration.

Np-Pt nanoparticles ( $\sim 20$ – $50$  nm particle size; pore size  $\sim 3$ – $5$  nm) have also been produced by a reduction method in the presence of a surface stabilizing agent. These nanoporous nanoparticles exhibited a larger surface area and a higher catalytic activity, such as for ethylene hydrogenation [1,269]. Meanwhile, the synthesis of Np-Pt nanowires (with an average diameter of  $\sim 68$  nm and pore sizes of  $\sim 6$ – $7$  nm) was reported using an electrochemical micelle assembly approach confined within a polycarbonate membrane template [270]. The said nanowires show high electrochemical performance toward methanol oxidation ( $\sim 2.7 \times$  higher normalized current density vs. a Pt black reference), which was even higher than the increase in electrochemical surface area ( $\sim 2 \times$ ), possibly pointing to an increased catalytic activity due to the nature of the nanoporous NW structure.

Hierarchical Np-Pd nanostructures are also interesting for catalysis. For example, hierarchical Np-Pd (pore size  $< 4$  nm) nanostructures (ligament size  $< 100$  nm, comprised of clustered fine nanoparticles of the size  $\sim 4$ – $5$  nm), which also present macropores (100–500 nm), were synthesized using a straightforward template-free approach [271]. This approach utilizes aggregation control in organic media by changing the dielectric constant of the medium. The synthesized hierarchical nanostructures were used for excellent catalytic reduction of 4-NTP to 4-aminophenol.

Another way to produce Np-metals is by galvanic replacement reactions, which allow for the controlled formation of hollow interiors and porous walls within metal nanostructures. Vital to this process is the occurrence of a replacement reaction between a metallic nano-template suspension and a salt precursor containing a more noble (i.e., less reactive) metal. This has been applied for the preparation of a wide range of nanostructures including hollow and porous ones based on Pd, Pt, and Au of various nanomorphologies,

such as single- or multi-walled NTs, nanoshells, nanotriangular rings, nanocages, and nanoboxes (prismatic and cubic). Such hollow porous nanostructures exhibit interesting properties such as tunable optical properties from visible to NIR range and unexpected higher strength than solid non-porous counterparts [228].

Np-metals are also used for actuators, which was discovered with Np-Pt in 2003 by Weismüller et al. [272]. In the said work, they created a continuous mesh structure made of Pt with nanoscale porosity and measured the change in electrochemical potential upon immersion in different electrolytes, where they found a linear and reversible relationship between the strain and potential. This paved the way for the development of Np-metals for the fabrication of metallic artificial muscles. The way these materials operate as actuators is based on electrochemical actuation, which involves changing the material's surface stress by adjusting its free electron density at its interface. Since Np-metals have a high surface-to-volume ratio, they are particularly responsive to these changes, leading to detectable, reversible changes in their size or shape when exposed to an electrochemical stimulus, making them attractive for actuation [273].

Since then, researchers explored the actuation properties of precious metals like Ag, Au, and Pd, and have achieved favorable deformation rates [232,234,274]. To enhance surface stress changes and obtain a large strain amplitude, efforts were made to decrease the pore and ligament sizes of the Np-metals to increase their specific surface areas [234]. Np-Ag was produced by selectively dissolving Al from Ag-Al alloys, resulting in an actuator with reversible strains of 0.2–0.5%, comparable to what can be achieved with Np-Au and Np-Pt [232]. A maximum strain amplitude of 1.3% was also obtained for nanoporous gold-platinum (Np-AuPt) with a ~5 nm ligament/pore size [233]. Subsequently, Zhang and co-workers demonstrated that Np-Pd could achieve a driving strain of 3.28% by controlled hydrogen adsorption/absorption coupling [234], making this material attractive not only for electrochemical actuation but also for H<sub>2</sub> storage applications.

#### 4.2.2. Porous Non-Precious Metals, MOFs, and Their Nanostructures

While precious metals exhibit excellent performance in many respects for various applications, they are too expensive for practical use and researchers are, therefore, constantly searching for new ways to reduce costs. One way is by exploring non-precious metals as replacements or as more sustainable alternatives. As such, in a new class of porous hybrid nanomaterial, i.e., metal-organic-frameworks (MOFs), non-precious metals are more commonly used. Though these inorganic-organic hybrid nanomaterials could also contain precious metals [275], most common MOFs contain non-precious ones. As such, MOFs and nanoMOFs will be included in this subsection. In addition to cost reduction and sustainable sourcing, in certain applications, these non-precious metals outperform precious metals. For this reason, a subsection is devoted to the development of porous non-precious metals and their hierarchical nanostructures.

A prime example where non-precious metals are developed to replace precious metals is in catalysis, such as for water-splitting. The standard catalyst for HER is Pt or Pt-based (e.g., Pt/C), having excellent HER catalytic activity [276–278]. Ir and Ru are also precious metals showing outstanding HER activities [277,278]. Due to the reasons mentioned above, for the past few years, catalysts based on transition metals, such as Fe, Zr, Co, Nb, Ni, and V, have been explored as alternatives [277–283].

Ni-based catalysts, for example, are attractive since they exhibit alkaline stability and alkaline electroactivity [277–283]. One modification of Ni to improve its electrocatalytic activity is via the formation of nanoparticles/nanostructures (including porous ones) on the surface, which achieves this by enhancing the conductivity [284,285]. For example, Ni, Co-based porous (micro- to) nanospheres have been produced for HER catalysis [286]. Self-standing nanoporous Mo-NiO/Ni HER electrocatalysts with high specific surface area and appropriate energy for hydrogen adsorption–desorption has also been prepared by simple dealloying preparation resulting in low overpotential and stable measurements [287]. Bimetallic NiMo-nitride porous nanotubes (50 nm wall thickness, 140 nm inner tube

diameter) have also been produced as bifunctional catalysts for electrochemical (EC) water-splitting, delivering excellent stability and high current density for the overall water-splitting [283].

Strategies to fabricate hierarchical trimodal and bimodal porous copper by dealloying CuAl intermetallics using HCl and NaOH solutions were also presented by Kong et al. [288]. A one-pot route to produce hierarchical bimodal (macro-, meso-)porous Cu was reported by Liu et al. by dealloying CuAl alloys using NaOH at elevated temperatures. Porous Cu (~140 nm ligament/pore size) can also be produced by dealloying CuMn alloy in an ammonium sulfate solution at 85 °C [289]. The latter has been applied to 3D printed (by selective laser melting) structures to achieve hierarchical porous Cu. Meanwhile, Grosu and co-workers explored the near-eutectic compositions of CuMg alloys to create hierarchical trimodal nanoporous Cu (Np-Cu), with the smallest pores in the range of 10–90 nm [290]. Further, they observed that at these compositions, an excess of Mg results in the trimodal porosity, whereas an excess of Cu, creates large inclusions of the intermetallic CuMg<sub>2</sub>, which can help stiffen the structure. A similar approach was used previously to produce bimodal Np-Cu [291]. Such Np-Cu structures have been used in glucose sensing and electrocatalytic CO<sub>2</sub>RR [292,293].

Non-precious metals are also used in producing actuators. The actuation of Np-metals was first discovered and explored for precious metals and at present, most of the electrochemical actuators based on Np-metals are still made of precious metals. However, due to their slow response rate, poor stability, and small actuation amplitude, in addition to their cost, non-precious Np-metals are being explored. Note though that the principles of actuation of the Np-metals are slightly different for these two types. While they are both based on the changes in the lattice parameters and valence state, in precious metals, the former occurs due to their stability against chemical reactions, whereas in non-precious metals, the changes occur due to electric field-induced redox reactions. Of these non-precious metal actuators, Ni exhibits better performance, while Cu and Ti have also been explored [273]. Ternary alloys have also been developed for actuators. An example is nanoporous CoCuAl (Np-CCA) which shows stability during actuation in an alkaline environment and exhibits a strain amplitude higher than Np-Pt and Np-Ag. Its maximum strain rate ( $2.3 \times 10^{-5} \text{ s}^{-1}$ ) also showed its sensitivity to electrochemical stimulation [294].

Though technically not inorganic, and rather a hybrid of inorganic and organic materials, metal-organic frameworks (MOFs) are an important class of novel porous nanomaterials. They are highly ordered structures derived from organic ligands and transition metals via coordination polymerization [10,26]. MOFs are included in this subsection as most of them are made from non-precious metals, although, as mentioned, they can also be prepared using precious metals. Common metals used in MOFs include Zn, Ni, Fe, Mn, Co, Cu, Cr, and Zr. Interesting as well is the fact that MOFs can be used as templates for the synthesis of some porous inorganic nanostructures. Moreover, as of late, there has been a growing interest in nanoscale MOFs (nanoMOFs), which fit well the concept of nanomaterials that contain small-scale (micro-, meso-, nano-)porosity [10]. These nanoMOFs present numerous benefits, including the following:

- Having a small size, suitable for use in biomedicine;
- Their assembly into different possible nanostructures for separation applications, energy conversion and storage, and related devices (possible also due to their small size);
- Enhanced kinetics related to adsorption–desorption;
- Better active site accessibility resulting in enhanced catalytic performance.

MOFs have been used for the preparation of porous nanomaterials, including non-precious transition metal-based catalysts [93,210,295]. For example, Liang et al. produced Ni-, Co-based bimetallic phosphides as bifunctional electrocatalysts for EC water-splitting using nanoMOFs made of NiCo [295]. Such nanoMOFs prepared by hydrothermal synthesis present a flower-like hierarchical structure consisting of mesoporous MOF nanosheets (~50 nm thickness, ~500 nm width, and > 5 μm length). After phosphorization, the

resulting mesoporous nanoparticles (10–20 nm) arranged in a sheetlike array (due to initial precursor assembly) were used as catalysts.

Because of their small size, biocompatibility, and physiological stability, among other interesting properties, nanoMOFs are mainly used in biomedicine and biotechnology (drug delivery, bioimaging, therapy, biosensing), though they have yet to be established for clinical use [10,26,27,296]. Their device integration is also expected to be better due to their smaller size. NanoMOFs and their metal nanocomposites are also very attractive for catalysis due to the aforementioned benefits and the superior catalytic performance afforded by the nanocomposites [10,297]. The push for sustainability and green chemistry has also influenced the synthesis of MOFs towards green MOFs, especially for biomedical use. Biomaterial-based MOFs (bio-MOFs) are also being developed, addressing in the process the requirement towards biocompatibility and sustainability [26]. Further, exploiting mixed-component MOFs can result in more sophisticated MOFs (and nanoMOFs) [28]. An in-depth discussion on this topic will not be given here. Rather, the readers are pointed to excellent reviews and articles on MOFs and nanoMOFs [2,10,26–33].

#### 4.3. Porous Carbon Nanostructures and Derivatives

There are several allotropes of carbon for a wide range of applications. These include bulk materials, such as diamond, chars, and graphite, and nanomaterials, such as carbon nanotubes (CNTs) and graphene [13]. From graphite, one can derive porous carbon, although porous non-graphitic carbons also exist, such as activated carbons [298]. The latter contains a twisted network of defective graphene layers, which are cross-linked by aliphatic bridging groups. The substantial porosity in these materials comes from the imperfect packing and bending of the layers, which results in micro-voids/micropores of a needle-like shape. Perret and Ruland have carried out detailed SAXS studies on different types of microporous carbons, describing the changes in porosity due to certain treatment procedures [299]. Among the most prominent porous carbons are charcoals, carbon blacks, carbon fibers, glassy carbons, and various types of activated carbons [300]. A large variety of organic materials, such as wood, synthetic polymers, and phenolic resins, and small organic molecules such as furfuryl alcohol produce porous carbons upon suitable carbonization and activation processes. Activated carbons are thus one of the most prominent classes of porous materials with a plethora of possible industrial applications, such as gas separation (e.g., nitrogen from oxygen), gas purification, and catalysis [60].

Since then, developments have been made to explore and further exploit the use of porous carbons for modern technology [13]. Considering that other carbon allotropes existing as nanomaterials (i.e., nanocarbons) can also be porous, especially in the presence of defects, or depending on their synthesis and treatment, a plethora of newer porous carbon materials and applications can be found in the literature [13,15,46,47]. Some of them are therefore given here, especially those in view of hierarchical structures.

With the push for more economically sustainable approaches, porous carbon is being extracted from waste and other “non-precious” sources. For example, porous graphitic carbon has been extracted from an invasive plant and then used for low-cost perovskite solar cells as both the sustainable hole-transporting material and the counter electrode, achieving with the best-performing device a power conversion efficiency (PCE) of 8.52% [301].

Porous carbon materials with low dimensionality (low D) have also become attractive for various applications requiring large specific surface areas and high electrical conductivity. Such applications include electrochemical actuators, for which the properties of these low-D porous carbon materials result in large capacitance and ion storage and high electrochemical-mechanical performance. Examples of these materials include single-walled CNTs (SWCNTs), vertically aligned CNT arrays, and 3D nanocomposite of porous carbons [302–305]. The last one includes the work of Lu et al., which presents a nanocomposite made of porous carbon comprising multi-walled CNTs (MWCNTs) and reduced graphene oxide (RGO) [304]. The electrodes made of pure RGO and MWCNT have an average pore size of ~4 nm and ~21 nm, respectively, whereas the RGO/MWCNT hybrid

presents a small average pore size of ~6.5 nm (similar to RGO) but increased range of up to 70 nm (similar to MWCNT), indicating a likely restacked RGO nanosheets in the porous network which could make the ion migration difficult and consequently resulting in a frequency-dependent volume expansion and quantum mechanical elongation.

Specifically, graphene oxide (GO) can be considered a form of the allotrope graphene, or an intermediate that can be reduced to RGO to somehow return to the graphene structure. The porous carbon nanomaterial graphene has been considered a wonder material. Since its discovery in 2004 [306], graphene has been quickly developed and characterized, including its many synthesis procedures for different applications. Specifically, there has been an interest in improving its dispersion and preventing its re-stacking or aggregation to fully utilize its large surface area and desirable electronic properties. An approach developed to address this is to form a hierarchical 3D network structure of these porous 2D sheets (also known as graphene sponges, aerogels, templates, and foams). The result is a material with very low density but high conductivity and strength due to the increased surface area and pore volume. This approach has also been applied to CNTs, GOs and RGOs [47]. For interest in this topic, one can take a look at the reviews of Kausar [46], Chabot et al. [47], and Pavlenko et al. [13]. The last one especially provides an updated and comprehensive review of templated porous carbons (including those of carbon sponges), their applications, and the effects of confinement of different proteins and liquids within the porous carbon matrices.

Interestingly, a similar hierarchical structure formation can be done with pores also at smaller scales. Firstly, template-synthesis approaches can be used to form pores of various sizes, including macro-meso-microporous scale, even with just hard templates—as usually soft templates are needed for the smaller pores [307]. Ordered pore structuring, even at the mesopore scale, down to several hundreds of nanometers in thickness, has been achieved in the past [308]. Using hard (silica) templates and polyaramide precursors, functionalized, hierarchical OM carbon (OMC) materials that replicate closely the silica templates at the nano- and micrometer scale were achieved using nanocasting [309]. Additionally, the hierarchical 3D-interconnected network of OMCs has also proved useful for microwave absorption (when the microstructure and thickness are optimized for the purpose) [310] and for high performance of lithium-ion batteries (since they can be used for binder-free anodes, enabling electron transport and accessibility of Li ions) [311]. Unsurprisingly as well, such known strategies to control the pore structure have now afforded the creation of hierarchical porous OMC nanomaterials. For example, OMC nanorods have been created as a supercapacitor electrode material with a soft template-based self-assembly procedure [312]. Moreover, the nanorods show bimodal meso-, nano-porosity of ~4 nm and ~16 nm pore diameters, with the order staying intact. These porous nanorods showed excellent supercapacitor performance, likely due to their high specific surface area, in addition to their unique porous nanostructure (Figure 10). Through a templated approach, a porous carbon nanowire array (140 nm nanowire diameter, 15  $\mu$ m nanowire length, and ~50 nm pore size) has also been developed for SERS (Figure 3a), resulting in a high EF ~  $10^6$  achieved via chemical mechanism (charge-transfer resonance) [68].

With the advent of new materials, which can also be used as host materials, more sophisticated structures of porous OMC nanomaterials have been possible. An example is the construction of a 2D-2D heterostructured composite between MXene-derived carbon and OMC (MDC-OMC) (Figure 11), which, due to its unique structure and the synergy of the components, exhibits outstanding supercapacitor performance compared to its pristine 2D counterparts [313].

MXenes, which are 2D (early) transition metal carbides (and/or nitrides), have also been made porous [314]. Of interest to this review is the formation of in-plane pores within these 2D sheets, which affords more exposed surface sites enabling efficient transport properties of guest molecules/materials/ions. For example, Ren et al. used oxidative etching catalyzed by metallic ions to form porous  $\text{Ti}_3\text{C}_2\text{T}_x$  MXenes, in effect converting some sites into  $\text{TiO}_2$ . The formed metal oxide is then removed with HF, revealing a uniformly mesoporous  $\text{Ti}_3\text{C}_2\text{T}_x$  (pore size ~4–6 nm) [314,315].

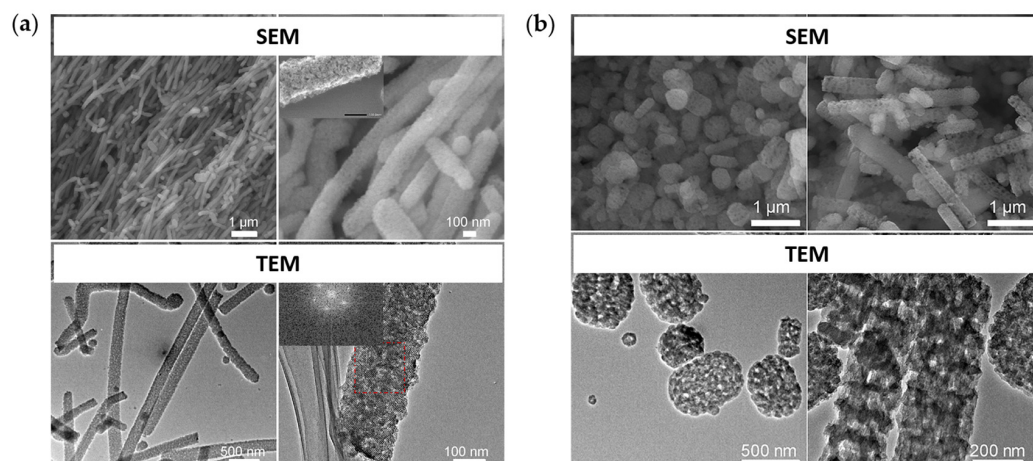


**Figure 10.** Hierarchically ordered mesoporous carbon (OMC) nanorods prepared using surfactant and polymer templates: (a) SEM (top) and TEM (bottom) images of the OMC nanorods; (b) SEM (top) and TEM (bottom) showing the changes in the nanomorphology with the change of the polymer used (left images—with polymer L31; right images—with L35). Reprinted (adapted) with permission from Du, G.; Wang, H.; Liu, J.; Sun, P.; Chen, T. Hierarchically Porous and Orderly Mesostructured Carbon Nanorods with Excellent Supercapacitive Performance. *ACS Appl. Nano Mater.* 2022, 5, 13384–13394, doi:10.1021/acsanm.2c03040. Copyright 2022 American Chemical Society [312].

Metal oxides and conducting polymers have been added to nanocarbons to introduce more reactive sites; however, due to their poor miscibility, the conductivity and charge transfer of the resulting electrode are severely compromised. Doping was carried out to harness the intrinsic property of the porous carbon network and introduce electrochemical activity [305]. Part of the widespread efforts to develop carbon-based metal-free catalysts and devices is adjusting the porous carbon material's electronic structure by doping with heteroatoms [316]. OMC materials, for example, have been doped with heteroatoms, as was in the work of Sánchez-Sánchez et al. (N- and O-doped OMCs), to improve their (pseudo)capacitive properties [309]. Such heteroatom-doped carbon materials also show notable activities for ORR—comparable to Pt/C—and include doped CNT- and graphene-based materials [317–319]. N-doping is a prime candidate for such purposes—as it can modify the electronic structure locally and increase the ion interaction and the density of the surface charge—and has been explored for batteries and supercapacitors [320,321].

Hierarchical porous carbons (HPCs) containing pores at different scales have also been synthesized for applications such as energy storage and CO<sub>2</sub> capture. HPCs have been synthesized from materials derived from biomass and serve as attractive supports for metal catalysts such as Ru and Cu [322,323]. These materials can also be N-doped [323].

In terms of zinc-air batteries (ZABs), the application of carbon-based metal-free catalysts has been limited due to their poor OER performance and quite high overpotential. As such other porous carbon-derivatives were explored, including porous graphitic carbon nitride (g-C<sub>3</sub>N<sub>4</sub>), which Wang et al. combined with 2D black phosphorus (BP) covalently (BP-CN-c) to achieve a bifunctional metal-free catalytic material that exhibits both high OER and excellent ORR activities for use in ZABs [316].

Porous g-C<sub>3</sub>N<sub>4</sub> has also been incorporated in the development of an electrochemical/electromechanical ionic actuator (Figure 12). Specifically, hierarchically porous g-C<sub>3</sub>N<sub>4</sub> nanosheets were combined with a small amount of CNTs to stabilize the structure and with an interpenetrating electrolytic polymer network for fast ion migration to fabricate an ionic actuator with a fast and stable actuation response (~0.5% in 300 ms and up to 100,000 cycles) and a large equilibrium electromechanical strain of ~0.93% [305]. The authors attribute the actuator's high electromechanical motion (Figure 12a) from the increased charge density and enhanced cation-interaction of the nitrogen-active sites (Figure 12b), while the hierarchical

(micro-, meso-)porous network played a major role in the volume expansion of the electrode, especially those with pores close to the size of the cation enabling intercalation-deintercalation.

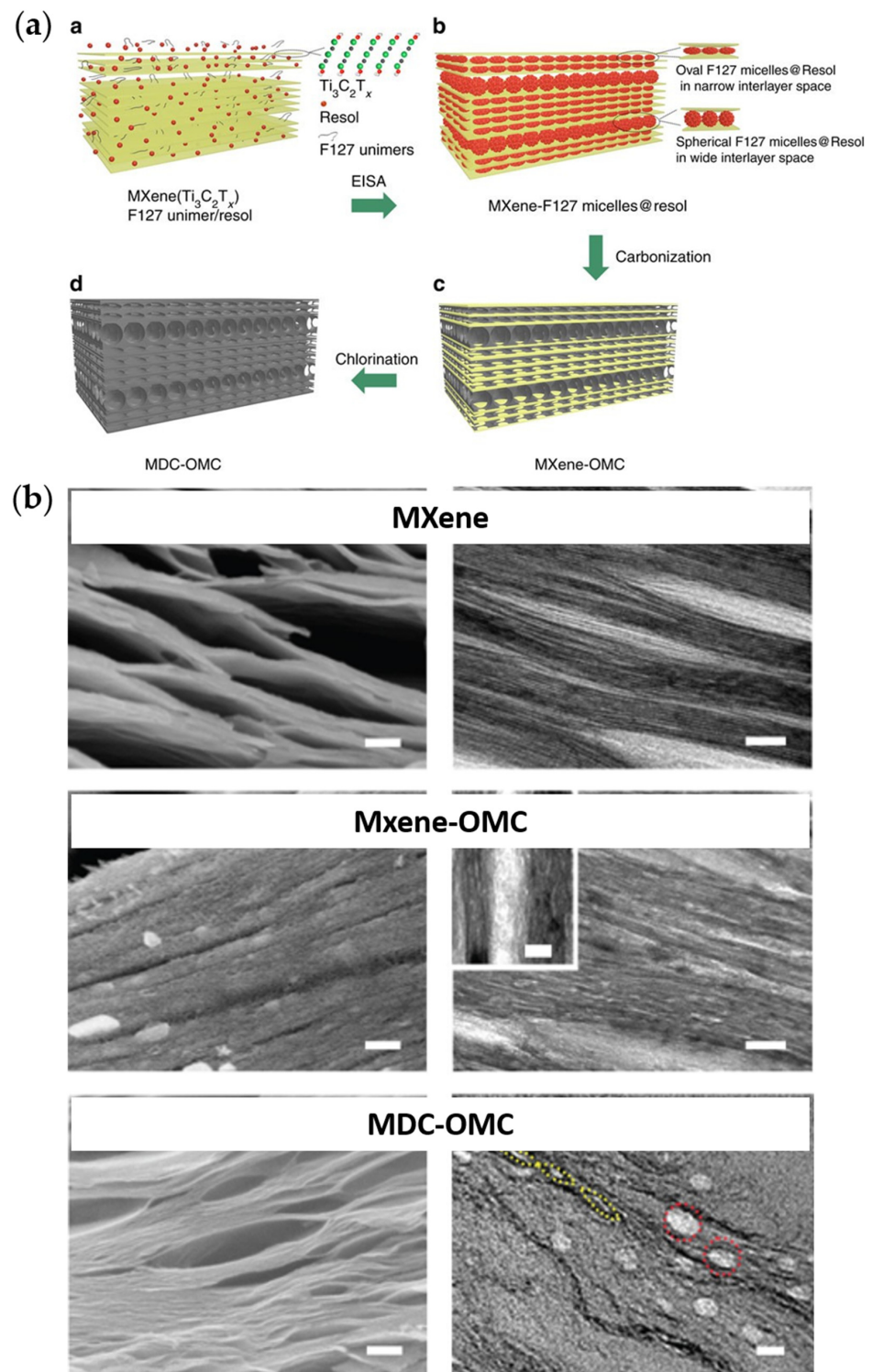


**Figure 11.** Hierarchical 2D-2D heterostructures of alternating MXene-derived carbon (MDC) layers and 2D ordered mesoporous carbon (OMC) layers (MDC-OMC): (a) a schematic diagram showing the preparation; (b) SEM (left) and TEM (right) images of the MXene, MXene-OMC, and MDC-OMC. Scale bars of 100 nm for images on the left and 20 nm for images on the right. Reprinted (adapted) with permission from [313]. Copyright 2017, The Author(s). Published by Springer Nature. CC BY 4.0 license.

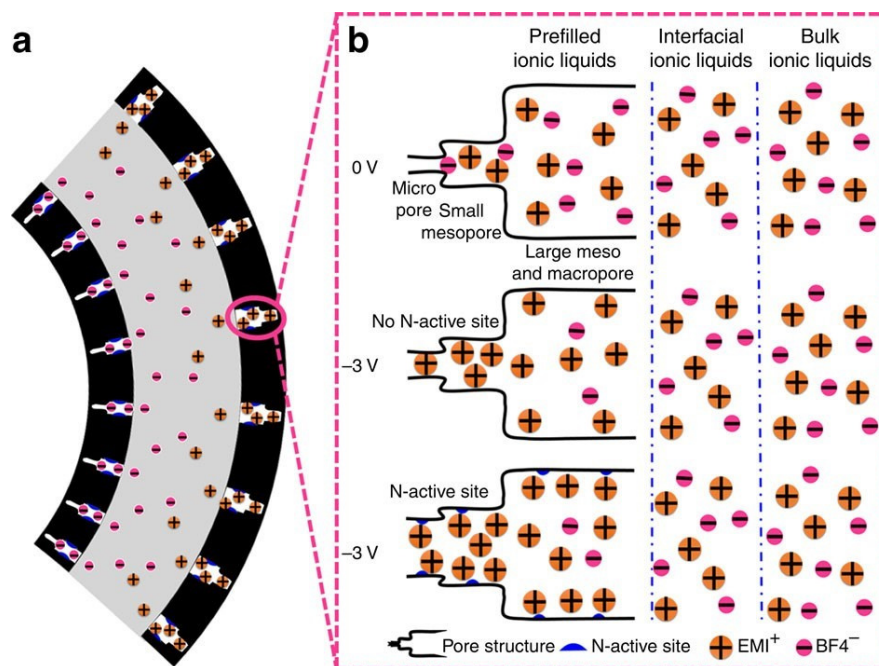


**Figure 12.** A schematic of the actuation mechanism of a porous graphitic carbon nitride ( $g\text{-C}_3\text{N}_4$ ) actuator: (a) illustration of the bending motion of the porous  $g\text{-C}_3\text{N}_4$  actuator; (b) a schematic representation of the pore structure and the actuator's mechanical output due to the cations. Reprinted (adapted) with permission from [305]. Copyright 2015, The Author(s). Published by Springer Nature. CC BY 4.0 license.

### 5. Technological Advancement and (Hierarchical) Porous Nanomaterials

As mentioned above, the advancements in porous materials and nanomaterials have seemingly merged, resulting in the creation of nanoporous nanomaterials. This has likely been a step towards a desired target architecture in terms of design complexity and functionality, which is pointing to hierarchical porous nanostructures. With the advancement in nanomaterial design and synthesis, technological advancements also come into play. These include digitalization, advancement in printing technologies, and AI.

Technology and nanomaterials development intertwine synergistically. That is, the advancements in nanomaterials contribute to technological development. In turn, technological advancements can also further push forward nanomaterial development. In the previous sections, the wide application of nanoporous nanomaterials in diverse fields has been presented. For example, porous nanomaterial incorporation into devices such as nano (bio)sensors have resulted in significant improvements in device functionality and performance. The large surface area afforded by these porous nanomaterials, for instance, resulted in increased sensitivity and specificity. Alongside this, the advent of AI resulted in the development of AI-based techniques. As such, the performance of devices such as biosensors can nowadays be further improved by combining the use of porous nanomaterials with AI-based diagnostic techniques. AI can analyze data from these nano biosensors to identify patterns and make accurate predictions about the presence or concentration of viruses. AI algorithms can process complex signals obtained from the interactions occurring at the nanoporous surfaces where viral particles are captured, enabling discernment between true signals and noise. Therefore, the combined use of advanced nanomaterials and AI techniques could further enhance the sensitivity and specificity of biosensors, enabling rapid, precise, and potentially human intervention-free detection of pathogens [324]. Similarly, nanopore-based sequencing and nanosensors have been applied for early diagnosis of pandemics and for discovering novel targets, whereas AI-based algorithms help significantly improve the accuracy, reliability, and performance of these nano diagnostics. For example, AI has been used in interpreting molecular profiling

from the data obtained using these nanomaterial-based technologies, including those that incorporate porous nanomaterials. AI is also being developed for biomarker profiling in intelligent bionanosensors [325]. Generally, devices in AI technologies, such as transistors can also be incorporated with nanomaterials for enhanced device performance and faster algorithm response [324].

In terms of therapeutics and nanomedicine, AI has also been applied for drug loading, therapeutic synergism (i.e., drug combination strategy), designing nanomedicine for personalized drug targeting, dosing and potency prediction, nanotheranostics, and nanotoxicity prediction. This is possible as AI is useful in intelligently handling big-data and omics profiling for optimized drug selection, optimizing drug combinations and potency, computer modeling, simulations, structure screening, de novo design, and properties prediction for drug discovery, drug repurposing, analyzing and pre-screening to identify targets (e.g., in patient stratification) and planning treatments. For interest in this topic, readers are directed to the review of Tan et al. [325].

In addition to the AI technologies that incorporate nanoporous materials and fields in which both AI and nanoporous nanomaterials are incorporated, such as the biomedical field for which applications are presented above, AI can also be used in guiding the design of porous nanomaterials and predicting their properties [39]. Further, AI can be used in the 3D printing of such nanoporous materials. While 3D printing has been vastly used and developed for porous polymer-based microstructures [326,327], it has also gained popularity for fabricating inorganic structures, including porous nanomaterials. For example, the recent work of Song and co-workers demonstrated the applicability of high-precision 3D microprinting to a vast variety of porous inorganic materials by solidification of inorganic nanocrystals [44]. The 3D microprinting of inorganic porous nanomaterials, especially AI-aided approaches, likely stemmed as a next step from the development of microprinting of inorganic structures such as porous/colloidal glasses [327,328] and the digitalization of the printing processes of such structures [329].

Three-dimensional microprinting using digital designs has also been developed for inorganic microstructures, such as metals [330–332], semiconductors [332], insulators/dielectrics [333], and their composites [334]. This technique has been demonstrated with nanoscale resolution using silica nanoparticles by Wen et al. [333]. Digitalization has also been incorporated into the control of the printing process such as in digital light processing (DLP), enabling the digitalized control of micromirror devices to produce patterned light, which together with photosensitive resins, allows the formation of detailed microstructures [335]. The 3D microprinting of hierarchical porous architectures (across seven orders of length scales) has also been demonstrated by a team at Cornell University using an ink made of zirconium oxide-based hybrid mesoporous photoresponsive ligand on inorganic core (PLIC) nanoparticles [336]. Muldoon et al. wrote a review on high-precision 3D microprinting of microstructure and nanostructures, including porous ones, for biomedical and electronic devices [45]. Readers are encouraged to read the said review.

In summary, the link between modern technologies such as AI, digitalization, and 3D microprinting to porous nanomaterials has not only been by the incorporation of these nanomaterials in such technologies or combining the use of these advanced nanomaterials with these new technologies in various applications such as the above-presented biomedical ones. These technological advancements have also been implemented and are currently still being developed towards progressing porous nanomaterials in terms of their design and fabrication. These technologies enable the formation of functional, customizable, and even intricate (hierarchical) porous nanomaterials/nanostructures.

## 6. Conclusions

Porous inorganic nanomaterials are being developed to incorporate or enhance specific material properties, such as increased surface area and associated functionalities, for various applications. Here, it has become apparent that the growing complexity in nanos-

structural design across different material compositions is gearing towards hierarchical porous nanomaterials. The trend towards hierarchical nanostructures highlights the essential role of porous nanomaterials in advancing nanostructure evolution to meet diverse technological needs. This is not surprising considering the prevalence of hierarchy in nature. By incorporating hierarchy in materials design, several functionalities can be provided that are difficult to achieve otherwise. Here, this is evident for porous nanomaterials.

In addition to naturally existing porous nanomaterials, synthetic ones have been prepared by different approaches which may or may not include the use of templates, and in many examples, use combined techniques. Though different approaches are preferred for certain material types, common techniques have been used across different material types. This includes hydrothermal, templated, and sol-gel techniques, as examples. Dealloying techniques are prevalently seen for metallic nanostructures, and despite the selective nature of retaining more noble elements in this process, they have been extensively applied for both precious and non-precious metals. Studies include approaches of not only resorting to the usage of smaller amounts of the noble elements and more of the non-precious transition elements but also playing around with certain phase transitions (for example, eutectic compositions in Cu-Mg for Np-Cu) to further tweak the porosity and other properties of the resulting porous material.

Further, the different material types considered here have different properties unique to them, which result in differences in the details of their preparation and use. Nevertheless, their (nano)porous nature and their nanoscale size result in common characteristics beneficial for the plethora of applications that they have been developed for. These include:

1. Small (nano) size;
2. Large surface area;
3. Accessibility of more active/adsorption sites due to the pores/porous network;
4. Relatively more reactive/active sites due to the exposed surface (uncoordinated atoms);
5. Lightweight (compared to bulk; both due to the dimension and presence of voids).

These common characteristics make these porous nanomaterials attractive for small device integration. Their high surface area also results in their incorporation, or at least consideration, for (bio)sensing, SERS, and electrode use.

In porous amorphous nanomaterials, the contradicting results obtained for different examples regarding the effect of porosity on the material's mechanical properties point to the need for further investigations. Some studies show the benefits of the presence of pores on their mechanical properties [183], whereas it has also been prevalent that pores can degrade the mechanical properties to the point of failure due to the formation of microcracks [201].

A common trend seen for inorganic porous nanomaterials is their use as templates/precursors to fabricate other porous nanomaterials (i.e., producing novel porous nanostructures from existing porous nanostructures). This approach adds another level of ingenuity, allowing for the creation of even more sophisticated novel materials in the future—considering the novel materials as well, such as MOFs and MXenes, their hierarchical structures, hybrids, and composites. Such new materials would lead to the formation of more complex but interesting hierarchical porous structures. Moreover, this trend is likely to continue and due to the increasing amounts of designed/discovered (hierarchical) porous nanomaterials, it can be expected that this will further contribute to the exponential increase in designed/engineered porous nanostructures/nanomaterials.

The complexity in the design of porous nanomaterials in the future is expected not only through the formation of hierarchical porous structures but also by resorting to the formation of mixed components or composites as seen in many examples presented here (mixed-component MOFs and hierarchical heterostructures, for instance). Such design complexity is expected to increase with the increasing demand for multifunctional materials. In turn, more studies to understand the influence of each component and the degree of heterogeneity and complexity on the material property need to be carried out. Doing so

will enable further design optimization, future design evolution, and obtaining valuable inputs for possible use in predictive technologies (e.g., through the use of AI).

The advent of new technologies, such as highly precise 3D microprinting combined with AI prediction of nanoporous materials, present almost endless opportunities for creating hierarchical porous nanomaterials. These are expected to even further increase the achievable amount and complexity of hierarchical porous nanostructures that can be designed and engineered in the future (as apparent in the latter parts of Section 5). A recent article on high-precision 3D microprinting of a multiscale porous gold structure, made from a few nanometers of multibranched, interconnected thick Au wires/fibers, has effectively illustrated how one could expect these advanced technologies to enable the fabrication of nanoporous gold and other metals in the future [38].

On the other hand, the vast amount of synthesized novel porous nanomaterials for biomedical applications, such as nanoMOFs, would also entail further biocompatibility, nanotoxicology, and nanosafety tests and clinical trials so that they can be used for therapeutic and nanomedicine. The increasing push for sustainability and green chemistry will also require changes in porous nanomaterial fabrication towards more eco-friendly approaches. As such, it is expected that not only biomaterial-based porous (inorganic) nanomaterials and hybrids (e.g., bio-MOFs [26]) will increasingly become more popular, but also that the reactants, solvents, other materials, and other details of the synthesis steps will be biocompatible and sustainable.

**Author Contributions:** Conceptualization, C.J.Q.; formal analysis, A.J., T.M., N.F.-N. and C.J.Q.; data curation, C.J.Q.; writing—original draft preparation, A.J., T.M., N.F.-N. and C.J.Q.; writing—review and editing, A.J., T.M., N.F.-N. and C.J.Q.; visualization, C.J.Q.; supervision, C.J.Q.; project administration, C.J.Q. All authors have read and agreed to the published version of the manuscript.

**Funding:** This research received no funding.

**Data Availability Statement:** No new data were created. Data on the research count presented here is available from Web of Science. Data sharing does not apply to this article.

**Acknowledgments:** The authors would like to thank all the scientists they had fruitful discussions with regarding porous nanomaterials and hierarchical nanostructures. C.J.Q. especially acknowledges Inez Weidinger (TU Dresden), Hoang Khoa Ly (TU Dresden), Ibrahim Halil Öner (TU Dresden), Xia Wang (currently, in MPI CPFS), Minghao Yu (TU Dresden), Xinlian Feng (TU Dresden), Ahmad Omar (IFW Dresden), Andrea Voß (IFW Dresden), Viktoriia Shtefan (IFW Dresden), Annett Gebert (IFW Dresden), Daria Mikhailova (IFW Dresden), Paola Rizzi (UniTo), and Kirti Tiwari (UniTo) for the interesting research works they had involving inorganic porous (nano)materials.

**Conflicts of Interest:** The authors declare no conflicts of interest. The funders had no role in the design of the study; in the collection, analyses, or interpretation of data; in the writing of the manuscript; or in the decision to publish the results.

## References

1. Guo, D.-J.; Ding, Y. Porous Nanostructured Metals for Electrocatalysis. *Electroanalysis* **2012**, *24*, 2035–2043. [[CrossRef](#)]
2. Sheta, S.M.; El-Sheikh, S.M. Nanomaterials and Metal-Organic Frameworks for Biosensing Applications of Mutations of the Emerging Viruses. *Anal. Biochem.* **2022**, *648*, 114680. [[CrossRef](#)] [[PubMed](#)]
3. Baig, N.; Kammakakam, I.; Falath, W. Nanomaterials: A Review of Synthesis Methods, Properties, Recent Progress, and Challenges. *Mater. Adv.* **2021**, *2*, 1821–1871. [[CrossRef](#)]
4. Datt, A.; Ndiege, N.; Larsen, S.C. Development of Porous Nanomaterials for Applications in Drug Delivery and Imaging. In *Nanomaterials for Biomedicine*; ACS Symposium Series; American Chemical Society: Washington, DC, USA, 2012; Volume 1119, pp. 239–258. ISBN 978-0-8412-2718-7.
5. Quesada-González, D.; Merkoçi, A. Nanomaterial-Based Devices for Point-of-Care Diagnostic Applications. *Chem. Soc. Rev.* **2018**, *47*, 4697–4709. [[CrossRef](#)] [[PubMed](#)]
6. Wen, N.; Zhang, L.; Jiang, D.; Wu, Z.; Li, B.; Sun, C.; Guo, Z. Emerging Flexible Sensors Based on Nanomaterials: Recent Status and Applications. *J. Mater. Chem. A* **2020**, *8*, 25499–25527. [[CrossRef](#)]
7. Kianfar, E.; Sayadi, H. Recent Advances in Properties and Applications of Nanoporous Materials and Porous Carbons. *Carbon Lett.* **2022**, *32*, 1645–1669. [[CrossRef](#)]

8. Du, C.; Li, P.; Zhuang, Z.; Fang, Z.; He, S.; Feng, L.; Chen, W. Highly Porous Nanostructures: Rational Fabrication and Promising Application in Energy Electrocatalysis. *Coord. Chem. Rev.* **2022**, *466*, 214604. [[CrossRef](#)]
9. Gleiter, H. Nanostructured Materials: Basic Concepts and Microstructure. *Acta Mater.* **2000**, *48*, 1–29. [[CrossRef](#)]
10. Cai, X.; Xie, Z.; Li, D.; Kassymova, M.; Zang, S.Q.; Jiang, H.L. Nano-Sized Metal-Organic Frameworks: Synthesis and Applications. *Coord. Chem. Rev.* **2020**, *417*, 213366. [[CrossRef](#)]
11. Querebillo, C.J. A Review on Nano Ti-Based Oxides for Dark and Photocatalysis: From Photoinduced Processes to Bioimplant Applications. *Nanomaterials* **2023**, *13*, 982. [[CrossRef](#)] [[PubMed](#)]
12. Yang, X.-Y.; Léonard, A.; Lemaire, A.; Tian, G.; Su, B.-L. Self-Formation Phenomenon to Hierarchically Structured Porous Materials: Design, Synthesis, Formation Mechanism and Applications. *Chem. Commun.* **2011**, *47*, 2763–2786. [[CrossRef](#)] [[PubMed](#)]
13. Pavlenko, V.; Khosravi, H.S.; Żóttowska, S.; Haruna, A.B.; Zahid, M.; Mansurov, Z.; Supiyeva, Z.; Galal, A.; Ozoemena, K.I.; Abbas, Q.; et al. A Comprehensive Review of Template-Assisted Porous Carbons: Modern Preparation Methods and Advanced Applications. *Mater. Sci. Eng. R Rep.* **2022**, *149*, 100682. [[CrossRef](#)]
14. Scandura, G.; Kumari, P.; Palmisano, G.; Karanikolos, G.N.; Orwa, J.; Dumée, L.F. Nanoporous Dealloyed Metal Materials Processing and Applications—A Review. *Ind. Eng. Chem. Res.* **2023**, *62*, 1736–1763. [[CrossRef](#)]
15. Fang, B.; Kim, J.H.; Kim, M.-S.; Yu, J.-S. Hierarchical Nanostructured Carbons with Meso–Macroporosity: Design, Characterization, and Applications. *Acc. Chem. Res.* **2013**, *46*, 1397–1406. [[CrossRef](#)] [[PubMed](#)]
16. Charkhi, A.; Kazemini, M.; Ahmadi, S.J.; Kazemian, H. Fabrication of Granulated NaY Zeolite Nanoparticles Using a New Method and Study the Adsorption Properties. *Powder Technol.* **2012**, *231*, 1–6. [[CrossRef](#)]
17. Dzyazko, Y.S.; Rozhdestvenska, L.M.; Kudelko, K.O.; Fedina, I.V.; Ponomaryova, L.M.; Nikovska, G.M.; Dzyazko, O.G. Hydrated Iron Oxide Embedded to Natural Zeolite: Effect of Nanoparticles and Microparticles on Sorption Properties of Composites. *Water Air Soil Pollut.* **2022**, *233*, 205. [[CrossRef](#)]
18. Zou, L.; Ge, M.; Zhao, C.; Meng, Q.; Wang, H.; Liu, X.; Lin, C.-H.; Xiao, X.; Lee, W.-K.; Shen, Q.; et al. Designing Multiscale Porous Metal by Simple Dealloying with 3D Morphological Evolution Mechanism Revealed via X-Ray Nano-Tomography. *ACS Appl. Mater. Interfaces* **2020**, *12*, 2793–2804. [[CrossRef](#)] [[PubMed](#)]
19. Lee, S.; Lee, Y.; Kim, D.H.; Moon, J.H. Carbon-Deposited TiO<sub>2</sub> 3D Inverse Opal Photocatalysts: Visible-Light Photocatalytic Activity and Enhanced Activity in a Viscous Solution. *ACS Appl. Mater. Interfaces* **2013**, *5*, 12526–12532. [[CrossRef](#)] [[PubMed](#)]
20. Wharry, J.P.; Nemets, G.; Marrero, E.; Emerson, J.; Gehmlich, N.; Okuniewski, M.A.; Clement, C.D.; Mao, K.S. Multimodal Characterization of Porosity in Advanced Manufactured and Welded Nuclear Structural Alloys. *Microsc. Microanal.* **2023**, *29*, 1536–1537. [[CrossRef](#)]
21. Zhao, B.; Collinson, M.M. Well-Defined Hierarchical Templates for Multimodal Porous Material Fabrication. *Chem. Mater.* **2010**, *22*, 4312–4319. [[CrossRef](#)]
22. Smått, J.-H.; Schunk, S.; Lindén, M. Versatile Double-Templating Synthesis Route to Silica Monoliths Exhibiting a Multimodal Hierarchical Porosity. *Chem. Mater.* **2003**, *15*, 2354–2361. [[CrossRef](#)]
23. Hessian, M.; Prouzet, E. Synthesis of Hierarchical Porous Silica by Sol-Gel of Sodium Silicate and Nanoemulsion Templating: Effective Combination Conditions. *ChemistrySelect* **2021**, *6*, 1440–1447. [[CrossRef](#)]
24. Chen, L.-H.; Li, Y.; Su, B.-L. Hierarchy in Materials for Maximized Efficiency. *Natl. Sci. Rev.* **2020**, *7*, 1626–1630. [[CrossRef](#)] [[PubMed](#)]
25. Liao, H.-C.; Tsao, C.-S.; Jao, M.-H.; Shyue, J.-J.; Hsu, C.-P.; Huang, Y.-C.; Tian, K.-Y.; Chen, C.-Y.; Su, C.-J.; Su, W.-F. Hierarchical i-p and i-n Porous Heterojunction in Planar Perovskite Solar Cells. *J. Mater. Chem. A* **2015**, *3*, 10526–10535. [[CrossRef](#)]
26. Rabiee, N.; Atarod, M.; Tavakolizadeh, M.; Asgari, S.; Rezaei, M.; Akhavan, O.; Pourjavadi, A.; Jouyandeh, M.; Lima, E.C.; Hamed Mashhadzadeh, A.; et al. Green Metal-Organic Frameworks (MOFs) for Biomedical Applications. *Microporous Mesoporous Mater.* **2022**, *335*, 111670. [[CrossRef](#)]
27. Chattopadhyay, K.; Mandal, M.; Maiti, D.K. Smart Metal-Organic Frameworks for Biotechnological Applications: A Mini-Review. *ACS Appl. Bio Mater.* **2021**, *4*, 8159–8171. [[CrossRef](#)] [[PubMed](#)]
28. Viciano-Chumillas, M.; Liu, X.; Leyva-Pérez, A.; Armentano, D.; Ferrando-Soria, J.; Pardo, E. Mixed Component Metal-Organic Frameworks: Heterogeneity and Complexity at the Service of Application Performances. *Coord. Chem. Rev.* **2022**, *451*, 214273. [[CrossRef](#)]
29. Lahcen, A.A.; Surya, S.G.; Beduk, T.; Vijjapu, M.T.; Lamaoui, A.; Durmus, C.; Timur, S.; Shekhah, O.; Mani, V.; Amine, A.; et al. Metal–Organic Frameworks Meet Molecularly Imprinted Polymers: Insights and Prospects for Sensor Applications. *ACS Appl. Mater. Interfaces* **2022**, *14*, 49399–49424. [[CrossRef](#)]
30. Beg, S.; Rahman, M.; Jain, A.; Saini, S.; Midoux, P.; Pichon, C.; Ahmad, F.J.; Akhter, S. Nanoporous Metal Organic Frameworks as Hybrid Polymer–Metal Composites for Drug Delivery and Biomedical Applications. *Drug Discov. Today* **2017**, *22*, 625–637. [[CrossRef](#)] [[PubMed](#)]
31. Zhang, H.; Hu, Q.; Liu, J.; Zhang, P.; Fu, S.; Wu, S. Iron–Organic Framework Nanoparticle-Supported Tungstosilicic Acid as a Catalyst for the Biginelli Reaction. *ACS Appl. Nano Mater.* **2022**, *5*, 16987–16995. [[CrossRef](#)]
32. Kalaj, M.; Bentz, K.C.; Ayala, S.; Palomba, J.M.; Barcus, K.S.; Katayama, Y.; Cohen, S.M. MOF-Polymer Hybrid Materials: From Simple Composites to Tailored Architectures. *Chem. Rev.* **2020**, *120*, 8267–8302. [[CrossRef](#)] [[PubMed](#)]
33. Wang, Z.; Zou, J.; Wang, Y.; Fu, A.; Guo, Y.-G.; Li, H. (Ni)MOF Interpenetrated with MnO<sub>2</sub> Nanothorns Anchored on Porous Carbon Cloth as Self-Standing Cathode for High-Performance Supercapacitors. *Int. J. Electrochem. Sci.* **2022**, *17*, 220843. [[CrossRef](#)]

34. McCue, I.; Benn, E.; Gaskey, B.; Erlebacher, J. Dealloying and Dealloyed Materials. *Annu. Rev. Mater. Res.* **2016**, *46*, 263–286. [[CrossRef](#)]
35. Gu, D.; Schüth, F. Synthesis of Non-Siliceous Mesoporous Oxides. *Chem. Soc. Rev.* **2013**, *43*, 313–344. [[CrossRef](#)] [[PubMed](#)]
36. Cundy, C.S.; Cox, P.A. The Hydrothermal Synthesis of Zeolites: History and Development from the Earliest Days to the Present Time. *Chem. Rev.* **2003**, *103*, 663–702. [[CrossRef](#)] [[PubMed](#)]
37. Yu, J.; Ran, R.; Zhong, Y.; Zhou, W.; Ni, M.; Shao, Z. Advances in Porous Perovskites: Synthesis and Electrocatalytic Performance in Fuel Cells and Metal–Air Batteries. *Energy Environ. Mater.* **2020**, *3*, 121–145. [[CrossRef](#)]
38. Derakhshankhah, H.; Jafari, S.; Sarvari, S.; Barzegari, E.; Moakedi, F.; Ghorbani, M.; Varnamkhasti, B.S.; Jaymand, M.; Izadi, Z.; Tayebi, L. Biomedical Applications of Zeolitic Nanoparticles, with an Emphasis on Medical Interventions. *Int. J. Nanomed.* **2020**, *15*, 363–386. [[CrossRef](#)] [[PubMed](#)]
39. Sastre, G.; Daeyaert, F.F. (Eds.) *AI-Guided Design and Property Prediction for Zeolites and Nanoporous Materials*; John Wiley and Sons Ltd.: Hoboken, NJ, USA, 2023; ISBN 978-1-119-81975-2.
40. Xu, D.; Lv, H.; Liu, B. Encapsulation of Metal Nanoparticle Catalysts Within Mesoporous Zeolites and Their Enhanced Catalytic Performances: A Review. *Front. Chem.* **2018**, *6*, 550. [[CrossRef](#)] [[PubMed](#)]
41. Schlumberger, C.; Thommes, M. Characterization of Hierarchically Ordered Porous Materials by Physisorption and Mercury Porosimetry—A Tutorial Review. *Adv. Mater. Interfaces* **2021**, *8*, 2002181. [[CrossRef](#)]
42. Van der Zalm, J.; Chen, S.; Huang, W.; Chen, A. Review—Recent Advances in the Development of Nanoporous Au for Sensing Applications. *J. Electrochem. Soc.* **2020**, *167*, 037532. [[CrossRef](#)]
43. Xiao, S.; Wang, S.; Wang, X.; Xu, P. Nanoporous Gold: A Review and Potentials in Biotechnological and Biomedical Applications. *Nano Sel.* **2021**, *2*, 1437–1458. [[CrossRef](#)]
44. Song, M.; Kim, Y.; Baek, D.S.; Kim, H.Y.; Gu, D.H.; Li, H.; Cuning, B.V.; Yang, S.E.; Heo, S.H.; Lee, S.; et al. 3D Microprinting of Inorganic Porous Materials by Chemical Linking-Induced Solidification of Nanocrystals. *Nat. Commun.* **2023**, *14*, 8460. [[CrossRef](#)] [[PubMed](#)]
45. Muldoon, K.; Song, Y.; Ahmad, Z.; Chen, X.; Chang, M.-W. High Precision 3D Printing for Micro to Nano Scale Biomedical and Electronic Devices. *Micromachines* **2022**, *13*, 642. [[CrossRef](#)] [[PubMed](#)]
46. Kausar, A. Scientific Worth of Polymer and Graphene Foam-Based Nanomaterials. *J. Chin. Adv. Mater. Soc.* **2018**, *6*, 779–800. [[CrossRef](#)]
47. Chabot, V.; Higgins, D.; Yu, A.; Xiao, X.; Chen, Z.; Zhang, J. A Review of Graphene and Graphene Oxide Sponge: Material Synthesis and Applications to Energy and the Environment. *Energy Environ. Sci.* **2014**, *7*, 1564. [[CrossRef](#)]
48. Sing, K.S.W. Reporting Physisorption Data for Gas/Solid Systems with Special Reference to the Determination of Surface Area and Porosity (Recommendations 1984). *Pure Appl. Chem.* **1985**, *57*, 603–619. [[CrossRef](#)]
49. Klobes, P.; Meyer, K.; Munro, R.G. *Porosity and Specific Surface Area Measurements for Solid Materials*; National Institute of Standards and Technology: Gaithersburg, MD, USA, 2006.
50. Zdravkov, B.; Čermák, J.; Šefara, M.; Janků, J. Pore Classification in the Characterization of Porous Materials: A Perspective. *Open Chem.* **2007**, *5*, 385–395. [[CrossRef](#)]
51. Du, X.; He, J. Hierarchically Mesoporous Silica Nanoparticles: Extraction, Amino-Functionalization, and Their Multipurpose Potentials. *Langmuir* **2011**, *27*, 2972–2979. [[CrossRef](#)] [[PubMed](#)]
52. Wawrzyńczak, A.; Nowak, I.; Woźniak, N.; Chudzińska, J.; Feliczak-Guzik, A. Synthesis and Characterization of Hierarchical Zeolites Modified with Polysaccharides and Its Potential Role as a Platform for Drug Delivery. *Pharmaceutics* **2023**, *15*, 535. [[CrossRef](#)] [[PubMed](#)]
53. Mansoori, G.A.; Soelaiman, T.F. Nanotechnology—An Introduction for the Standards Community. *J. ASTM Int.* **2005**, *2*, JAI13110. [[CrossRef](#)]
54. Bayda, S.; Adeel, M.; Tuccinardi, T.; Cordani, M.; Rizzolio, F. The History of Nanoscience and Nanotechnology: From Chemical–Physical Applications to Nanomedicine. *Molecules* **2019**, *25*, 112. [[CrossRef](#)]
55. Mekuye, B.; Abera, B. Nanomaterials: An Overview of Synthesis, Classification, Characterization, and Applications. *Nano Sel.* **2023**, *4*, 486–501. [[CrossRef](#)]
56. Feynman, R.P. There’s Plenty of Room at the Bottom. *Eng. Sci.* **1960**, *23*, 22–36.
57. Taniguchi, N. On The Basic Concept of Nano-Technology. In Proceedings of the International Conference on Production Engineering, Tokyo, Japan, 26–29 August 1974; pp. 18–23.
58. Buzzea, C.; Pacheco, I.L.; Robbie, K. Nanomaterials and Nanoparticles: Sources and Toxicity. *Biointerphases* **2007**, *2*, MR17–MR71. [[CrossRef](#)] [[PubMed](#)]
59. Xie, L.; Jin, Z.; Dai, Z.; Chang, Y.; Jiang, X.; Wang, H. Porous Carbons Synthesized by Templating Approach from Fluid Precursors and Their Applications in Environment and Energy Storage: A Review. *Carbon* **2020**, *170*, 100–118. [[CrossRef](#)]
60. Polarz, S.; Smarsly, B. Nanoporous Materials. *J. Nanosci. Nanotechnol.* **2002**, *2*, 581–612. [[CrossRef](#)]
61. Manzano, M.; Vallet-Regí, M. Mesoporous Silica Nanoparticles for Drug Delivery. *Adv. Funct. Mater.* **2020**, *30*, 1902634. [[CrossRef](#)]
62. Innocenzi, P.; Costacurta, S.; Kidchob, T.; Malfatti, L.; Falcaro, P.; Soler-Illia, G. Mesoporous Thin Films: Properties and Applications. In *Proceedings of the Sol-Gel Methods for Materials Processing*; Innocenzi, P., Zub, Y.L., Kessler, V.G., Eds.; Springer: Dordrecht, The Netherlands, 2008; pp. 105–123.

63. Grosso, D.; Cagnol, F.; Soler-Illia, G.J.A.A.; Crepaldi, E.L.; Amenitsch, H.; Brunet-Bruneau, A.; Bourgeois, A.; Sanchez, C. Fundamentals of Mesostructuring Through Evaporation-Induced Self-Assembly. *Adv. Funct. Mater.* **2004**, *14*, 309–322. [[CrossRef](#)]
64. Sakatani, Y.; Boissière, C.; Grosso, D.; Nicole, L.; Soler-Illia, G.J.A.A.; Sanchez, C. Coupling Nanobuilding Block and Breath Figures Approaches for the Designed Construction of Hierarchically Templated Porous Materials and Membranes. *Chem. Mater.* **2008**, *20*, 1049–1056. [[CrossRef](#)]
65. Ahn, S.H.; Kim, D.J.; Chi, W.S.; Kim, J.H. Hierarchical Double-Shell Nanostructures of TiO<sub>2</sub> Nanosheets on SnO<sub>2</sub> Hollow Spheres for High-Efficiency, Solid-State, Dye-Sensitized Solar Cells. *Adv. Funct. Mater.* **2014**, *24*, 5037–5044. [[CrossRef](#)]
66. Wang, L.; Zhu, Q.; Zhao, J.; Guan, Y.; Liu, J.; An, Z.; Xu, B. Nitrogen-Doped Hierarchical Porous Carbon for Supercapacitors with High Rate Performance. *Microporous Mesoporous Mater.* **2019**, *279*, 439–445. [[CrossRef](#)]
67. Qiu, D.; Cao, T.; Zhang, J.; Zhang, S.-W.; Zheng, D.; Wu, H.; Lv, W.; Kang, F.; Yang, Q.-H. Precise Carbon Structure Control by Salt Template for High Performance Sodium-Ion Storage. *J. Energy Chem.* **2019**, *31*, 101–106. [[CrossRef](#)]
68. Chen, N.; Xiao, T.-H.; Luo, Z.; Kitahama, Y.; Hiramatsu, K.; Kishimoto, N.; Itoh, T.; Cheng, Z.; Goda, K. Porous Carbon Nanowire Array for Surface-Enhanced Raman Spectroscopy. *Nat. Commun.* **2020**, *11*, 4772. [[CrossRef](#)] [[PubMed](#)]
69. Kumar, S.; Bhushan, P.; Bhattacharya, S. Fabrication of Nanostructures with Bottom-up Approach and Their Utility in Diagnostics, Therapeutics, and Others. In *Environmental, Chemical and Medical Sensors*; Bhattacharya, S., Agarwal, A.K., Chanda, N., Pandey, A., Sen, A.K., Eds.; Energy, Environment, and Sustainability; Springer: Singapore, 2018; pp. 167–198. ISBN 978-981-10-7750-0.
70. Galarneau, A.; Mehlhorn, D.; Guenneau, F.; Coasne, B.; Villemot, F.; Minoux, D.; Aquino, C.; Dath, J.-P. Specific Surface Area Determination for Microporous/Mesoporous Materials: The Case of Mesoporous FAU-Y Zeolites. *Langmuir* **2018**, *34*, 14134–14142. [[CrossRef](#)] [[PubMed](#)]
71. Kumar, S.; Malik, M.M.; Purohit, R. Synthesis of High Surface Area Mesoporous Silica Materials Using Soft Templating Approach. *Mater. Today Proc.* **2018**, *5*, 4128–4133. [[CrossRef](#)]
72. Yang, P.; Zhao, D.; Margolese, D.I.; Chmelka, B.F.; Stucky, G.D. Generalized Syntheses of Large-Pore Mesoporous Metal Oxides with Semicrystalline Frameworks. *Nature* **1998**, *396*, 152–155. [[CrossRef](#)]
73. Yang, P.; Deng, T.; Zhao, D.; Feng, P.; Pine, D.; Chmelka, B.F.; Whitesides, G.M.; Stucky, G.D. Hierarchically Ordered Oxides. *Science* **1998**, *282*, 2244–2246. [[CrossRef](#)] [[PubMed](#)]
74. Zhang, R.; Dai, H.; Du, Y.; Zhang, L.; Deng, J.; Xia, Y.; Zhao, Z.; Meng, X.; Liu, Y. P123-PMMA Dual-Templating Generation and Unique Physicochemical Properties of Three-Dimensionally Ordered Macroporous Iron Oxides with Nanovoids in the Crystalline Walls. *Inorg. Chem.* **2011**, *50*, 2534–2544. [[CrossRef](#)] [[PubMed](#)]
75. Ryu, J.; Yun, J.; Lee, J.; Lee, K.; Jang, J. Hierarchical Mesoporous Silica Nanoparticles as Superb Light Scattering Materials. *Chem. Commun.* **2016**, *52*, 2165–2168. [[CrossRef](#)] [[PubMed](#)]
76. Huang, X.; Zhao, G.; Wang, G.; Irvine, J.T.S. Synthesis and Applications of Nanoporous Perovskite Metal Oxides. *Chem. Sci.* **2018**, *9*, 3623–3637. [[CrossRef](#)]
77. Suzuki, N.; Osada, M.; Billah, M.; Allothman, Z.A.; Bando, Y.; Yamauchi, Y.; Hossain, M.S.A. Origin of Thermally Stable Ferroelectricity in a Porous Barium Titanate Thin Film Synthesized through Block Copolymer Templating. *APL Mater.* **2017**, *5*, 076111. [[CrossRef](#)]
78. Li, K.; Yang, J.; Huang, R.; Lin, S.; Gu, J. Ordered Large-Pore MesoMOFs Based on Synergistic Effects of TriBlock Polymer and Hofmeister Ion. *Angew. Chem.* **2020**, *132*, 14228–14232. [[CrossRef](#)]
79. Li, K.; Yang, J.; Gu, J. Hierarchically Porous MOFs Synthesized by Soft-Template Strategies. *Acc. Chem. Res.* **2022**, *55*, 2235–2247. [[CrossRef](#)]
80. Szcześniak, B.; Choma, J.; Jaroniec, M. Recent Advances in Mechanochemical Synthesis of Mesoporous Metal Oxides. *Mater. Adv.* **2021**, *2*, 2510–2523. [[CrossRef](#)]
81. Bashir, J.; Chowdhury, M.B.; Kathak, R.R.; Dey, S.; Tasnim, A.T.; Amin, M.A.; Kaneti, Y.V.; Masud, M.K.; Hossain, M.S.A. Electrochemical Fabrication of Mesoporous Metal-Alloy Films. *Mater. Adv.* **2023**, *4*, 408–431. [[CrossRef](#)]
82. Iqbal, M.; Li, C.; Wood, K.; Jiang, B.; Takei, T.; Dag, Ö.; Baba, D.; Nugraha, A.S.; Asahi, T.; Whitten, A.E.; et al. Continuous Mesoporous Pd Films by Electrochemical Deposition in Nonionic Micellar Solution. *Chem. Mater.* **2017**, *29*, 6405–6413. [[CrossRef](#)]
83. Li, C.; Jiang, B.; Wang, Z.; Li, Y.; Hossain, M.S.A.; Kim, J.H.; Takei, T.; Henzie, J.; Dag, Ö.; Bando, Y.; et al. First Synthesis of Continuous Mesoporous Copper Films with Uniformly Sized Pores by Electrochemical Soft Templating. *Angew. Chem. Int. Ed.* **2016**, *55*, 12746–12750. [[CrossRef](#)] [[PubMed](#)]
84. Tan, Y.; Steinmiller, E.M.P.; Choi, K.-S. Electrochemical Tailoring of Lamellar-Structured ZnO Films by Interfacial Surfactant Templating. *Langmuir* **2005**, *21*, 9618–9624. [[CrossRef](#)] [[PubMed](#)]
85. Jiokeng, S.L.Z.; Tonle, I.K.; Walcarius, A. Amino-Attapulgit/Mesoporous Silica Composite Films Generated by Electro-Assisted Self-Assembly for the Voltammetric Determination of Diclofenac. *Sens. Actuators B Chem.* **2019**, *287*, 296–305. [[CrossRef](#)]
86. Lytle, J.C.; Yan, H.; Turgeon, R.T.; Stein, A. Multistep, Low-Temperature Pseudomorphic Transformations of Nanostructured Silica to Titania via a Titanium Oxyfluoride Intermediate. *Chem. Mater.* **2004**, *16*, 3829–3837. [[CrossRef](#)]
87. Wen, X.; Zhang, D.; Yan, T.; Zhang, J.; Shi, L. Three-Dimensional Graphene-Based Hierarchically Porous Carbon Composites Prepared by a Dual-Template Strategy for Capacitive Deionization. *J. Mater. Chem. A* **2013**, *1*, 12334–12344. [[CrossRef](#)]
88. Chen, Y.; Su, X.; Esmail, D.; Buck, E.; Tran, S.D.; Szkopek, T.; Cerruti, M. Dual-Templating Strategy for the Fabrication of Graphene Oxide, Reduced Graphene Oxide and Composite Scaffolds with Hierarchical Architectures. *Carbon* **2022**, *189*, 186–198. [[CrossRef](#)]

89. Hou, J.; Tu, X.; Wu, X.; Shen, M.; Wang, X.; Wang, C.; Cao, C.; Pang, H.; Wang, G. Remarkable Cycling Durability of Lithium-Sulfur Batteries with Interconnected Mesoporous Hollow Carbon Nanospheres as High Sulfur Content Host. *Chem. Eng. J.* **2020**, *401*, 126141. [[CrossRef](#)]
90. Trovagunta, R.; Kelley, S.S.; Lavoine, N. Dual-Templating Approach for Engineering Strong, Biodegradable Lignin-Based Foams. *ACS Sustain. Chem. Eng.* **2022**, *10*, 15058–15067. [[CrossRef](#)]
91. Inagaki, M.; Toyoda, M.; Soneda, Y.; Tsujimura, S.; Morishita, T. Templated Mesoporous Carbons: Synthesis and Applications. *Carbon* **2016**, *107*, 448–473. [[CrossRef](#)]
92. Liu, H.-J.; Cui, W.-J.; Jin, L.-H.; Wang, C.-X.; Xia, Y.-Y. Preparation of Three-Dimensional Ordered Mesoporous Carbon Sphere Arrays by a Two-Step Templating Route and Their Application for Supercapacitors. *J. Mater. Chem.* **2009**, *19*, 3661–3667. [[CrossRef](#)]
93. Kumar, A.; Bhattacharyya, S. Porous NiFe-Oxide Nanocubes as Bifunctional Electrocatalysts for Efficient Water-Splitting. *ACS Appl. Mater. Interfaces* **2017**, *9*, 41906–41915. [[CrossRef](#)] [[PubMed](#)]
94. Xu, Y.; Dhainaut, J.; Rochard, G.; Dacquin, J.-P.; Mamede, A.-S.; Giraudon, J.-M.; Lamonier, J.-F.; Zhang, H.; Royer, S. Hierarchical Porous  $\epsilon$ -MnO<sub>2</sub> from Perovskite Precursor: Application to the Formaldehyde Total Oxidation. *Chem. Eng. J.* **2020**, *388*, 124146. [[CrossRef](#)]
95. Yang, W.; Li, J.; Wang, Y.; Zhu, F.; Shi, W.; Wan, F.; Xu, D. A Facile Synthesis of Anatase TiO<sub>2</sub> Nanosheets -Based Hierarchical Spheres with over 90% {001} Facets for Dye -Sensitized Solar Cells. *Chem. Commun.* **2011**, *47*, 1809–1811. [[CrossRef](#)] [[PubMed](#)]
96. Ge, Z.; Wang, C.; Chen, Z.; Wang, T.; Chen, T.; Shi, R.; Yu, S.; Liu, J. Investigation of the TiO<sub>2</sub> Nanoparticles Aggregation with High Light Harvesting for High-Efficiency Dye-Sensitized Solar Cells. *Mater. Res. Bull.* **2021**, *135*, 111148. [[CrossRef](#)]
97. Chaida-Chenni, F.Z.; Belhadj, F.; Grande Casas, M.S.; Márquez-Álvarez, C.; Hamacha, R.; Bengueddach, A.; Pérez-Pariente, J. Synthesis of Mesoporous-Zeolite Materials Using Beta Zeolite Nanoparticles as Precursors and Their Catalytic Performance in m-Xylene Isomerization and Disproportionation. *Appl. Catal. A Gen.* **2018**, *568*, 148–156. [[CrossRef](#)]
98. Nguyen, K.; Hoa, N.D.; Hung, C.M.; Le, D.T.T.; Duy, N.V.; Hieu, N.V. A Comparative Study on the Electrochemical Properties of Nanoporous Nickel Oxide Nanowires and Nanosheets Prepared by a Hydrothermal Method. *RSC Adv.* **2018**, *8*, 19449–19455. [[CrossRef](#)] [[PubMed](#)]
99. Li, A.; Zhang, Y.; Heard, C.J.; Gołabek, K.; Ju, X.; Čejka, J.; Mazur, M. Encapsulating Metal Nanoparticles into a Layered Zeolite Precursor with Surface Silanol Nests Enhances Sintering Resistance\*\*. *Angew. Chem. Int. Ed.* **2023**, *62*, e202213361. [[CrossRef](#)] [[PubMed](#)]
100. Zhang, Y.; Ouyang, B.; Xu, J.; Chen, S.; Rawat, R.S.; Fan, H.J. 3D Porous Hierarchical Nickel–Molybdenum Nitrides Synthesized by RF Plasma as Highly Active and Stable Hydrogen-Evolution-Reaction Electrocatalysts. *Adv. Energy Mater.* **2016**, *6*, 1600221. [[CrossRef](#)]
101. Liu, G.; Chen, H.; Xia, L.; Wang, S.; Ding, L.-X.; Li, D.; Xiao, K.; Dai, S.; Wang, H. Hierarchical Mesoporous/Macroporous Perovskite La<sub>0.5</sub>Sr<sub>0.5</sub>CoO<sub>3-x</sub> Nanotubes: A Bifunctional Catalyst with Enhanced Activity and Cycle Stability for Rechargeable Lithium Oxygen Batteries. *ACS Appl. Mater. Interfaces* **2015**, *7*, 22478–22486. [[CrossRef](#)] [[PubMed](#)]
102. Pang, C.; Zhu, S.; Xu, W.; Liang, Y.; Li, Z.; Wu, S.; Jiang, H.; Wang, H.; Cui, Z. Self-Standing Mo-NiO/Ni Electrocatalyst with Nanoporous Structure for Hydrogen Evolution Reaction. *Electrochim. Acta* **2023**, *439*, 141621. [[CrossRef](#)]
103. Chuang, A.; Erlebacher, J. Challenges and Opportunities for Integrating Dealloying Methods into Additive Manufacturing. *Materials* **2020**, *13*, 3706. [[CrossRef](#)] [[PubMed](#)]
104. Graf, M.; Roschning, B.; Weissmüller, J. Nanoporous Gold by Alloy Corrosion: Method-Structure-Property Relationships. *J. Electrochem. Soc.* **2017**, *164*, C194. [[CrossRef](#)]
105. Weissmüller, J.; Sieradzki, K. Dealloyed Nanoporous Materials with Interface-Controlled Behavior. *MRS Bull.* **2018**, *43*, 14–19. [[CrossRef](#)]
106. Bao, J.; Chen, H.; Yang, S.; Zhang, P. Mechanochemical Redox-Based Synthesis of Highly Porous Co<sub>x</sub>Mn<sub>1-x</sub>O<sub>y</sub> Catalysts for Total Oxidation. *Chin. J. Catal.* **2020**, *41*, 1846–1854. [[CrossRef](#)]
107. Frišćić, T.; Mottillo, C.; Titi, H.M. Mechanochemistry for Synthesis. *Angew. Chem. Int. Ed.* **2020**, *59*, 1018–1029. [[CrossRef](#)] [[PubMed](#)]
108. Rahmanivahid, B.; Pinilla-de Dios, M.; Haghghi, M.; Luque, R. Mechanochemical Synthesis of CuO/MgAl<sub>2</sub>O<sub>4</sub> and MgFe<sub>2</sub>O<sub>4</sub> Spinels for Vanillin Production from Isoeugenol and Vanillyl Alcohol. *Molecules* **2019**, *24*, 2597. [[CrossRef](#)] [[PubMed](#)]
109. Chakravarty, R.; Chakraborty, S.; Shukla, R.; Bahadur, J.; Ram, R.; Mazumder, S.; Sarma, H.D.; Kumar Tyagi, A.; Dash, A. Mechanochemical Synthesis of Mesoporous Tin Oxide: A New Generation Nanosorbent for 68 Ge/68 Ga Generator Technology. *Dalton Trans.* **2016**, *45*, 13361–13372. [[CrossRef](#)]
110. Plowman, B.J.; Jones, L.A.; Bhargava, S.K. Building with Bubbles: The Formation of High Surface Area Honeycomb-like Films via Hydrogen Bubble Templated Electrodeposition. *Chem. Commun.* **2015**, *51*, 4331–4346. [[CrossRef](#)] [[PubMed](#)]
111. Cherevko, S.; Chung, C.-H. Direct Electrodeposition of Nanoporous Gold with Controlled Multimodal Pore Size Distribution. *Electrochem. Commun.* **2011**, *13*, 16–19. [[CrossRef](#)]
112. Dorofeeva, T.S.; Seker, E. Electrically Tunable Pore Morphology in Nanoporous Gold Thin Films. *Nano Res.* **2015**, *8*, 2188–2198. [[CrossRef](#)]
113. Wittstock, G.; Bäumer, M.; Dononelli, W.; Klüner, T.; Lührs, L.; Mahr, C.; Moskaleva, L.V.; Oezaslan, M.; Risse, T.; Rosenauer, A.; et al. Nanoporous Gold: From Structure Evolution to Functional Properties in Catalysis and Electrochemistry. *Chem. Rev.* **2023**, *123*, 6716–6792. [[CrossRef](#)] [[PubMed](#)]

114. Kwon, H.; Barad, H.-N.; Silva Olaya, A.R.; Alarcón-Correa, M.; Hahn, K.; Richter, G.; Wittstock, G.; Fischer, P. Ultra-Pure Nanoporous Gold Films for Electrocatalysis. *ACS Catal.* **2023**, *13*, 11656–11665. [[CrossRef](#)]
115. Anka, G.N.; Pareek, A.; Cherevko, S.; Topalov, A.A.; Rohwerder, M.; Renner, F.U. The Influence of Halides on the Initial Selective Dissolution of Cu<sub>3</sub>Au (111). *Electrochim. Acta* **2012**, *85*, 384–392. [[CrossRef](#)]
116. Xiao, X.; Ou, W.; Du, P.; Lyu, F.; Diao, Y.; Lu, J.; Li, Y.Y. Ultrafine Nanoporous Gold via Thiol Compound-Mediated Chemical Dealloying. *J. Phys. Chem. C* **2020**, *124*, 10026–10031. [[CrossRef](#)]
117. Xu, C.; Wang, R.; Chen, M.; Zhang, Y.; Ding, Y. Dealloying to Nanoporous Au/Pt Alloys and Their Structure Sensitive Electrocatalytic Properties. *Phys. Chem. Chem. Phys.* **2010**, *12*, 239–246. [[CrossRef](#)] [[PubMed](#)]
118. Zhao, B.Y.; Wei, Q.; Xu, C.; Li, H.; Wu, D.; Cai, Y.; Mao, K.; Cui, Z.; Du, B. Label-Free Electrochemical Immunosensor for Sensitive Detection of Kanamycin. *Sens. Actuators B Chem.* **2011**, *155*, 618–625. [[CrossRef](#)]
119. Qian, L.H.; Yan, X.Q.; Fujita, T.; Inoue, A.; Chen, M.W. Surface Enhanced Raman Scattering of Nanoporous Gold: Smaller Pore Sizes Stronger Enhancements. *Appl. Phys. Lett.* **2007**, *90*, 153120. [[CrossRef](#)]
120. Chen, C.; Liu, Z.; Cai, C.; Qi, Z. Facile Fabrication of Nanoporous Gold Films for Surface Plasmon Resonance (SPR) Sensing and SPR-Based SERS. *J. Mater. Chem. C* **2021**, *9*, 6815–6822. [[CrossRef](#)]
121. Morrish, R.; Dorame, K.; Muscat, A.J. Formation of Nanoporous Au by Dealloying AuCu Thin Films in HNO<sub>3</sub>. *Scr. Mater.* **2011**, *64*, 856–859. [[CrossRef](#)]
122. Kim, J.; Song, J.T.; Oh, J. Facile Electrochemical Synthesis of Dilute AuCu Alloy Nanostructures for Selective and Long-Term Stable CO<sub>2</sub> Electrolysis. *J. Chem. Phys.* **2020**, *153*, 054702. [[CrossRef](#)] [[PubMed](#)]
123. Chen, A.Y.; Shi, S.S.; Qiu, Y.D.; Xie, X.F.; Ruan, H.H.; Gu, J.F.; Pan, D. Pore-Size Tuning and Optical Performances of Nanoporous Gold Films. *Microporous Mesoporous Mater.* **2015**, *202*, 50–56. [[CrossRef](#)]
124. Huang, W.; Wang, M.; Zheng, J.; Li, Z. Facile Fabrication of Multifunctional Three-Dimensional Hierarchical Porous Gold Films via Surface Rebuilding. *J. Phys. Chem. C* **2009**, *113*, 1800–1805. [[CrossRef](#)]
125. Sulka, G.D. (Ed.) Chapter One—Introduction to Anodization of Metals. In *Nanostructured Anodic Metal Oxides*; Micro and Nano Technologies; Elsevier: Amsterdam, The Netherlands, 2020; pp. 1–34. ISBN 978-0-12-816706-9.
126. Reghunath, S.; Pinheiro, D.; Kr, S.D. A Review of Hierarchical Nanostructures of TiO<sub>2</sub>: Advances and Applications. *Appl. Surf. Sci. Adv.* **2021**, *3*, 100063. [[CrossRef](#)]
127. Lee, J.; Hwan Ko, S. Fundamentals of Hierarchical Nanostructures. In *Hierarchical Nanostructures for Energy Devices*; Ko, S.H., Grigoropoulos, C.P., Eds.; The Royal Society of Chemistry: London, UK, 2014; pp. 7–25. ISBN 978-1-84973-628-2.
128. Qin, Z.; Buehler, M.J. Hierarchical Nanostructures for Functional Materials. *Nanotechnology* **2018**, *29*, 280201. [[CrossRef](#)] [[PubMed](#)]
129. Arroyo-Currás, N.; Scida, K.; Ploense, K.L.; Kippin, T.E.; Plaxco, K.W. High Surface Area Electrodes Generated via Electrochemical Roughening Improve the Signaling of Electrochemical Aptamer-Based Biosensors. *Anal. Chem.* **2017**, *89*, 12185–12191. [[CrossRef](#)] [[PubMed](#)]
130. Downs, A.M.; Gerson, J.; Hossain, M.N.; Ploense, K.; Pham, M.; Kraatz, H.-B.; Kippin, T.; Plaxco, K.W. Nanoporous Gold for the Miniaturization of In Vivo Electrochemical Aptamer-Based Sensors. *ACS Sens.* **2021**, *6*, 2299–2306. [[CrossRef](#)]
131. Antonelli, D.M.; Ying, J.Y. Synthesis of Hexagonally Packed Mesoporous TiO<sub>2</sub> by a Modified Sol–Gel Method. *Angew. Chem. Int. Ed. Engl.* **1995**, *34*, 2014–2017. [[CrossRef](#)]
132. Gong, D.; Grimes, C.A.; Varghese, O.K.; Hu, W.; Singh, R.S.; Chen, Z.; Dickey, E.C. Titanium Oxide Nanotube Arrays Prepared by Anodic Oxidation. *J. Mater. Res.* **2001**, *16*, 3331–3334. [[CrossRef](#)]
133. Macak, J.M.; Zlamal, M.; Krysa, J.; Schmuki, P. Self-Organized TiO<sub>2</sub> Nanotube Layers as Highly Efficient Photocatalysts. *Small* **2007**, *3*, 300–304. [[CrossRef](#)] [[PubMed](#)]
134. Teodorescu-Soare, C.T.; Catrinescu, C.; Dobromir, M.; Stoian, G.; Arvinte, A.; Luca, D. Growth and Characterization of TiO<sub>2</sub> Nanotube Arrays under Dynamic Anodization. Photocatalytic Activity. *J. Electroanal. Chem.* **2018**, *823*, 388–396. [[CrossRef](#)]
135. Querebillo, C.J.; Öner, I.H.; Hildebrandt, P.; Ly, K.H.; Weidinger, I.M. Accelerated Photo-Induced Degradation of Benzidine-p-Aminothiophenolate Immobilized at Light-Enhancing TiO<sub>2</sub> Nanotube Electrodes. *Chem. A Eur. J.* **2019**, *25*, 16048–16053. [[CrossRef](#)] [[PubMed](#)]
136. Oener, H.I.; Querebillo, C.J.; David, C.; Gernert, U.; Walter, C.; Driess, M.; Leimkühler, S.; Ly, K.H.; Weidinger, I.M. High Electromagnetic Field Enhancement of TiO<sub>2</sub> Nanotubes Electrodes. *Angew. Chem. Int. Ed.* **2018**, *57*, 7225–7229. [[CrossRef](#)] [[PubMed](#)]
137. Kapusta-Kołodziej, J.; Chudecka, A.; Sulka, G.D. 3D Nanoporous Titania Formed by Anodization as a Promising Photoelectrode Material. *J. Electroanal. Chem.* **2018**, *823*, 221–233. [[CrossRef](#)]
138. Zhang, C.; Smirnov, A.I.; Hahn, D.; Grebel, H. Surface Enhanced Raman Scattering of Biospecies on Anodized Aluminum Oxide Films. *Chem. Phys. Lett.* **2007**, *440*, 239–243. [[CrossRef](#)]
139. Huang, X.; Mutlu, H.; Théato, P. The Toolbox of Porous Anodic Aluminum Oxide-Based Nanocomposites: From Preparation to Application. *Colloid Polym. Sci.* **2021**, *299*, 325–341. [[CrossRef](#)]
140. Poinern, G.E.J.; Ali, N.; Fawcett, D. Progress in Nano-Engineered Anodic Aluminum Oxide Membrane Development. *Materials* **2011**, *4*, 487–526. [[CrossRef](#)] [[PubMed](#)]
141. Macak, J.M.; Tsuchiya, H.; Taveira, L.; Ghicov, A.; Schmuki, P. Self-Organized Nanotubular Oxide Layers on Ti-6Al-7Nb and Ti-6Al-4V Formed by Anodization in NH<sub>4</sub>F Solutions. *J. Biomed. Mater. Res. Part A* **2005**, *75A*, 928–933. [[CrossRef](#)] [[PubMed](#)]

142. Roshchina, M.Y.; Querebillo, C.J.; Dmitrieva, E.; Voss, A.; Israel, N.; Gemming, T.; Giebeler, L.; Pilz, S.; Roehrer, S.; Hoffmann, V.; et al. Corrosion Behavior of an Oxide Nanotube-Coated  $\beta$ -Type Ti-45Nb Implant Alloy in a Simulated Inflammatory Solution. *Corros. Sci.* **2024**, *227*, 111767. [[CrossRef](#)]
143. Kumaravel, V.; Nair, K.M.; Mathew, S.; Bartlett, J.; Kennedy, J.E.; Manning, H.G.; Whelan, B.J.; Leyland, N.S.; Pillai, S.C. Antimicrobial TiO<sub>2</sub> Nanocomposite Coatings for Surfaces, Dental and Orthopaedic Implants. *Chem. Eng. J.* **2021**, *416*, 129071. [[CrossRef](#)] [[PubMed](#)]
144. O'Regan, B.; Grätzel, M. A Low-Cost, High-Efficiency Solar Cell Based on Dye-Sensitized Colloidal TiO<sub>2</sub> Films. *Nature* **1991**, *353*, 737–740. [[CrossRef](#)]
145. Li, Z.; Zhou, Y.; Xue, G.; Yu, T.; Liu, J.; Zou, Z. Fabrication of Hierarchically Assembled Microspheres Consisting of Nanoporous ZnO Nanosheets for High-Efficiency Dye-Sensitized Solar Cells. *J. Mater. Chem.* **2012**, *22*, 14341–14345. [[CrossRef](#)]
146. Yan, G.; Li, G.; Tan, H.; Gu, Y.; Li, Y. Spinel-Type Ternary Multimetal Hybrid Oxides with Porous Hierarchical Structure Grown on Ni Foam as Large-Current-Density Water Oxidation Electrocatalyst. *J. Alloys Compd.* **2020**, *838*, 155662. [[CrossRef](#)]
147. Singh, K.P.; Shin, C.-H.; Lee, H.-Y.; Razmjooei, F.; Sinhamahapatra, A.; Kang, J.; Yu, J.-S. TiO<sub>2</sub>/ZrO<sub>2</sub> Nanoparticle Composites for Electrochemical Hydrogen Evolution. *ACS Appl. Nano Mater.* **2020**, *3*, 3634–3645. [[CrossRef](#)]
148. Vij, V.; Sultan, S.; Harzandi, A.M.; Meena, A.; Tiwari, J.N.; Lee, W.-G.; Yoon, T.; Kim, K.S. Nickel-Based Electrocatalysts for Energy-Related Applications: Oxygen Reduction, Oxygen Evolution, and Hydrogen Evolution Reactions. *ACS Catal.* **2017**, *7*, 7196–7225. [[CrossRef](#)]
149. Brezesinski, T.; Groenewolt, M.; Antonietti, M.; Smarsly, B. Crystal-to-Crystal Phase Transition in Self-Assembled Mesoporous Iron Oxide Films. *Angew. Chem. Int. Ed.* **2006**, *45*, 781–784. [[CrossRef](#)]
150. Tian, B.; Liu, X.; Yang, H.; Xie, S.; Yu, C.; Tu, B.; Zhao, D. General Synthesis of Ordered Crystallized Metal Oxide Nanoarrays Replicated by Microwave-Digested Mesoporous Silica. *Adv. Mater.* **2003**, *15*, 1370–1374. [[CrossRef](#)]
151. Zakaria, M.B.; Belik, A.A.; Liu, C.-H.; Hsieh, H.-Y.; Liao, Y.-T.; Malgras, V.; Yamauchi, Y.; Wu, K.C.-W. Prussian Blue Derived Nanoporous Iron Oxides as Anticancer Drug Carriers for Magnetic-Guided Chemotherapy. *Chem. Asian J.* **2015**, *10*, 1457–1462. [[CrossRef](#)] [[PubMed](#)]
152. Lv, L.; Peng, M.; Wu, L.; Dong, Y.; You, G.; Duan, Y.; Yang, W.; He, L.; Liu, X. Progress in Iron Oxides Based Nanostructures for Applications in Energy Storage. *Nanoscale Res. Lett.* **2021**, *16*, 138. [[CrossRef](#)] [[PubMed](#)]
153. Prakasam, H.E.; Varghese, O.K.; Paulose, M.; Mor, G.K.; Grimes, C.A. Synthesis and Photoelectrochemical Properties of Nanoporous Iron (III) Oxide by Potentiostatic Anodization. *Nanotechnology* **2006**, *17*, 4285. [[CrossRef](#)]
154. Fu, K.; Chen, W.; Jiang, F.; Chen, X.; Liu, J. Research Progress of Perovskite-Based Bifunctional Oxygen Electrocatalyst in Alkaline Conditions. *Molecules* **2023**, *28*, 7114. [[CrossRef](#)] [[PubMed](#)]
155. Zhang, J.; Zhao, Y.; Zhao, X.; Liu, Z.; Chen, W. Porous Perovskite LaNiO<sub>3</sub> Nanocubes as Cathode Catalysts for Li-O<sub>2</sub> Batteries with Low Charge Potential. *Sci. Rep.* **2014**, *4*, 6005. [[CrossRef](#)]
156. Hussain, S.; Javed, M.S.; Ullah, N.; Shaheen, A.; Aslam, N.; Ashraf, I.; Abbas, Y.; Wang, M.; Liu, G.; Qiao, G. Unique Hierarchical Mesoporous LaCrO<sub>3</sub> Perovskite Oxides for Highly Efficient Electrochemical Energy Storage Applications. *Ceram. Int.* **2019**, *45*, 15164–15170. [[CrossRef](#)]
157. Li, Z.; Zhang, W.; Wang, H.; Yang, B. Two-Dimensional Perovskite LaNiO<sub>3</sub> Nanosheets with Hierarchical Porous Structure for High-Rate Capacitive Energy Storage. *Electrochim. Acta* **2017**, *258*, 561–570. [[CrossRef](#)]
158. Jiang, S.; Liang, F.; Zhou, W.; Shao, Z. Hierarchical Porous Cobalt-Free Perovskite Electrode for Highly Efficient Oxygen Reduction. *J. Mater. Chem.* **2012**, *22*, 16214–16218. [[CrossRef](#)]
159. Cuan, J.; Zhang, D.; Xing, W.; Han, J.; Zhou, H.; Zhou, Y. Confining CsPbX<sub>3</sub> Perovskites in a Hierarchically Porous MOF as Efficient and Stable Phosphors for White LED. *Chem. Eng. J.* **2021**, *425*, 131556. [[CrossRef](#)]
160. Hu, E.; Feng, Y.; Nai, J.; Zhao, D.; Hu, Y.; Lou, X.W.D. Construction of Hierarchical Ni-Co-P Hollow Nanobricks with Oriented Nanosheets for Efficient Overall Water Splitting. *Energy Environ. Sci.* **2018**, *11*, 872–880. [[CrossRef](#)]
161. Chassaing, S.; Bénétiau, V.; Pale, P. Green Catalysts Based on Zeolites for Heterocycle Synthesis. *Curr. Opin. Green Sustain. Chem.* **2018**, *10*, 35–39. [[CrossRef](#)]
162. Rahimi, M.; Ng, E.-P.; Bakhtiari, K.; Vinciguerra, M.; Ahmad, H.A.; Awala, H.; Mintova, S.; Daghighi, M.; Bakhshandeh Rostami, F.; de Vries, M.; et al. Zeolite Nanoparticles for Selective Sorption of Plasma Proteins. *Sci. Rep.* **2015**, *5*, 17259. [[CrossRef](#)] [[PubMed](#)]
163. Li, Y.; Li, L.; Yu, J. Applications of Zeolites in Sustainable Chemistry. *Chem* **2017**, *3*, 928–949. [[CrossRef](#)]
164. Zimmermann, N.E.R.; Haranczyk, M. History and Utility of Zeolite Framework-Type Discovery from a Data-Science Perspective. *Cryst. Growth Des.* **2016**, *16*, 3043–3048. [[CrossRef](#)]
165. Fan, W.; Snyder, M.A.; Kumar, S.; Lee, P.-S.; Yoo, W.C.; McCormick, A.V.; Lee Penn, R.; Stein, A.; Tsapatsis, M. Hierarchical Nanofabrication of Microporous Crystals with Ordered Mesoporosity. *Nat. Mater.* **2008**, *7*, 984–991. [[CrossRef](#)] [[PubMed](#)]
166. Seljak, K.B.; Kocbek, P.; Gašperlin, M. Mesoporous Silica Nanoparticles as Delivery Carriers: An Overview of Drug Loading Techniques. *J. Drug Deliv. Sci. Technol.* **2020**, *59*, 101906. [[CrossRef](#)]
167. Rastegari, E.; Hsiao, Y.-J.; Lai, W.-Y.; Lai, Y.-H.; Yang, T.-C.; Chen, S.-J.; Huang, P.-I.; Chiou, S.-H.; Mou, C.-Y.; Chien, Y. An Update on Mesoporous Silica Nanoparticle Applications in Nanomedicine. *Pharmaceutics* **2021**, *13*, 1067. [[CrossRef](#)] [[PubMed](#)]
168. Yanagisawa, T.; Shimizu, T.; Kuroda, K.; Kato, C. The Preparation of Alkyltrimethylammonium-Kanemite Complexes and Their Conversion to Microporous Materials. *Bull. Chem. Soc. Jpn.* **1990**, *63*, 988–992. [[CrossRef](#)]

169. Pal, N.; Lee, J.-H.; Cho, E.-B. Recent Trends in Morphology-Controlled Synthesis and Application of Mesoporous Silica Nanoparticles. *Nanomaterials* **2020**, *10*, 2122. [[CrossRef](#)] [[PubMed](#)]
170. McGrath, K.M.; Dabbs, D.M.; Yao, N.; Edler, K.J.; Aksay, I.A.; Gruner, S.M. Silica Gels with Tunable Nanopores through Templating of the L3 Phase. *Langmuir* **2000**, *16*, 398–406. [[CrossRef](#)]
171. Izquierdo-Barba, I.; Ruiz-González, L.; Doadrio, J.C.; González-Calbet, J.M.; Vallet-Regí, M. Tissue Regeneration: A New Property of Mesoporous Materials. *Solid State Sci.* **2005**, *7*, 983–989. [[CrossRef](#)]
172. Huang, L.; Ma, J.; Wang, X.; Zhang, P.; Yu, L.; Zhang, S. Mesoporous Silica Nanoparticles-Loaded Methyl 3-(3,5-Di-Tert-Butyl-4-Hydroxyphenyl) Propanoate as a Smart Antioxidant of Synthetic Ester Oil. *Tribol. Int.* **2018**, *121*, 114–120. [[CrossRef](#)]
173. Liu, M.; Li, T.; Zhang, C.; Zheng, Y.; Wu, C.; Zhang, J.; Zhang, K.; Zhang, Z. Fluorescent Carbon Dots Embedded in Mesoporous Silica Nanospheres: A Simple Platform for Cr(VI) Detection in Environmental Water. *J. Hazard. Mater.* **2021**, *415*, 125699. [[CrossRef](#)] [[PubMed](#)]
174. Pal, N.; Cho, E.-B.; Kim, D. Synthesis of Ordered Mesoporous Silica/Ceria–Silica Composites and Their High Catalytic Performance for Solvent-Free Oxidation of Benzyl Alcohol at Room Temperature. *RSC Adv.* **2014**, *4*, 9213–9222. [[CrossRef](#)]
175. Mikšík, F.; Miyazaki, T.; Inada, M. Detailed Investigation on Properties of Novel Commercial Mesoporous Silica Materials. *Microporous Mesoporous Mater.* **2019**, *289*, 109644. [[CrossRef](#)]
176. Armstrong, E.; O'Dwyer, C. Artificial Opal Photonic Crystals and Inverse Opal Structures—Fundamentals and Applications from Optics to Energy Storage. *J. Mater. Chem. C* **2015**, *3*, 6109–6143. [[CrossRef](#)]
177. Fathi, F.; Monirinasab, H.; Ranjbar, F.; Nejadi-Koshki, K. Inverse Opal Photonic Crystals: Recent Advances in Fabrication Methods and Biological Applications. *J. Drug Deliv. Sci. Technol.* **2022**, *72*, 103377. [[CrossRef](#)]
178. Jiang, Y.; Zheng, P.; Li, D.; Zhou, L.; Tian, L.; Wang, J.; Yang, B.; Wang, X.; Zhang, X.; Gao, J. Enzyme-Containing Silica Inverse Opals Prepared by Using Water-Soluble Colloidal Crystal Templates: Characterization and Application. *Biochem. Eng. J.* **2016**, *112*, 123–129. [[CrossRef](#)]
179. Pham, K.; Temerov, F.; Saarinen, J.J. Multicomponent Inverse Opal Structures with Gold Nanoparticles for Visible Light Photocatalytic Activity. *Mater. Des.* **2020**, *194*, 108886. [[CrossRef](#)]
180. Sakamoto, J.S.; Dunn, B. Hierarchical Battery Electrodes Based on Inverted Opal Structures. *J. Mater. Chem.* **2002**, *12*, 2859–2861. [[CrossRef](#)]
181. Von Freymann, G.; Kitaev, V.; Lotsch, B.V.; Ozin, G.A. Bottom-up Assembly of Photonic Crystals. *Chem. Soc. Rev.* **2013**, *42*, 2528–2554. [[CrossRef](#)] [[PubMed](#)]
182. Ma, Y.; Zhang, H.; Lin, R.; Ai, Y.; Lan, K.; Duan, L.; Chen, W.; Duan, X.; Ma, B.; Wang, C.; et al. Remodeling Nanodroplets into Hierarchical Mesoporous Silica Nanoreactors with Multiple Chambers. *Nat. Commun.* **2022**, *13*, 6136. [[CrossRef](#)] [[PubMed](#)]
183. Brothers, A.H.; Dunand, D.C. Porous and Foamed Amorphous Metals. *MRS Bull.* **2007**, *32*, 639–643. [[CrossRef](#)]
184. Jones, J.R.; Lee, P.D.; Hench, L.L. Hierarchical Porous Materials for Tissue Engineering. *Phil. Trans. R. Soc. A* **2006**, *364*, 263–281. [[CrossRef](#)] [[PubMed](#)]
185. Li, T.H.; Wong, P.C.; Chang, S.F.; Tsai, P.H.; Jang, J.S.C.; Huang, J.C. Biocompatibility Study on Ni-Free Ti-Based and Zr-Based Bulk Metallic Glasses. *Mater. Sci. Eng. C* **2017**, *75*, 1–6. [[CrossRef](#)]
186. Du, P.; Li, B.; Chen, J.; Li, K.; Xie, G. Novel Ti-Based Bulk Metallic Glass Free of Toxic and Noble Elements for Bio-Implant Applications. *J. Alloys Compd.* **2023**, *934*, 167996. [[CrossRef](#)]
187. Trexler, M.M.; Thadhani, N.N. Mechanical Properties of Bulk Metallic Glasses. *Prog. Mater. Sci.* **2010**, *55*, 759–839. [[CrossRef](#)]
188. Inoue, A.; Takeuchi, A. Recent Development and Application Products of Bulk Glassy Alloys. *Acta Mater.* **2011**, *59*, 2243–2267. [[CrossRef](#)]
189. Liu, Y.; Pang, S.; Li, H.; Hu, Q.; Chen, B.; Zhang, T. Formation and Properties of Ti-Based Ti–Zr–Cu–Fe–Sn–Si Bulk Metallic Glasses with Different (Ti + Zr)/Cu Ratios for Biomedical Application. *Intermetallics* **2016**, *72*, 36–43. [[CrossRef](#)]
190. Wang, C.; Hua, N.; Liao, Z.; Yang, W.; Pang, S.; Liaw, P.K.; Zhang, T. Ti-Cu-Zr-Fe-Sn-Si-Ag-Pd Bulk Metallic Glasses with Potential for Biomedical Applications. *Met. Mater. Trans A* **2021**, *52*, 1559–1567. [[CrossRef](#)]
191. Liens, A.; Etienne, A.; Rivory, P.; Balvay, S.; Pelletier, J.-M.; Cardinal, S.; Fabrègue, D.; Kato, H.; Steyer, P.; Munhoz, T.; et al. On the Potential of Bulk Metallic Glasses for Dental Implantology: Case Study on Ti<sub>40</sub>Zr<sub>10</sub>Cu<sub>36</sub>Pd<sub>14</sub>. *Materials* **2018**, *11*, 249. [[CrossRef](#)] [[PubMed](#)]
192. Biały, M.; Hasiak, M.; Łaszcz, A. Review on Biocompatibility and Prospect Biomedical Applications of Novel Functional Metallic Glasses. *J. Funct. Biomater.* **2022**, *13*, 245. [[CrossRef](#)] [[PubMed](#)]
193. Gostin, P.F.; Addison, O.; Morrell, A.P.; Zhang, Y.; Cook, A.J.M.C.; Liens, A.; Stoica, M.; Ignatyev, K.; Street, S.R.; Wu, J.; et al. In Situ Synchrotron X-Ray Diffraction Characterization of Corrosion Products of a Ti-Based Metallic Glass for Implant Applications. *Adv. Healthc. Mater.* **2018**, *7*, 1800338. [[CrossRef](#)] [[PubMed](#)]
194. Blanquer, A.; Hynowska, A.; Nogués, C.; Ibáñez, E.; Sort, J.; Baró, M.D.; Özkale, B.; Pané, S.; Pellicer, E.; Barrios, L. Effect of Surface Modifications of Ti<sub>40</sub>Zr<sub>10</sub>Cu<sub>38</sub>Pd<sub>12</sub> Bulk Metallic Glass and Ti-6Al-4V Alloy on Human Osteoblasts In Vitro Biocompatibility. *PLoS ONE* **2016**, *11*, e0156644. [[CrossRef](#)] [[PubMed](#)]
195. Oak, J.-J.; Inoue, A.; Rao, K.V.; Chun, H.-H.; Park, Y.H. Surface Modified Ti Based Metallic Glasses for Bioactivation by Electrochemical Treatment Technique. *J. Alloys Compd.* **2014**, *615*, S136–S141. [[CrossRef](#)]
196. Sharma, A.; Zadorozhnyy, V. Review of the Recent Development in Metallic Glass and Its Composites. *Metals* **2021**, *11*, 1933. [[CrossRef](#)]

197. Zhang, C.; Li, X.; Liu, S.-Q.; Liu, H.; Yu, L.-J.; Liu, L. 3D Printing of Zr-Based Bulk Metallic Glasses and Components for Potential Biomedical Applications. *J. Alloys Compd.* **2019**, *790*, 963–973. [[CrossRef](#)]
198. Shen, X.-J.; Zhang, C.; Yang, Y.-G.; Liu, L. On the Microstructure, Mechanical Properties and Wear Resistance of an Additively Manufactured Ti64/Metallic Glass Composite. *Addit. Manuf.* **2019**, *25*, 499–510. [[CrossRef](#)]
199. Du, P.; Xiang, T.; Yang, X.; Xie, G. Optimization of Bioactivity and Antibacterial Properties of Porous Ti-Based Bulk Metallic Glass through Chemical Treatment. *Ceram. Int.* **2023**, *49*, 13960–13971. [[CrossRef](#)]
200. Du, P.; Xiang, T.; Yang, X.; Xie, G. Enhanced Mechanical and Antibacterial Properties of Cu-Bearing Ti-Based Bulk Metallic Glass by Controlling Porous Structure. *J. Alloys Compd.* **2022**, *904*, 164005. [[CrossRef](#)]
201. Zhang, P.; Tan, J.; Tian, Y.; Yan, H.; Yu, Z. Research Progress on Selective Laser Melting (SLM) of Bulk Metallic Glasses (BMGs): A Review. *Int. J. Adv. Manuf. Technol.* **2022**, *118*, 2017–2057. [[CrossRef](#)]
202. Kunz, C.; Müller, F.; Gräf, S. Multifunctional Hierarchical Surface Structures by Femtosecond Laser Processing. *Materials* **2018**, *11*, 789. [[CrossRef](#)] [[PubMed](#)]
203. Badria, A. Click Chemistry: A Promising Tool for Building Hierarchical Structures. *Polymers* **2022**, *14*, 4077. [[CrossRef](#)] [[PubMed](#)]
204. Mishnaevsky, L.; Tsapatsis, M. Hierarchical Materials: Background and Perspectives. *MRS Bull.* **2016**, *41*, 661–664. [[CrossRef](#)]
205. Huang, Y.; Zha, G.; Luo, Q.; Zhang, J.; Zhang, F.; Li, X.; Zhao, S.; Zhu, W.; Li, X. The Construction of Hierarchical Structure on Ti Substrate with Superior Osteogenic Activity and Intrinsic Antibacterial Capability. *Sci. Rep.* **2014**, *4*, 6172. [[CrossRef](#)]
206. Liu, Y.; Luo, D.; Wang, T. Hierarchical Structures of Bone and Bioinspired Bone Tissue Engineering. *Small* **2016**, *12*, 4611–4632. [[CrossRef](#)] [[PubMed](#)]
207. Zhang, Y.; Wang, X.; Li, Y.; Liang, J.; Jiang, P.; Huang, Q.; Yang, Y.; Duan, H.; Dong, X.; Rui, G.; et al. Cell Osteogenic Bioactivity Mediated Precisely by Varying Scaled Micro-Pits on Ordered Micro/Nano Hierarchical Structures of Titanium. *Regen. Biomater.* **2022**, *9*, rbac046. [[CrossRef](#)] [[PubMed](#)]
208. Öner, I.H.; David, C.; Querebillo, C.J.; Weidinger, I.M.; Ly, K.H. Electromagnetic Field Enhancement of Nanostructured TiN Electrodes Probed with Surface-Enhanced Raman Spectroscopy. *Sensors* **2022**, *22*, 487. [[CrossRef](#)] [[PubMed](#)]
209. Dai, J.; Zhu, Y.; Zhong, Y.; Miao, J.; Lin, B.; Zhou, W.; Shao, Z. Enabling High and Stable Electrocatalytic Activity of Iron-Based Perovskite Oxides for Water Splitting by Combined Bulk Doping and Morphology Designing. *Adv. Mater. Interfaces* **2019**, *6*, 1801317. [[CrossRef](#)]
210. Hou, X.; Pan, L.; Huang, S.; Wei, O.-Y.; Chen, X. Enhanced Efficiency and Stability of Perovskite Solar Cells Using Porous Hierarchical TiO<sub>2</sub> Nanostructures of Scattered Distribution as Scaffold. *Electrochim. Acta* **2017**, *236*, 351–358. [[CrossRef](#)]
211. Lombardi, J.R.; Birke, R.L. Theory of Surface-Enhanced Raman Scattering in Semiconductors. *J. Phys. Chem. C* **2014**, *118*, 11120–11130. [[CrossRef](#)]
212. Yang, H.-Y.; Rho, W.-Y.; Lee, S.; Kim, S.; Hahn, Y.-B. TiO<sub>2</sub> Nanoparticles/Nanotubes for Efficient Light Harvesting in Perovskite Solar Cells. *Nanomaterials* **2019**, *9*, 326. [[CrossRef](#)] [[PubMed](#)]
213. Pérez León, C.; Kador, L.; Peng, B.; Thelakkat, M. Characterization of the Adsorption of Ru-Bpy Dyes on Mesoporous TiO<sub>2</sub> Films with UV-Vis, Raman, and FTIR Spectroscopies. *J. Phys. Chem. B* **2006**, *110*, 8723–8730. [[CrossRef](#)] [[PubMed](#)]
214. Blackburn, R.L.; Johnson, C.S.; Hupp, J.T. Surface Intervalence Enhanced Raman Scattering from Ferrocyanide on Colloidal Titanium Dioxide. A Mode-by-Mode Description of the Franck-Condon Barrier to Interfacial Charge Transfer. *J. Am. Chem. Soc.* **1991**, *113*, 1060–1062. [[CrossRef](#)]
215. Qi, D.; Lu, L.; Wang, L.; Zhang, J. Improved SERS Sensitivity on Plasmon-Free TiO<sub>2</sub> Photonic Microarray by Enhancing Light-Matter Coupling. *J. Am. Chem. Soc.* **2014**, *136*, 9886–9889. [[CrossRef](#)] [[PubMed](#)]
216. Öner, I.H.; Querebillo, C.J.; David, C.; Gernert, U.; Walter, C.; Driess, M.; Leimkühler, S.; Ly, K.H.; Weidinger, I.M. Hohe Elektromagnetische Feldverstärkung in Nanotubularen TiO<sub>2</sub>-Elektroden. *Angew. Chem.* **2018**, *130*, 7344–7348. [[CrossRef](#)]
217. Gesesse, G.D.; Li, C.; Paineau, E.; Habibi, Y.; Remita, H.; Colbeau-Justin, C.; Ghazzal, M.N. Enhanced Photogenerated Charge Carriers and Photocatalytic Activity of Biotemplated Mesoporous TiO<sub>2</sub> Films with a Chiral Nematic Structure. *Chem. Mater.* **2019**, *31*, 4851–4863. [[CrossRef](#)]
218. Zhang, X.; John, S. Enhanced Photocatalysis by Light-Trapping Optimization in Inverse Opals. *J. Mater. Chem. A* **2020**, *8*, 18974–18986. [[CrossRef](#)]
219. Huo, J.; Yuan, C.; Wang, Y. Nanocomposites of Three-Dimensionally Ordered Porous TiO<sub>2</sub> Decorated with Pt and Reduced Graphene Oxide for the Visible-Light Photocatalytic Degradation of Waterborne Pollutants. *ACS Appl. Nano Mater.* **2019**, *2*, 2713–2724. [[CrossRef](#)]
220. Chen, J.L.L.; Von Freymann, G.; Choi, S.Y.; Kitaev, V.; Ozin, G.A. Slow Photons in the Fast Lane in Chemistry. *J. Mater. Chem.* **2008**, *18*, 369–373. [[CrossRef](#)]
221. Sordello, F.; Duca, C.; Maurino, V.; Minero, C. Photocatalytic Metamaterials: TiO<sub>2</sub> Inverse Opals. *Chem. Commun.* **2011**, *47*, 6147–6149. [[CrossRef](#)] [[PubMed](#)]
222. Maznichenko, D.; Venkatakrisnan, K.; Tan, B. Stimulating Multiple SERS Mechanisms by a Nano Fi Brous Three- Dimensional Network Structure of Titanium Dioxide (TiO<sub>2</sub>). *J. Phys. Chem. C* **2013**, *117*, 578–583. [[CrossRef](#)]
223. Han, X.X.; Köhler, C.; Kozuch, J.; Kuhlmann, U.; Paasche, L.; Sivanesan, A.; Weidinger, I.M.; Hildebrandt, P. Potential-Dependent Surface-Enhanced Resonance Raman Spectroscopy at Nanostructured TiO<sub>2</sub>: A Case Study on Cytochrome B5. *Small* **2013**, *9*, 4175–4181. [[CrossRef](#)] [[PubMed](#)]
224. Zhang, X.; Lei, L.; Zhang, J.; Chen, Q.; Bao, J.; Fang, B. A Novel CdS/S-TiO<sub>2</sub> Nanotubes Photocatalyst with High Visible Light Activity. *Sep. Purif. Technol.* **2009**, *66*, 417–421. [[CrossRef](#)]

225. Shin, S.W.; Lee, J.Y.; Ahn, K.-S.; Kang, S.H.; Kim, J.H. Visible Light Absorbing TiO<sub>2</sub> Nanotube Arrays by Sulfur Treatment for Photoelectrochemical Water Splitting. *J. Phys. Chem. C* **2015**, *119*, 13375–13383. [[CrossRef](#)]
226. Feng, X.; Sloppy, J.D.; LaTempa, T.J.; Paulose, M.; Komarneni, S.; Bao, N.; Grimes, C.A. Synthesis and Deposition of Ultrafine Pt Nanoparticles within High Aspect Ratio TiO<sub>2</sub> Nanotube Arrays: Application to the Photocatalytic Reduction of Carbon Dioxide. *J. Mater. Chem.* **2011**, *21*, 13429. [[CrossRef](#)]
227. Teng, X.; Wei, M.; Yi, W.; Li, J.; Yin, M.; Xi, G. General Synthesis of Large-Area Transition Metal Nitride Porous Arrays for Highly Sensitive Surface-Enhanced Raman Scattering Substrates with Ultrahigh Durability. *Small Struct.* **2023**, *4*, 2300127. [[CrossRef](#)]
228. Lu, X.; Chen, J.; Skrabalak, S.E.; Xia, Y. Galvanic Replacement Reaction: A Simple and Powerful Route to Hollow and Porous Metal Nanostructures. *Proc. Inst. Mech. Eng. Part N J. Nanoeng. Nanosyst.* **2007**, *221*, 1–16. [[CrossRef](#)]
229. Fujita, T.; Qian, L.-H.; Inoke, K.; Erlebacher, J.; Chen, M.-W. Three-Dimensional Morphology of Nanoporous Gold. *Appl. Phys. Lett.* **2008**, *92*, 251902. [[CrossRef](#)]
230. Carabineiro, S.A.C. Supported Gold Nanoparticles as Catalysts for the Oxidation of Alcohols and Alkanes. *Front. Chem.* **2019**, *7*, 702. [[CrossRef](#)] [[PubMed](#)]
231. Wu, T.; Lu, Y.; Liu, J.; Zhang, S.; Zhang, X. In Situ Monitoring of Catalytic Reaction on Single Nanoporous Gold Nanowire with Tuneable SERS and Catalytic Activity. *Talanta* **2020**, *218*, 121181. [[CrossRef](#)]
232. Detsi, E.; Sellès, M.S.; Onck, P.R.; De Hosson, J.T.M. Nanoporous Silver as Electrochemical Actuator. *Scr. Mater.* **2013**, *69*, 195–198. [[CrossRef](#)]
233. Jin, H.-J.; Wang, X.-L.; Parida, S.; Wang, K.; Seo, M.; Weissmüller, J. Nanoporous Au–Pt Alloys As Large Strain Electrochemical Actuators. *Nano Lett.* **2010**, *10*, 187–194. [[CrossRef](#)] [[PubMed](#)]
234. Zhang, J.; Bai, Q.; Zhang, Z. Dealloying-Driven Nanoporous Palladium with Superior Electrochemical Actuation Performance. *Nanoscale* **2016**, *8*, 7287–7295. [[CrossRef](#)] [[PubMed](#)]
235. Yogeswaran, U.; Chen, S.-M. A Review on the Electrochemical Sensors and Biosensors Composed of Nanowires as Sensing Material. *Sensors* **2008**, *8*, 290–313. [[CrossRef](#)]
236. Klinghammer, S.; Uhlig, T.; Patrovsky, F.; Böhm, M.; Schütt, J.; Pütz, N.; Baraban, L.; Eng, L.M.; Cuniberti, G. Plasmonic Biosensor Based on Vertical Arrays of Gold Nanoantennas. *ACS Sens.* **2018**, *3*, 1392–1400. [[CrossRef](#)] [[PubMed](#)]
237. Bollella, P. Porous Gold: A New Frontier for Enzyme-Based Electrodes. *Nanomaterials* **2020**, *10*, 722. [[CrossRef](#)] [[PubMed](#)]
238. Choi, H.K.; Lee, M.-J.; Lee, S.N.; Kim, T.-H.; Oh, B.-K. Noble Metal Nanomaterial-Based Biosensors for Electrochemical and Optical Detection of Viruses Causing Respiratory Illnesses. *Front. Chem.* **2021**, *9*, 672739. [[CrossRef](#)] [[PubMed](#)]
239. Zhang, X.; Li, D.; Bourgeois, L.; Wang, H.; Webley, P.A. Direct Electrodeposition of Porous Gold Nanowire Arrays for Biosensing Applications. *ChemPhysChem* **2009**, *10*, 436–441. [[CrossRef](#)] [[PubMed](#)]
240. Logan, B.E.; Rabaey, K. Conversion of Wastes into Bioelectricity and Chemicals by Using Microbial Electrochemical Technologies. *Science* **2012**, *337*, 686–690. [[CrossRef](#)] [[PubMed](#)]
241. Ortac, I.; Simberg, D.; Yeh, Y.; Yang, J.; Messmer, B.; Trogler, W.C.; Tsien, R.Y.; Esener, S. Dual-Porosity Hollow Nanoparticles for the Immunoprotection and Delivery of Nonhuman Enzymes. *Nano Lett.* **2014**, *14*, 3023–3032. [[CrossRef](#)] [[PubMed](#)]
242. Usman, M.; Sarwar, Y.; Abbasi, R.; Ishaq, H.M.; Iftikhar, M.; Hussain, I.; Demirdogen, R.E.; Ihsan, A. Nanogold Morphologies with the Same Surface Chemistry Provoke a Different Innate Immune Response: An in-Vitro and in-Vivo Study. *NanoImpact* **2022**, *28*, 100419. [[CrossRef](#)] [[PubMed](#)]
243. Abeyweera, S.C.; Yu, J.; Perdew, J.P.; Yan, Q.; Sun, Y. Hierarchically 3D Porous Ag Nanostructures Derived from Silver Benzenethiolate Nanoboxes: Enabling CO<sub>2</sub> Reduction with a Near-Unity Selectivity and Mass-Specific Current Density over 500 A/g. *Nano Lett.* **2020**, *20*, 2806–2811. [[CrossRef](#)] [[PubMed](#)]
244. Cheng, C.; Lühns, L. Robust Metallic Actuators Based on Nanoporous Gold Rapidly Dealloyed from Gold–Nickel Precursors. *Adv. Funct. Mater.* **2021**, *31*, 2107241. [[CrossRef](#)]
245. Pareek, A.; Anka, G.N.; Cherevko, S.; Ebbinghaus, P.; Mayrhofer, K.J.J.; Erbe, A.; Renner, F.U. Effect of Thiol Self-Assembled Monolayers and Plasma Polymer Films on Dealloying of Cu–Au Alloys. *RSC Adv.* **2013**, *3*, 6586. [[CrossRef](#)]
246. Ateya, B.G.; Geh, G.; Carim, A.H.; Pickering, H.W. Selective Dissolution below the Critical Potential and Back Alloying in Copper–Gold Alloy. *J. Electrochem. Soc.* **2002**, *149*, B27. [[CrossRef](#)]
247. Erlebacher, J.; Aziz, M.J.; Karma, A.; Dimitrov, N.; Sieradzki, K. Evolution of Nanoporosity in Dealloying. *Nature* **2001**, *410*, 450–453. [[CrossRef](#)] [[PubMed](#)]
248. Anka, G.N.; Pareek, A.; Cherevko, S.; Zegenhagen, J.; Renner, F.U. Hierarchical Nanoporous Films Obtained by Surface Cracking on Cu–Au and Ethanethiol on Au(001). *Electrochim. Acta* **2014**, *140*, 352–358. [[CrossRef](#)]
249. Ding, Y.; Chen, M. Nanoporous Metals for Catalytic and Optical Applications. *MRS Bull.* **2009**, *34*, 569–576. [[CrossRef](#)]
250. Sun, H.; Mowbray, D.J.; Migani, A.; Zhao, J.; Petek, H.; Rubio, A. Comparing Quasiparticle H<sub>2</sub>O Level Alignment on Anatase and Rutile TiO<sub>2</sub>. *ACS Catal.* **2015**, *5*, 4242–4254. [[CrossRef](#)]
251. Collinson, M.M. Nanoporous Gold Electrodes and Their Applications in Analytical Chemistry. *ISRN Anal. Chem.* **2013**, *2013*, 692484. [[CrossRef](#)]
252. Qi, Z.; Weissmüller, J. Hierarchical Nested-Network Nanostructure by Dealloying. *ACS Nano* **2013**, *7*, 5948–5954. [[CrossRef](#)] [[PubMed](#)]
253. Xing, X.-F.; Han, D.-Q.; Wu, Y.-F.; Guan, Y.; Bao, N.; Xu, X.-H. Fabrication and Electrochemical Property of Hierarchically Porous Au–Cu Films. *Mater. Lett.* **2012**, *71*, 108–110. [[CrossRef](#)]

254. Zhang, Y.; Wang, Y.; Yu, B.; Yin, K.; Zhang, Z. Hierarchically Structured Black Gold Film with Ultrahigh Porosity for Solar Steam Generation. *Adv. Mater.* **2022**, *34*, 2200108. [[CrossRef](#)] [[PubMed](#)]
255. Sohn, Y.; Joo, J.B.; Kim, P. Chemically Dealloyed Pt–Au–Cu Ternary Electrocatalysts with Enhanced Stability in Electrochemical Oxygen Reduction. *Res. Chem. Intermed.* **2018**, *44*, 3697–3712. [[CrossRef](#)]
256. Lee, M.N.; Santiago-Cordoba, M.A.; Hamilton, C.E.; Subbaiyan, N.K.; Duque, J.G.; Obrey, K.A.D. Developing Monolithic Nanoporous Gold with Hierarchical Bicontinuity Using Colloidal Bijels. *J. Phys. Chem. Lett.* **2014**, *5*, 809–812. [[CrossRef](#)] [[PubMed](#)]
257. Ding, Y.; Erlebacher, J. Nanoporous Metals with Controlled Multimodal Pore Size Distribution. *J. Am. Chem. Soc.* **2003**, *125*, 7772–7773. [[CrossRef](#)] [[PubMed](#)]
258. Liu, Z.; Searson, P.C. Single Nanoporous Gold Nanowire Sensors. *J. Phys. Chem. B* **2006**, *110*, 4318–4322. [[CrossRef](#)] [[PubMed](#)]
259. Yoo, S.-H.; Park, S. Platinum-Coated, Nanoporous Gold Nanorod Arrays: Synthesis and Characterization. *Adv. Mater.* **2007**, *19*, 1612–1615. [[CrossRef](#)]
260. Samanman, S.; Thammakhet, C.; Kanatharana, P.; Buranachai, C.; Thavarungkul, P. Novel Template-Assisted Fabrication of Porous Gold Nanowire Arrays Using a Conductive-Layer-Free Anodic Alumina Oxide Membrane. *Electrochim. Acta* **2013**, *102*, 342–350. [[CrossRef](#)]
261. Wu, Y.; Markmann, J.; Lilleodden, E.T. Electro-Chemo-Mechanical Coupling of Nanoporous Gold at the Microscale. *Appl. Phys. Lett.* **2019**, *115*, 251602. [[CrossRef](#)]
262. Schubert, I.; Huck, C.; Kröber, P.; Neubrech, F.; Pucci, A.; Toimil-Molares, M.E.; Trautmann, C.; Vogt, J. Porous Gold Nanowires: Plasmonic Response and Surface-Enhanced Infrared Absorption. *Adv. Opt. Mater.* **2016**, *4*, 1838–1845. [[CrossRef](#)]
263. Awada, C.; Dab, C.; Grimaldi, M.G.; Alshoabi, A.; Ruffino, F. High Optical Enhancement in Au/Ag Alloys and Porous Au Using Surface-Enhanced Raman Spectroscopy Technique. *Sci. Rep.* **2021**, *11*, 4714. [[CrossRef](#)] [[PubMed](#)]
264. Wiriayakun, N.; Pankhluab, K.; Boonrungsiman, S.; Laocharoensuk, R. Site-Selective Controlled Dealloying Process of Gold-Silver Nanowire Array: A Simple Approach towards Long-Term Stability and Sensitivity Improvement of SERS Substrate. *Sci. Rep.* **2016**, *6*, 39115. [[CrossRef](#)] [[PubMed](#)]
265. Chandra, D.; Yang, S. Capillary-Force-Induced Clustering of Micropillar Arrays: Is It Caused by Isolated Capillary Bridges or by the Lateral Capillary Interaction Force? *Langmuir* **2009**, *25*, 10430–10434. [[CrossRef](#)]
266. Ou, F.S.; Hu, M.; Naumov, I.; Kim, A.; Wu, W.; Bratkovsky, A.M.; Li, X.; Williams, R.S.; Li, Z. Hot-Spot Engineering in Polygonal Nanofinger Assemblies for Surface Enhanced Raman Spectroscopy. *Nano Lett.* **2011**, *11*, 2538–2542. [[CrossRef](#)] [[PubMed](#)]
267. Tian, C.; Li, J.; Ma, C.; Wang, P.; Sun, X.; Fang, J. An Ordered Mesoporous Ag Superstructure Synthesized via a Template Strategy for Surface-Enhanced Raman Spectroscopy. *Nanoscale* **2015**, *7*, 12318–12324. [[CrossRef](#)] [[PubMed](#)]
268. Capaccio, A.; Sasso, A.; Rusciano, G. A Simple and Reliable Approach for the Fabrication of Nanoporous Silver Patterns for Surface-Enhanced Raman Spectroscopy Applications. *Sci. Rep.* **2021**, *11*, 22295. [[CrossRef](#)]
269. Lee, H.; Habas, S.E.; Kweskin, S.; Butcher, D.; Somorjai, G.A.; Yang, P. Morphological Control of Catalytically Active Platinum Nanocrystals. *Angew. Chem. Int. Ed.* **2006**, *45*, 7824–7828. [[CrossRef](#)] [[PubMed](#)]
270. Li, C.; Malgras, V.; Alshehri, S.M.; Kim, J.H.; Yamauchi, Y. Electrochemical Synthesis of Mesoporous Pt Nanowires with Highly Electrocatalytic Activity toward Methanol Oxidation Reaction. *Electrochim. Acta* **2015**, *183*, 107–111. [[CrossRef](#)]
271. Halder, A.; Patra, S.; Viswanath, B.; Munichandraiah, N.; Ravishankar, N. Porous, Catalytically Active Palladium Nanostructures by Tuning Nanoparticle Interactions in an Organic Medium. *Nanoscale* **2011**, *3*, 725–730. [[CrossRef](#)] [[PubMed](#)]
272. Weissmüller, J.; Viswanath, R.N.; Kramer, D.; Zimmer, P.; Würschum, R.; Gleiter, H. Charge-Induced Reversible Strain in a Metal. *Science* **2003**, *300*, 312–315. [[CrossRef](#)] [[PubMed](#)]
273. Deng, Q.; Jia, H.; An, C.; Wu, S.; Zhao, S.; Hu, N. Progress and Prospective of Electrochemical Actuator Materials. *Compos. Part A Appl. Sci. Manuf.* **2023**, *165*, 107336. [[CrossRef](#)]
274. Kramer, D.; Viswanath, R.N.; Weissmüller, J. Surface-Stress Induced Macroscopic Bending of Nanoporous Gold Cantilevers. *Nano Lett.* **2004**, *4*, 793–796. [[CrossRef](#)]
275. Zheng, G.; Pastoriza-Santos, I.; Pérez-Juste, J.; Liz-Marzán, L.M. Plasmonic Metal-organic Frameworks. *SmartMat* **2021**, *2*, 446–465. [[CrossRef](#)]
276. Hansen, J.N.; Prats, H.; Toudahl, K.K.; Mørch Secher, N.; Chan, K.; Kibsgaard, J.; Chorkendorff, I. Is There Anything Better than Pt for HER? *ACS Energy Lett.* **2021**, *6*, 1175–1180. [[CrossRef](#)] [[PubMed](#)]
277. Zhang, S.; Zhang, X.; Rui, Y.; Wang, R.; Li, X. Recent Advances in Non-Precious Metal Electrocatalysts for pH-Universal Hydrogen Evolution Reaction. *Green Energy Environ.* **2021**, *6*, 458–478. [[CrossRef](#)]
278. Cao, X.; Wang, T.; Jiao, L. Transition-Metal (Fe, Co, and Ni)-Based Nanofiber Electrocatalysts for Water Splitting. *Adv. Fiber Mater.* **2021**, *3*, 210–228. [[CrossRef](#)]
279. Xie, Y.; Zhao, B.; Tang, K.; Qin, W.; Tan, C.; Yao, J.; Li, Y.; Jiang, L.; Wang, X.; Sun, Y. In-Situ Phase Transition Induced Nanoheterostructure for Overall Water Splitting. *Chem. Eng. J.* **2021**, *409*, 128156. [[CrossRef](#)]
280. Zhang, M.; Shao, X.; Liu, L.; Xu, X.; Pan, J.; Hu, J. 3d Transition Metal Doping Induced Charge Rearrangement and Transfer to Enhance Overall Water-Splitting on Ni<sub>3</sub>S<sub>2</sub> (101) Facet: A First-Principles Calculation Study. *RSC Adv.* **2022**, *12*, 26866–26874. [[CrossRef](#)] [[PubMed](#)]
281. Zhang, J.; Zhang, Z.; Ji, Y.; Yang, J.; Fan, K.; Ma, X.; Wang, C.; Shu, R.; Chen, Y. Surface Engineering Induced Hierarchical Porous Ni<sub>12</sub>P<sub>5</sub>-Ni<sub>2</sub>P Polymorphs Catalyst for Efficient Wide pH Hydrogen Production. *Appl. Catal. B Environ.* **2021**, *282*, 119609. [[CrossRef](#)]

282. Baghban, A.; Habibzadeh, S.; Ashtiani, F.Z. New Insights into the Hydrogen Evolution Reaction Using Ni-ZIF8/67-Derived Electrocatalysts. *Sci. Rep.* **2023**, *13*, 8359. [[CrossRef](#)] [[PubMed](#)]
283. Yin, Z.; Sun, Y.; Zhu, C.; Li, C.; Zhang, X.; Chen, Y. Bimetallic Ni–Mo Nitride Nanotubes as Highly Active and Stable Bifunctional Electrocatalysts for Full Water Splitting. *J. Mater. Chem. A* **2017**, *5*, 13648–13658. [[CrossRef](#)]
284. Zhou, W.; Lu, X.-F.; Chen, J.-J.; Zhou, T.; Liao, P.-Q.; Wu, M.; Li, G.-R. Hierarchical Porous Prism Arrays Composed of Hybrid Ni–NiO–Carbon as Highly Efficient Electrocatalysts for Overall Water Splitting. *ACS Appl. Mater. Interfaces* **2018**, *10*, 38906–38914. [[CrossRef](#)]
285. Peng, L.; Liang, Y.; Wu, S.; Li, Z.; Sun, H.; Jiang, H.; Zhu, S.; Cui, Z.; Li, L. Nanoporous Ni/NiO Catalyst for Efficient Hydrogen Evolution Reaction Prepared by Partial Electro-Oxidation after Dealloying. *J. Alloys Compd.* **2022**, *911*, 165061. [[CrossRef](#)]
286. Xu, Y.; Wang, R.; Zheng, Y.; Zhang, L.; Jiao, T.; Peng, Q.; Liu, Z. Facile Preparation of Self-Assembled Ni/Co Phosphates Composite Spheres with Highly Efficient HER Electrocatalytic Performances. *Appl. Surf. Sci.* **2020**, *509*, 145383. [[CrossRef](#)]
287. Pham, N.N.T.; Kang, S.G.; Kim, H.-J.; Pak, C.; Han, B.; Lee, S.G. Catalytic Activity of Ni<sub>3</sub>Mo Surfaces for Hydrogen Evolution Reaction: A Density Functional Theory Approach. *Appl. Surf. Sci.* **2021**, *537*, 147894. [[CrossRef](#)]
288. Kong, Q.; Lian, L.; Liu, Y.; Zhang, J. Hierarchical Porous Copper Materials: Fabrication and Characterisation. *Micro Nano Lett.* **2013**, *8*, 432–435. [[CrossRef](#)]
289. Zhang, Y.; Sun, X.; Nomura, N.; Fujita, T. Hierarchical Nanoporous Copper Architectures via 3D Printing Technique for Highly Efficient Catalysts. *Small* **2019**, *15*, 1805432. [[CrossRef](#)] [[PubMed](#)]
290. Grosu, Y.; Zaki, A.; Faik, A. Trimodal Hierarchical Nanoporous Copper with Tunable Porosity Prepared by Dealloying Mg–Cu Alloys of Close-to-Eutectic Compositions. *Appl. Surf. Sci.* **2019**, *475*, 748–753. [[CrossRef](#)]
291. Liu, W.B.; Zhang, S.C.; Li, N.; Zheng, J.W.; An, S.S.; Xing, Y.L. A General Dealloying Strategy to Nanoporous Intermetallics, Nanoporous Metals with Bimodal, and Unimodal Pore Size Distributions. *Corros. Sci.* **2012**, *58*, 133–138. [[CrossRef](#)]
292. Su, Y.-R.; Wu, T.-H.; Cheng, I.-C. Synthesis and Catalytic Properties of Hierarchical Nanoporous Copper from  $\theta$  and  $\eta$  Phases in CuAl Alloys. *J. Phys. Chem. Solids* **2021**, *151*, 109915. [[CrossRef](#)]
293. Li, X.; Huang, B.; Qiu, C.; Li, Z.; Shao, L.-H.; Liu, H. Hierarchical Nested-Network Porous Copper Fabricated by One-Step Dealloying for Glucose Sensing. *J. Alloys Compd.* **2016**, *681*, 109–114. [[CrossRef](#)]
294. Chen, X.; Tan, F.; Wang, J.; Zhao, K.; Wang, Y.; Zhang, J.; Liu, H. The Electrochemical Actuation Performances of Nanoporous Ternary AlCoCu Alloy with a Unique Nanosheet Structure. *Materials* **2023**, *16*, 6942. [[CrossRef](#)] [[PubMed](#)]
295. Liang, X.; Zheng, B.; Chen, L.; Zhang, J.; Zhuang, Z.; Chen, B. MOF-Derived Formation of Ni<sub>2</sub>P–CoP Bimetallic Phosphides with Strong Interfacial Effect toward Electrocatalytic Water Splitting. *ACS Appl. Mater. Interfaces* **2017**, *9*, 23222–23229. [[CrossRef](#)] [[PubMed](#)]
296. Guo, Y.; Li, Y.; Zhou, S.; Ye, Q.; Zan, X.; He, Y. Metal–Organic Framework-Based Composites for Protein Delivery and Therapeutics. *ACS Biomater. Sci. Eng.* **2022**, *8*, 4028–4038. [[CrossRef](#)] [[PubMed](#)]
297. Falcaro, P.; Hill, A.J.; Nairn, K.M.; Jasieniak, J.; Mardel, J.I.; Bastow, T.J.; Mayo, S.C.; Gimona, M.; Gomez, D.; Whitfield, H.J.; et al. A New Method to Position and Functionalize Metal–Organic Framework Crystals. *Nat. Commun.* **2011**, *2*, 237. [[CrossRef](#)]
298. Stoeckli, H.F.; Kraehenbuehl, F. The External Surface of Microporous Carbons, Derived from Adsorption and Immersion Studies. *Carbon* **1984**, *22*, 297–299. [[CrossRef](#)]
299. Perret, R.; Ruland, W. The Microstructure of PAN-Base Carbon Fibres. *J. Appl. Crystallogr.* **1970**, *3*, 525–532. [[CrossRef](#)]
300. Boehm, H.P. Book Review: Active Carbon. Manufacture, Properties and Applications. By M. Smišek and S. Černý. *Angew. Chem. Int. Ed. Engl.* **1971**, *10*, 360. [[CrossRef](#)]
301. Pitchaiya, S.; Eswaramoorthy, N.; Natarajan, M.; Santhanam, A.; Asokan, V.; Madurai Ramakrishnan, V.; Rangasamy, B.; Sundaram, S.; Ravirajan, P.; Velauthapillai, D. Perovskite Solar Cells: A Porous Graphitic Carbon Based Hole Transporter/Counter Electrode Material Extracted from an Invasive Plant Species *Eichhornia Crassipes*. *Sci. Rep.* **2020**, *10*, 6835. [[CrossRef](#)]
302. Mukai, K.; Asaka, K.; Sugino, T.; Kiyohara, K.; Takeuchi, I.; Terasawa, N.; Futaba, D.N.; Hata, K.; Fukushima, T.; Aida, T. Highly Conductive Sheets from Millimeter-Long Single-Walled Carbon Nanotubes and Ionic Liquids: Application to Fast-Moving, Low-Voltage Electromechanical Actuators Operable in Air. *Adv. Mater.* **2009**, *21*, 1582–1585. [[CrossRef](#)]
303. Liu, S.; Liu, Y.; Cebeci, H.; De Villoria, R.G.; Lin, J.; Wardle, B.L.; Zhang, Q.M. High Electromechanical Response of Ionic Polymer Actuators with Controlled-Morphology Aligned Carbon Nanotube/Nafion Nanocomposite Electrodes. *Adv. Funct. Mater.* **2010**, *20*, 3266–3271. [[CrossRef](#)] [[PubMed](#)]
304. Lu, L.; Liu, J.; Hu, Y.; Zhang, Y.; Randriamahazaka, H.; Chen, W. Highly Stable Air Working Bimorph Actuator Based on a Graphene Nanosheet/Carbon Nanotube Hybrid Electrode. *Adv. Mater.* **2012**, *24*, 4317–4321. [[CrossRef](#)] [[PubMed](#)]
305. Wu, G.; Hu, Y.; Liu, Y.; Zhao, J.; Chen, X.; Whoehling, V.; Plesse, C.; Nguyen, G.T.M.; Vidal, F.; Chen, W. Graphitic Carbon Nitride Nanosheet Electrode-Based High-Performance Ionic Actuator. *Nat. Commun.* **2015**, *6*, 7258. [[CrossRef](#)] [[PubMed](#)]
306. Novoselov, K.S.; Geim, A.K.; Morozov, S.V.; Jiang, D.; Zhang, Y.; Dubonos, S.V.; Grigorieva, I.V.; Firsov, A.A. Electric Field Effect in Atomically Thin Carbon Films. *Science* **2004**, *306*, 666–669. [[CrossRef](#)] [[PubMed](#)]
307. Ungureanu, S.; Birot, M.; Deleuze, H.; Schmitt, V.; Mano, N.; Backov, R. Triple Hierarchical Micro–Meso–Macroporous Carbonaceous Foams Bearing Highly Monodisperse Macroporosity. *Carbon* **2015**, *91*, 311–320. [[CrossRef](#)]
308. Meng, Y.; Gu, D.; Zhang, F.; Shi, Y.; Cheng, L.; Feng, D.; Wu, Z.; Chen, Z.; Wan, Y.; Stein, A.; et al. A Family of Highly Ordered Mesoporous Polymer Resin and Carbon Structures from Organic–Organic Self-Assembly. *Chem. Mater.* **2006**, *18*, 4447–4464. [[CrossRef](#)]

309. Sánchez-Sánchez, A.; Fierro, V.; Izquierdo, M.T.; Celzard, A. Functionalized, Hierarchical and Ordered Mesoporous Carbons for High-Performance Supercapacitors. *J. Mater. Chem. A* **2016**, *4*, 6140–6148. [[CrossRef](#)]
310. Zhou, P.; Zhang, J.; Song, Z.; Wang, L.; Zhang, Q. Ordered Mesoporous Carbon with Hierarchical Pore Structure for High-Efficiency Electromagnetic Wave Absorber under Thin Matching Thickness. *J. Mater. Res. Technol.* **2023**, *25*, 1560–1569. [[CrossRef](#)]
311. Zhou, Z.; Zhang, H.; Zhou, Y.; Qiao, H.; Gurung, A.; Naderi, R.; Elbohy, H.; Smirnova, A.L.; Lu, H.; Chen, S.; et al. Binder Free Hierarchical Mesoporous Carbon Foam for High Performance Lithium Ion Battery. *Sci. Rep.* **2017**, *7*, 1440. [[CrossRef](#)] [[PubMed](#)]
312. Du, G.; Wang, H.; Liu, J.; Sun, P.; Chen, T. Hierarchically Porous and Orderly Mesostructured Carbon Nanorods with Excellent Supercapacitive Performance. *ACS Appl. Nano Mater.* **2022**, *5*, 13384–13394. [[CrossRef](#)]
313. Wang, J.; Tang, J.; Ding, B.; Malgras, V.; Chang, Z.; Hao, X.; Wang, Y.; Dou, H.; Zhang, X.; Yamauchi, Y. Hierarchical Porous Carbons with Layer-by-Layer Motif Architectures from Confined Soft-Template Self-Assembly in Layered Materials. *Nat. Commun.* **2017**, *8*, 15717. [[CrossRef](#)] [[PubMed](#)]
314. Bu, F.; Zagho, M.M.; Ibrahim, Y.; Ma, B.; Elzatahry, A.; Zhao, D. Porous MXenes: Synthesis, Structures, and Applications. *Nano Today* **2020**, *30*, 100803. [[CrossRef](#)]
315. Ren, C.E.; Zhao, M.; Makaryan, T.; Halim, J.; Boota, M.; Kota, S.; Anasori, B.; Barsoum, M.W.; Gogotsi, Y. Porous Two-Dimensional Transition Metal Carbide (MXene) Flakes for High-Performance Li-Ion Storage. *ChemElectroChem* **2016**, *3*, 689–693. [[CrossRef](#)]
316. Wang, X.; Raghupathy, R.K.M.; Querebillo, C.J.; Liao, Z.; Li, D.; Lin, K.; Hantusch, M.; Sofer, Z.; Li, B.; Zschech, E.; et al. Interfacial Covalent Bonds Regulated Electron-Deficient 2D Black Phosphorus for Electrocatalytic Oxygen Reactions. *Adv. Mater.* **2021**, *33*, 2008752. [[CrossRef](#)] [[PubMed](#)]
317. Qu, L.; Liu, Y.; Baek, J.-B.; Dai, L. Nitrogen-Doped Graphene as Efficient Metal-Free Electrocatalyst for Oxygen Reduction in Fuel Cells. *ACS Nano* **2010**, *4*, 1321–1326. [[CrossRef](#)]
318. Jeon, I.; Zhang, S.; Zhang, L.; Choi, H.; Seo, J.; Xia, Z.; Dai, L.; Baek, J. Edge-Selectively Sulfurized Graphene Nanoplatelets as Efficient Metal-Free Electrocatalysts for Oxygen Reduction Reaction: The Electron Spin Effect. *Adv. Mater.* **2013**, *25*, 6138–6145. [[CrossRef](#)] [[PubMed](#)]
319. Yang, L.; Jiang, S.; Zhao, Y.; Zhu, L.; Chen, S.; Wang, X.; Wu, Q.; Ma, J.; Ma, Y.; Hu, Z. Boron-Doped Carbon Nanotubes as Metal-Free Electrocatalysts for the Oxygen Reduction Reaction. *Angew. Chem. Int. Ed.* **2011**, *50*, 7132–7135. [[CrossRef](#)]
320. Paek, E.; Pak, A.J.; Kweon, K.E.; Hwang, G.S. On the Origin of the Enhanced Supercapacitor Performance of Nitrogen-Doped Graphene. *J. Phys. Chem. C* **2013**, *117*, 5610–5616. [[CrossRef](#)]
321. Lee, W.J.; Maiti, U.N.; Lee, J.M.; Lim, J.; Han, T.H.; Kim, S.O. Nitrogen-Doped Carbon Nanotubes and Graphene Composite Structures for Energy and Catalytic Applications. *Chem. Commun.* **2014**, *50*, 6818. [[CrossRef](#)]
322. Pei, Y.; Zhao, J.; Shi, R.; Wang, X.; Li, Z.; Ren, J. Hierarchical Porous Carbon-Supported Copper Nanoparticles as an Efficient Catalyst for the Dimethyl Carbonate Synthesis. *Catal. Lett.* **2019**, *149*, 3184–3193. [[CrossRef](#)]
323. Tang, M.; Deng, J.; Li, M.; Li, X.; Li, H.; Chen, Z.; Wang, Y. 3D-Interconnected Hierarchical Porous N-Doped Carbon Supported Ruthenium Nanoparticles as an Efficient Catalyst for Toluene and Quinoline Hydrogenation. *Green Chem.* **2016**, *18*, 6082–6090. [[CrossRef](#)]
324. Ramalingam, M.; Jaisankar, A.; Cheng, L.; Krishnan, S.; Lan, L.; Hassan, A.; Sasmazel, H.T.; Kaji, H.; Deigner, H.-P.; Pedraz, J.L.; et al. Impact of Nanotechnology on Conventional and Artificial Intelligence-Based Biosensing Strategies for the Detection of Viruses. *Discov. Nano* **2023**, *18*, 58. [[CrossRef](#)]
325. Tan, P.; Chen, X.; Zhang, H.; Wei, Q.; Luo, K. Artificial Intelligence Aids in Development of Nanomedicines for Cancer Management. *Semin. Cancer Biol.* **2023**, *89*, 61–75. [[CrossRef](#)] [[PubMed](#)]
326. Dong, Z.; Cui, H.; Zhang, H.; Wang, F.; Zhan, X.; Mayer, F.; Nestler, B.; Wegener, M.; Levkin, P.A. 3D Printing of Inherently Nanoporous Polymers via Polymerization-Induced Phase Separation. *Nat. Commun.* **2021**, *12*, 247. [[CrossRef](#)]
327. Mayer, F.; Ryklin, D.; Wacker, I.; Curticean, R.; Čalkovský, M.; Niemeyer, A.; Dong, Z.; Levkin, P.A.; Gerthsen, D.; Schröder, R.R.; et al. 3D Two-Photon Microprinting of Nanoporous Architectures. *Adv. Mater.* **2020**, *32*, 2002044. [[CrossRef](#)] [[PubMed](#)]
328. Demirörs, A.F.; Poloni, E.; Chiesa, M.; Bargardi, F.L.; Binelli, M.R.; Woigk, W.; De Castro, L.D.C.; Kleger, N.; Coulter, F.B.; Sicher, A.; et al. Three-Dimensional Printing of Photonic Colloidal Glasses into Objects with Isotropic Structural Color. *Nat. Commun.* **2022**, *13*, 4397. [[CrossRef](#)]
329. Moore, D.G.; Barbera, L.; Masania, K.; Studart, A.R. Three-Dimensional Printing of Multicomponent Glasses Using Phase-Separating Resins. *Nat. Mater.* **2020**, *19*, 212–217. [[CrossRef](#)] [[PubMed](#)]
330. Duda, T.; Raghavan, L.V. 3D Metal Printing Technology: The Need to Re-Invent Design Practice. *AI Soc.* **2018**, *33*, 241–252. [[CrossRef](#)]
331. Park, S.H.; Su, R.; Jeong, J.; Guo, S.; Qiu, K.; Joung, D.; Meng, F.; McAlpine, M.C. 3D Printed Polymer Photodetectors. *Adv. Mater.* **2018**, *30*, 1803980. [[CrossRef](#)] [[PubMed](#)]
332. Kong, Y.L.; Tamargo, I.A.; Kim, H.; Johnson, B.N.; Gupta, M.K.; Koh, T.-W.; Chin, H.-A.; Steingart, D.A.; Rand, B.P.; McAlpine, M.C. 3D Printed Quantum Dot Light-Emitting Diodes. *Nano Lett.* **2014**, *14*, 7017–7023. [[CrossRef](#)] [[PubMed](#)]
333. Wen, X.; Zhang, B.; Wang, W.; Ye, F.; Yue, S.; Guo, H.; Gao, G.; Zhao, Y.; Fang, Q.; Nguyen, C.; et al. 3D-Printed Silica with Nanoscale Resolution. *Nat. Mater.* **2021**, *20*, 1506–1511. [[CrossRef](#)]
334. Zhou, N.; Bekenstein, Y.; Eisler, C.N.; Zhang, D.; Schwartzberg, A.M.; Yang, P.; Alivisatos, A.P.; Lewis, J.A. Perovskite Nanowire-Block Copolymer Composites with Digitally Programmable Polarization Anisotropy. *Sci. Adv.* **2019**, *5*, eaav8141. [[CrossRef](#)] [[PubMed](#)]

- 
335. Aubert, T.; Huang, J.-Y.; Ma, K.; Hanrath, T.; Wiesner, U. Porous Cage-Derived Nanomaterial Inks for Direct and Internal Three-Dimensional Printing. *Nat. Commun.* **2020**, *11*, 4695. [[CrossRef](#)] [[PubMed](#)]
336. Huang, J.-Y.; Xu, H.; Peretz, E.; Wu, D.-Y.; Ober, C.K.; Hanrath, T. Three-Dimensional Printing of Hierarchical Porous Architectures. *Chem. Mater.* **2019**, *31*, 10017–10022. [[CrossRef](#)]

**Disclaimer/Publisher’s Note:** The statements, opinions and data contained in all publications are solely those of the individual author(s) and contributor(s) and not of MDPI and/or the editor(s). MDPI and/or the editor(s) disclaim responsibility for any injury to people or property resulting from any ideas, methods, instructions or products referred to in the content.